Evaluating the Inflammatory and Tissue Remodeling Response to Novel Biomaterials in a Rabbit Model of Lumbar Colpopexy

by

Aimon Iftikhar

Bachelor of Science in Biomedical Engineering, University of Connecticut, 2013

Master of Science in Biomedical Engineering, Carnegie Mellon University, 2014

Submitted to the Graduate Faculty of the

Swanson School of Engineering in partial fulfillment

of the requirements for the degree of

Doctor of Philosophy

University of Pittsburgh

2020

UNIVERSITY OF PITTSBURGH

SWANSON SCHOOL OF ENGINEERING

This dissertation was presented

by

Aimon Iftikhar

It was defended on

February 3, 2020

and approved by

Pamela Moalli, MD, Ph.D., Associate Professor, Department of Obstetrics, Gynecology & Reproductive Sciences

Steven Abramowitch, Ph.D., Associate Professor, Department of Bioengineering

Julie Phillippi, Ph.D., Associate Professor, Department of Cardiothoracic Surgery

Dissertation Director: Bryan Brown, Ph.D., Associate Professor, Department of Bioengineering

Evaluating the Inflammatory and Tissue Remodeling Response to Novel Biomaterials in a Rabbit Model of Lumbar Colpopexy

Aimon Iftikhar, PhD

University of Pittsburgh, 2020

Pelvic floor disorders account for the weakened function of muscles and surrounding tissues with one of the most prevalent conditions being pelvic organ prolapse (POP). Over a million women each year in the United States are affected with over a quarter undergoing a reconstructive procedure, increasingly using polypropylene mesh. While mesh may provide the mechanical support necessary to treat POP, serious complications such as exposure, erosion, contraction, and pain limit successful outcomes in the long term. Researchers have found an increased inflammatory response to mesh to be correlated with mesh complications, both pre-clinically and in the clinic. The host-biomaterial interaction, with a specific focus on early macrophage behavior, has been accepted as an indicator of implant integration in the long term. However, to date, most research on the host response to mesh has not been performed using a relevant animal model, or has only been evaluated in the long term.

The present dissertation focuses on understanding the tissue specific micro-environment of pelvic floor repair by employing the New Zealand white rabbit to perform a "gold standard" lumbar colpopexy procedure to evaluate changes in the immunologic response at acute (14 days) stages and tissue remodeling outcomes at late stages (90 days) of mesh implantation. Additional comparisons were made with subcutaneous implantation sites relevant from previous models studying host response. Histological and gene expression analysis found evidence of acute and chronic inflammation surrounding mesh implants with tissue degradation and unresolved

inflammation. An overall heightened host response in vaginally implanted meshes was observed when considering macrophage presence, collagen deposition, elastic fiber changes and vascularity.

Further work to mitigate the observed tissue degradation and inflammation involved the immunomodulatory strategy of delivering interleukin-4 (IL-4) during the early stages of the host response. Studies in a mice subcutaneous implantation model have shown success in reducing fibrous capsule formation and encouraging a pro-remodeling response. We have taken this a step further in a novel clinically relevant New Zealand white rabbit lumbar colpopexy model. Results showed overall increased anti-inflammatory cytokine expression, with decreased tissue degradation, enhanced tissue integration, and an overall reduction in tissue adhesions.

Table of Contents

List of Tables

List of Figures

Preface

I am incredibly grateful for the opportunities and learning that being a part of the Brown lab has warranted. I remember coming into the PhD program with goals in mind of enhancing knowledge in the field of immunology, pathology, biochemistry, materials science, and broader concepts of clinically translational biomedical engineering and regenerative medicine. I can honestly say that I am satisfied with the achievement of these learning goals. I am thankful for the opportunities in working on so many interdisciplinary projects. With that being said, I am very thankful for my research advisor, Dr. Brown, and all of his guidance throughout the years. I am very appreciative of his abilities to remain calm and provide perspective whenever I had questions or was presented with difficult challenges. I am also very thankful to all the members of my committee; Drs. Phillippi, Moalli, and Abramowitch, for being supportive and providing insight to the project. Their feedback was always helpful and encouraging. I am so grateful to the NIH TL1 CTSI fellowship for their financial and academic support, which provided me with many opportunities for professional growth and development.

Everyone in the Brown Lab, past and present, has played a huge role in my life. I am thankful for being able to spend time learning and growing from everyone. I always loved the fact that we got along so well and took care of each other just like family. I'm also incredibly grateful for all the people I have met through utilizing all sorts of resources across campus. I learned so much across animal facilities and characterization, histology, and imaging labs.

More personally, I am very thankful for the support from my parents. They have encouraged the pursuit of such wonderful opportunities. I appreciate everything they have done for me to get me to where I am today and will forever be truly grateful. I also am so thankful for

my fiancé, Ariff, for providing me with so much encouragement and support. He is a complete inspiration to me and motivates me constantly to be better. There are so many more people I would love to mention by name, but I'm so thankful for all my friends who have given so much love and constant support.

1.0 Introduction

1.1 Pelvic Organ Prolapse (POP)

Pelvic organ prolapse is a condition characterized by the weakening of pelvic floor muscles over time resulting in the downward shift, or herniation of the pelvic organs into or beyond the vaginal canal. The vagina along with its connective tissues and muscles provides direct support to the pelvic organs, including the urethra, bladder, uterus, and rectum [2-6]. However, factors such as menopause, obesity, age, vaginal birth, congenital or acquired connective tissue abnormalities increase the susceptibility to experiencing pelvic organ prolapse [4, 7, 8]. While POP is not life threatening, symptoms such as pelvic pressure, observing a bulge protruding past the vaginal opening, pain with daily activities as well as dyspareunia, along with disruptions in bowel and urinary behavior can have a lasting impact on the quality of life for women [9-11]. While the degree and type of prolapse can vary, about 41% to 50% of the female population have presented symptoms of prolapse upon physical examination [12]. It is estimated that the number of women who have POP in the United States will increase by 46% to an approximate 4.9 million women by the year 2050 [12].

There are many variations in the types of prolapse that women may experience (See Table 1). Upper vaginal prolapse or vaginal vault, can occur after hysterectomy, when the top of the vagina descends down and bulges outward. Uterine prolapse is when the uterus descends into the vagina. Cystocele, or anterior vaginal wall prolapse, is when the bladder shifts downward, creating the bulge. Urethrocele is another form of the anterior vaginal wall prolapse, where the urethra will

fall into the anterior vaginal wall. Enterocele is when small bowel sinks into the posterior vaginal wall. Rectocele is when the rectum descends into the posterior vaginal wall [13].

Table 1: Classifications of Pelvic Organ Prolapse

Prolapse Type	Prolapse Description
Cystocele	Prolapse of the bladder into upper anterior vaginal wall
Urethrocele	Prolapse of the urethra into lower anterior vaginal wall
Enterocele	Prolapse of the small bowel into the upper posterior vaginal wall
Rectocele	Prolapse of the rectum into the posterior vaginal wall
Uterine prolapse	Prolapse of the uterus into the vagina
Vaginal Vault	Prolapse of the top of the vagina descends down, also known as upper vaginal prolapse; can occur after hysterectomy

POP patients often experience other forms of pelvic floor disorders in conjunction with their prolapse symptoms. It has been found that approximately 40% of POP patients have stress urinary incontinence, 50% experience fecal incontinence, and 37% have symptoms of an overactive bladder [11].

1.1.1 Anatomy of the Pelvic Floor

In the female pelvis, the anatomical support of the pelvic organs is provided by a physiologically intricate relationship between the pelvic floor muscles and connective tissue attachments. The pelvic floor muscles, also known as the levator ani muscles, hold the pelvic floor closed in such a way that usually prevents the abnormal descent of the pelvic organs. They consist of the coccygeous, pubococcygeous, ileo coccygeous muscles and it is through isotonic contraction that provides mechanical support to the pelvic organs [3-5, 14-24]. The connective tissue structural support is characterized by three levels, each with distinct contributions. Level I is defined by the cardinal and uterosacral ligaments attaching the upper third of the vagina and the cervix to the pelvic walls. Level II support is defined by the paravaginal attachment of the middle of the vagina laterally to the pelvic sidewalls via the arcus tendinous fascia. Level III is characterized by the distal vagina attachment to surrounding structures such as the levator ani muscles and the perineal body via endopelvic fascia [2-4, 25].

It is specifically loss of apical support (Level I) or a combination of these levels that has been found to contribute towards the development of POP [4, 5].

1.1.2 Clinical Treatment Options

Current statistics from the U.S. Food and Drug Administration (FDA) state that approximately 12.6% of women will undergo surgery to repair pelvic organ prolapse (POP) during their lifetime [12, 26, 27]. While treatment is individualized to each patient's circumstance and the symptoms that are being experienced, the primary goal is to always improve the condition and minimize any further progression. At times, this can be achieved with conservative nonsurgical

options, such as the use of a vaginal pessary, or with increased pelvic floor muscle training exercises. However, there are circumstances that necessitate a reconstructive surgery to correct POP by restoring mechanical support to the pelvic floor. This is done once a physician has completed the pelvic organ prolapse quantification system exam otherwise known as POP-Q [13]. It provides a standardized method of classifying the array of symptoms experienced by women through a series of defined anatomical points that serve as landmark references. During examination, physicians can determine any prolapse development through changes in measurements from these references. For example, the degree of prolapse is described in stages from 0 to 4, with a higher number indicative of a more severe progression.

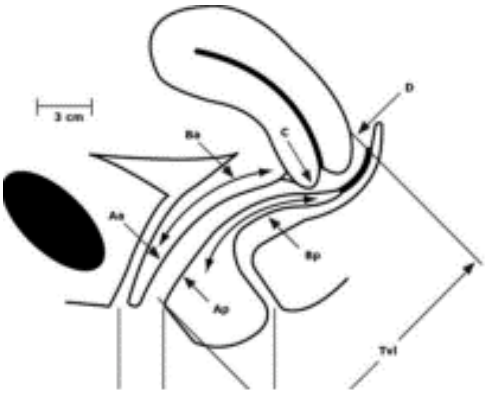

Point	Description	Range of Values
Aa	Anterior vaginal wall 3 cm proximal to the hymen	-3 cm to +3 cm
Ba	Most distal position of the remaining upper anterior vaginal wall	-3 cm to +tvl
C	Most distal edge of cervix or vaginal cuff scar	
D	Posterior fornix (N/A if post-hysterectomy)	
Ap	Posterior vaginal wall 3 cm proximal to the hymen	-3 cm to +3 cm
Bp	Most distal position of the remaining upper posterior vaginal wall	-3 cm to + tvl

Genital hiatus (gh) – Measured from middle of external urethral meatus to posterior midline hymen
Perineal body (pb) – Measured from posterior margin of gh to middle of anal opening
Total vaginal length (tvl) – Depth of vagina when point D or C is reduced to normal position

Figure 1 POP-Q landmark references and points referring to the range of values for quantitative measurements in determining the stages of prolapse. Public Domain. Retrieved from [2]

When it comes to surgical treatment, there are a wide variety of both abdominal and vaginal approaches that can be considered to resuspend the vaginal apex and anterior and posterior vaginal walls (See Table 2). It is well recognized that providing robust apical support is a fundamental component of successful long-term POP repair [28].

Table 2: Surgical Approaches to treat Pelvic Organ Prolapse

Vaginal Approaches [6, 29]	
Colporrhaphy	Anterior or posterior vaginal wall repair
McCall culdoplasty	Attaching uterosacral and cardinal ligaments to the peritoneal surface
Manchester repair	Amputation of the cervix with uterus suspension to the cardinal ligaments
Prespinous & sacrospinous colpopexy	Attachment of uterus or vagina to sacral anterior ligament
Abdominal Approaches (Either through open incision or via laparoscope)[6, 29]	
Sacral colpopexy	Attachment of uterus or vagina to sacral anterior ligament
Paravaginal repair	Attaching pelvic organs (bladder and urethra) to pelvic sidewalls
Vault suspending and uterosacral ligament plication	Suspending uterosacral ligament to the sacrum
Enterocele ligation and posterior vaginal wall repair	Repair surgery to stop rectum from bulging into the vagina

A variety of research has found that the sacral colpopexy surgical method has been associated with the best outcomes in terms of durability when compared to other procedures, especially those of the transvaginal route [30, 31]. However, the risk of recurrence still exists and it has been estimated that between 10 - 30% of all procedures required a secondary and sometimes multiple operations to resolve complications or recurring symptoms [9].

There are four classes of reconstructive materials used in the procedure to provide restore mechanical support that include: biologic, non-absorbable synthetic, absorbable synthetic, and

composite (any combination of the previous three). Autologous repairs are utilizing the patient's own native tissues for repair, however there is a higher chance of recurrence (40%) [9, 32]. Biologically derived materials such as allografts and xenografts create extracellular matrix scaffolds, but also have been shown to lack the mechanical robustness needed to provide reconstructive support long-term. Synthetic mesh materials such as polypropylene are increasingly used in reconstructive procedures, and maintain the mechanical strength necessary to provide support. However, the use of mesh is also not without complications, such as chronic pain, mesh erosion and exposure through the neighboring tissues [33-35].

1.1.3 Complications

The use of polypropylene mesh in pelvic floor repair has led to a significant reduction in the recurrence of prolapse, but is also associated with complications, including chronic pain and mesh erosion/exposure [9, 12, 36, 37]. In a meta-analysis conducted by the FDA reported in early 2019, 11 – 18% of women implanted with mesh experienced these complications in a time period of 1 – 6 years after prolapse repair, thus requiring surgical correction [12].

Further assessment has found that mesh-related complications are dependent on the anatomical placement of mesh during POP repair. It has been shown that abdominal approaches were associated with approximately 30% lower rate of complications than a transvaginal approach after 7 years post-surgery [38]. Additionally, complications can be correlated with two distinct pathways of failure. Mechanical mismatch and an unresolved inflammatory response leading to poor tissue integration are widely accepted phenomena associated with the failure of mesh in pelvic floor repair [9, 37, 38].

Synthetic mesh has originally been used to repair abdominal hernias for over half a century. Medical device companies, through 510k and the 1976 Medical Device Amendments Act, were able to resell the hernia repair mesh as a treatment for pelvic organ prolapse [26, 27]. However, with the increasing complications, in 2008 and 2011, the US Food and Drug Administration issued warnings to doctors and patients about mesh [27]. In January of 2016, the US Food and Drug Administration officially reclassified surgical mesh for transvaginal repair of pelvic organ prolapse from a class II, moderate risk device, to a class III, high-risk device [26].However, most recently in 2019, the sale of mesh intended for transvaginal repair was officially banned [12]. It is clear that there are deeper considerations that impact the understanding of the host response to synthetic mesh in vaginal tissue. Hernia repair focuses predominantly on the anatomical location of the abdomen and the transition to vaginal repair introduces increased vulnerabilities via inflammation and changes in the mechanical stresses.

2.0 Foreign Body Response to Mesh

While the material and mechanical properties associated with biomaterial implants are of significant importance both at the time of implantation and for the long-term function of materials within the body, the host inflammatory response which occurs at the host-biomaterial interface has long been considered as a key predictor of downstream success. That is, even in the presence of a robust design which meets the mechanical requirements at the site of implantation, materials may fail due to a reaction which degrades or inhibits their proper function over time. Such reactions have been a topic of study for many decades and advances in the understanding of the host response has been used to drive the development of novel materials and modification strategies.

It is well known that as soon as a material is implanted in the body, an orchestrated progression of cellular and biochemical phenomena including blood-material interactions, provisional matrix formation, acute inflammation, chronic inflammation, granulation tissue development, foreign body reaction, and fibrotic tissue deposition [1, 39-41]. The mechanisms underlying each of these phenomena have been studied in-depth and multiple strategies for their modification have been proposed in the field.

2.1 Acute vs. Chronic Response

The inflammatory response can be divided into two broad categories based upon temporal activities that have been widely observed, the acute phase and chronic phase of inflammation. The acute inflammatory stage begins immediately after implantation and can last two to four weeks.

Host proteins adsorb onto the implant surface and within hours the presence of neutrophils is observed, reacting by producing cytokines, chemokines, reactive oxygen species, and other enzymes such as metalloproteinases that lead to the recruitment of macrophages over the next few days [1, 39, 40, 42]. The presence of macrophages also leads to further secretion of cytokines, which, depending on the degradability and surface properties of the implant, will continue the inflammatory process [1, 39, 40]. Simultaneously, angiogenic factors are released and lymphocytes continue the inflammatory process. However, when the acute inflammatory response does not eliminate the invading foreign agent, the response moves into the next stage of chronic inflammation. At this point, macrophages can fuse into a foreign body giant cells, fibroblast recruitment is promoted, and an increased extracellular matrix can be observed surrounding the implant [1, 39, 40]. It is at this stage, where subsequent development of a dense collagen capsule with decreased potential for vascularization, that the implant may result in failure for its intended purpose.

2.2 The Role of Cytokines

Table 3 lists the critical cytokines present during the foreign body response which provide functional events determining later stages of inflammation. These will be referenced later in discussion. Cytokines are considered the molecular messengers that provide the necessary signals for inflammatory or anti-inflammatory events, such as macrophage activation that will determine immune response outcomes including collagen formation and angiogenesis [40, 43].

Table 3: Cytokines involved in wound healing and the foreign body reaction. Retrieved from [1]

Cytokine	*Function relative to the FBR*	*Produced by*
G-CSF	Chemotactic for and activator of PMNs	Fibroblast, macrophage, monocyte, PMN, T cell
GM-CSF	Activates PMN, eosinophil, monocyte Enhances phagocytosis in macrophage and PMN	EC, fibroblast, monocyte, T cell
IFNγ	Induces IL-1β, G-CSF, M-CSF production Inhibits growth of various cell types	Natural killer cell, T cell
IL-1	Acute-phase protein production, induces edema, fever, and cytokine and adhesion molecule production Fibroblast chemotaxis and proliferation	Fibroblast, keratinocyte, macrophage, monocyte, PMN, T cell
IL-2	T-cell proliferation, induces IFNγ, IL-1, and TNFα production Activates macrophages	T cell
IL-4	MnGC formation Inhibits IL-1 and TNFα production	T cell
IL-6	Acute-phase protein production, enhanced IL-1Ra and soluble TNFαR production Lowers TNFα, CXCL-2, GM-CSF, and IFNγ levels	Many cell types
IL-10	Reduces IL-1β, IL-6, TNFα, CXCL-1, and MIP-1α production Inhibits phagocytosis	Macrophage, Th2
IL-12	Enhances phagocytosis, increases IFNγ production by T cells	Macrophage, PMN
IL-13	MnGC formation, inhibits IL-1β, IL-6, TNFα, CXCL-8, and CCL3 production IL-1RA, CR3, and CR4 upregulation	T cell
M-CSF	Survival, proliferation, and differentiation of phagocytes Proangiogenic	B cell, EC, fibroblast, monocyte, PMN, T cell
PDGF	Vessel maturation and chemotactic for fibroblasts and SMC	EC, fibroblast, macrophage, mast cell, platelet
TGFβ	Increases ECM production Macrophage, fibroblast, and PMN chemoattractant PMN and macrophage activator Induces TGFβ production in macrophages	EC, fibroblast, keratinocyte, macrophage, mast cell, platelet, PMN
TNFα	Enhances phagocytosis and chemotaxis Induces chemokine production	Fibroblast, keratinocyte, macrophage, mast cell, monocyte, natural killer cell, PMN, Th
VEGF	Angiogenic, mitogen for EC Induces vascular permeability and vasodilatation	EC, fibroblast, keratinocyte, macrophage, mast cell, platelet, PMN

2.3 The Role of Macrophages

Macrophages are widely accepted as protagonists during the inflammatory process. Preliminary work has shown that the implantation of mesh is associated with a foreign body response, consisting predominantly of activated, proinflammatory M1 macrophages [33, 44, 45]. It is commonly known that macrophages can exist on a spectrum ranging from the classically activated, M1 type to the alternatively activated, pro-remodeling M2 phenotypic profile depending on the nature of signaling cues received [44, 46-49]. Previous evaluation of the host response to mesh implanted in human patients who experienced complications found a prolonged presence of the activated, pro-inflammatory response lasting beyond 8 years (30, 31).

Classically activated macrophages appear initially to the site of injury and proceed with phagocytic functions and the production of oxidative metabolites and pro-inflammatory cytokines. Typically, there is a phenotypic switch to the anti-inflammatory M2 macrophage population, with an upregulation of anti-inflammatory cytokines focused on tissue remodeling and constructive processes to resolve inflammation.

Macrophage polarization is a concept that is a focus for immunomodulation. It is widely known that shifting the macrophage phenotype during the foreign body response from the pro-inflammatory profile to the more anti-inflammatory, pro-tissue remodeling profile early on after implantation of a biomaterial has been associated with a beneficial host response [44, 49, 50]. It has also been correlated with better integration of the implant into the surrounding tissue, thus mitigating the negative effects of a chronic inflammatory response.

3.0 The Concept of Immunomodulation

There have been many developments in strategies to modulate the immune response to biomaterials specifically related to macrophage polarization. Macrophage polarization has been modeled *in vitro* with the administration of cytokines capable of shifting phenotypic properties. Inflammatory mediators (lipopolysaccharide (LPS) and interferon-gamma (IFN-γ) are known to activate the M1 macrophage phenotype. Interleukin-4 (IL-4), interleukin-13, (IL-13) and other cytokines are known to support activation of the M2 macrophage phenotype. Immunomodulatory approaches focus on the temporal release of specific cytokines or other molecules capable of mitigating inflammation and promoting a regenerative bioactive response.

While there are strategies that have focused on inhibiting the effects of known pro-inflammatory agents, such as tumor necrosis factor alpha (TNF-α) and have shown promise for faster wound healing, there is increased attention towards strategies of promoting the phenotypic shift of M1 towards an M2-like profile during the early stages of the immune response [44, 45, 49-51]. This is accomplished using anti-inflammatory agents, such as interleukin-10 (IL-10), IL-4, IL-13, or even glucocorticosteroids. However, the method of exposing macrophages to these crucial mediators is also an area of development in which researchers will embed the molecules in a material scaffold and utilize different controlled release strategies [45, 50, 52-57]. Scaffolds can range from materials such as synthetic polymers to extracellular matrix derived biologic scaffolds. These strategies are motivated by the natural healing process of tissues. To date, preclinical findings have shown potential, more research is needed to move forward with clinical studies of such approaches.

3.1 Layer-by-Layer

The last decades have brought significant development in the field of novel materials as well as the available methods of modifying the surface of implants. This has led to an array of changing properties increasing the characteristics associated with the host material. While there are numerous methods to fabricate a polymer film, the layer-by-layer assembly method provides many benefits in its mild process including versatility and the ability to incorporate functional biomolecules. Using the concept of electrostatic interactions, the layer-by-layer method quite literally refers to the deposition of alternating layers of a cationic polyelectrolyte followed by an anionic polyelectrolyte. This mechanism can be applied to several charged materials, including nucleic acids, saccharides and other proteins. However, in our laboratory, a previously developed layer-by-layer system incorporating chitosan as a cationic polymer and dermatan sulfate as an anionic polymer has shown great success in the release of bioactive IL-4 [50]. While the applications of layer-by-layer technology can go beyond what will be discussed further in this dissertation, there are several aspects of using polyelectrolyte layers for the release of bioactive molecules that highlight implant functionality.

4.0 Animal Models Examining Mesh Host Response

There are many *in vivo* models utilized to undergo the vast task of understanding the host response to mesh. Animal surgical models continue to be an essential component in preclinical testing. However, there are several models that can accurately represent the pathophysiological parameters surround pelvic organ prolapse.

Rodents have been previously employed to assess the inflammatory response to materials, especially at the early stages of development. Subcutaneous and partial thickness abdominal wall defects are common procedures providing detailed information on material-tissue interactions. More recently, a lysyl oxidase like-1 (LOXL1)-deficient group of mice have been used as a clinically relevant parallel to prolapse, having found that LOXL1-deficient mice develop prolapse after delivery [58, 59]. This comes with the knowledge that LOXL1 is the enzyme critical in elastin metabolism and thus removing it from mice allows researchers to mimic prolapse symptoms due to the associated weakness in the pelvic floor [59]. Other groups have looked at fibulin-5 knockouts in mice or disrupting motifs that are responsible for the matrix metalloproteinases [59-61]. Previous work using modifications such extracellular matrix coatings or incorporation of immunomodulatory cytokines has also served as the groundwork towards shifting to a larger animal model, thereby enhancing preclinical knowledge [50, 62].

To date, rabbit studies have focused on the external vagina in which the mesh is simply placed under the vaginal wall and therefore, do not mimic a prolapse surgical repair [42, 63]. Additionally, there are several studies that have also continued the trend of abdominal wall implantations in rabbits, which cannot necessarily relate back to prolapse repair [64, 65].

Sheep closely mimic the anatomical and physiological properties of the female pelvic floor, and was shown to elicit the same mesh placed in the abdominal wall and implanted transvaginally found greater fibrotic response and tissue degradation in the vaginal implants. However, the use of a sheep model has resulted in numerous studies of implanting mesh in the abdominal wall and transvaginally [64, 66-69].

A nonhuman primate sacrocolpopexy model allows for the gold standard pelvic floor repair procedure. Numerous studies have contributed significantly to the field in discovering the effects of mesh implantation on vaginal tissues. Researchers found substantial reduction in the vaginal smooth muscle layer along with decreased collagen and elastin content and increased active metalloproteinases, all indicative of vaginal degeneration [35, 70, 71]. While nonhuman primate model outcomes have provided tremendous insight into the mechanisms behind complications, the host response has only been observed at later time points (> 3 months) due to the high cost and limited availability of this model.

5.0 Hypothesis and Specific Aims

In order to better understand vaginal tissue degradation in mesh implantation patients, the current dissertation describes the development and utilization of a surgical model to assess the impact of different microenvironments based upon anatomical location. As noted previously, the early host response in a clinically relevant environment remains largely uncharacterized. Based on previous contributions from animal models of mesh implantation, our research objective consisted of two main aims.

Aim 1: To develop and utilize a clinically relevant rabbit pelvic prolapse reconstruction model to assess the host response to implanted mesh in the vagina and abdomen.

Sub Aim 1.1: To analyze the tissue composition in the abdomen and vagina, and how that deviates with the implantation of polypropylene mesh at early inflammatory and late tissue remodeling time points.

Hypothesis: Implantation of mesh in the vagina and abdomen will be consequently associated with an increased inflammatory profile in the vagina related to increased tissue degradation downstream. We hypothesize differences in the extracellular matrix deposition based on the anatomical location at early and late time points, such that the abdomen is not a representative indicator of mesh implantation outcome in the vagina.

Aim 2: To scale up the controlled release of IL-4 from a layer-by-layer coating as an immunomodulatory strategy to improve downstream outcomes following mesh implantation.

Hypothesis: The controlled release of IL-4 from a coated mesh will modulate the immune response to promote an improved tissue remodeling and decreased inflammatory response. Thus, modifying the polypropylene mesh to maintain its original functionality but with a coating using a drug delivery mechanism to release cytokines to promote tissue remodeling will be beneficial in creating an enhanced mesh implant associated with improved tissue integration post-implantation.

6.0 Aim 1: To Utilize a Clinically Relevant Rabbit Pelvic Reconstruction Model to Assess the Acute and Chronic Host Response to Polypropylene Mesh in the Vagina and the Abdomen

6.1 Introduction

Previous studies of clinically available as well as novel biomaterials have shown that the early inflammatory profile following implantation is a strong indicator of overall tissue integration downstream across multiple tissue and organ systems [33, 42, 44, 50, 72-74]. However, the early host response to polypropylene mesh in the vaginal microenvironment remains largely unstudied. While a nonhuman primate sacrocolpopexy model allows for the gold standard pelvic floor repair procedure, the host response has only been observed at later time points (> 3 months) due to the high cost and limited availability of this model [33, 64, 71]. Similarly, a sheep model has resulted in numerous studies of implanting mesh transvaginally, but the same constraint of a later time point (> 3 months) remains [64, 66, 67, 69]. While there is prior work conducted in a rodent abdominal defect model defining the response at earlier time points, the host response to mesh in this model is not truly representative to a relevant pelvic floor model [62, 64, 68, 74-77]. To date, rabbit studies have focused on the external vagina in which the mesh is simply placed under the vaginal wall and therefore, do not mimic a prolapse surgical repair [63, 73]. Thus, there is a clinical need for a cost-effective model that allows for the assessment of biomaterials in relevant anatomical locations at time points relevant to shifts in the immune response.

A rabbit lumbar colpopexy model may represent an ideal, cost-effective model system due to the ability to create an adapted method of pelvic reconstruction closely mimicking sacrocolpopexy affording the possibility of assessing early and late immune responses. In this aim,

Gynemesh PS (Ethicon, Somerville, NJ), a commercially available polypropylene mesh, was implanted via lumbar colpopexy in 6-month-old New Zealand white rabbits. At 14- and 90-days post-implantation, the mesh-vagina complexes were extracted for evaluation of the acute and chronic immune and tissue remodeling response. Results from this aim provided insight into the dynamic remodeling process of the mesh host response captured in a clinically relevant model.

6.2 Materials & Methods

6.2.1 Animal Subjects

A total of 12 nulliparous New Zealand White Rabbits aged 4 – 6 months (~4 kg) were used in this study. Animals were obtained from Covance, Inc. (Princeton, NJ). All animals were housed in the Center for Preclinical Studies at the McGowan Institute for Regenerative Medicine (MIRM) for at least 7 days prior to the start of any procedure. All animals were examined by staff veterinarians and determined to be in good health prior to admission into any study. All animals were monitored daily. All procedures were approved by the Institutional Animal Care and Use Committee at the University of Pittsburgh.

Rabbits were kept with fresh bedding and enrichment along with access to food and water in accordance to National Institutes of Health Animal Care Guidelines for rabbit care. Extra enrichment was provided in the form of preferential snacks such as blueberries, pineapple, celery, strawberries, grapes and romaine lettuce. The rabbits were exposed to a 12-hour light/dark cycle and monitored for signs of distress throughout the study.

6.2.2 Surgical Design (Lumbar Colpopexy vs Subcutaneous)

Rabbits were sedated with acepromazine (1 mg/kg) followed by intramuscular injection of ketamine/xylazine (35 mg/kg & 5 mg/kg). Animals were then incubated and a surgical plane of anesthesia was achieved via inhalation of 2% isofluorane.

A midline longitudinal incision was performed opening the peritoneal space with the bowels packed away followed by identification of the uterine horn and reproductive organs (Figure 2A). A hysterectomy was performed followed by trimming and collection of the proximal vagina of the rabbit to serve as a positive control for histological, biochemical and gene expression analysis (Figure 2B). Once the uterus was removed, space was dissected along the vaginal wall on both sides between the bladder and the rectum (Figure 3A). Two 3 x 12 cm^2 pieces of Gynemesh PS (Ethicon, Somerville, NJ) were secured with 3-0 PDS suture along the posterior and anterior vaginal walls (Figure 3B). The remaining flaps at the top were then attached to a ligament in the lumbar spine with 2-0 PDS creating support to the pelvic organs (Figure 4A & 4B). The peritoneal cavity was continuously hydrated (Figure 5) and sutured closed with continuous stitching using 3-0 PDS. A 2 x 2 cm^2 piece of mesh was implanted subcutaneously (Figure 6B) onto the abdominal musculature via 3-0 PDS prior to closing the initial abdominal incision in the skin with subcuticular stitches. Post-surgically, all animals were monitored closely to ensure full recovery from anesthesia.

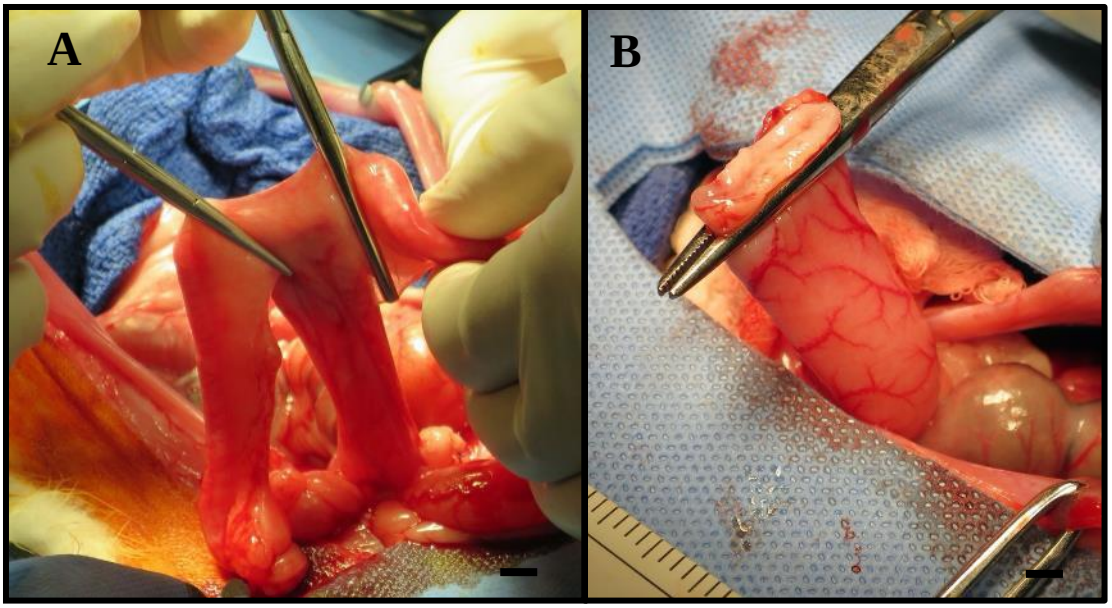

Figure 2: A. Identification of the uterus prior to performing hysterectomy B. Partial removal of proximal vagina. All scale bars indicate 0.5 cm.

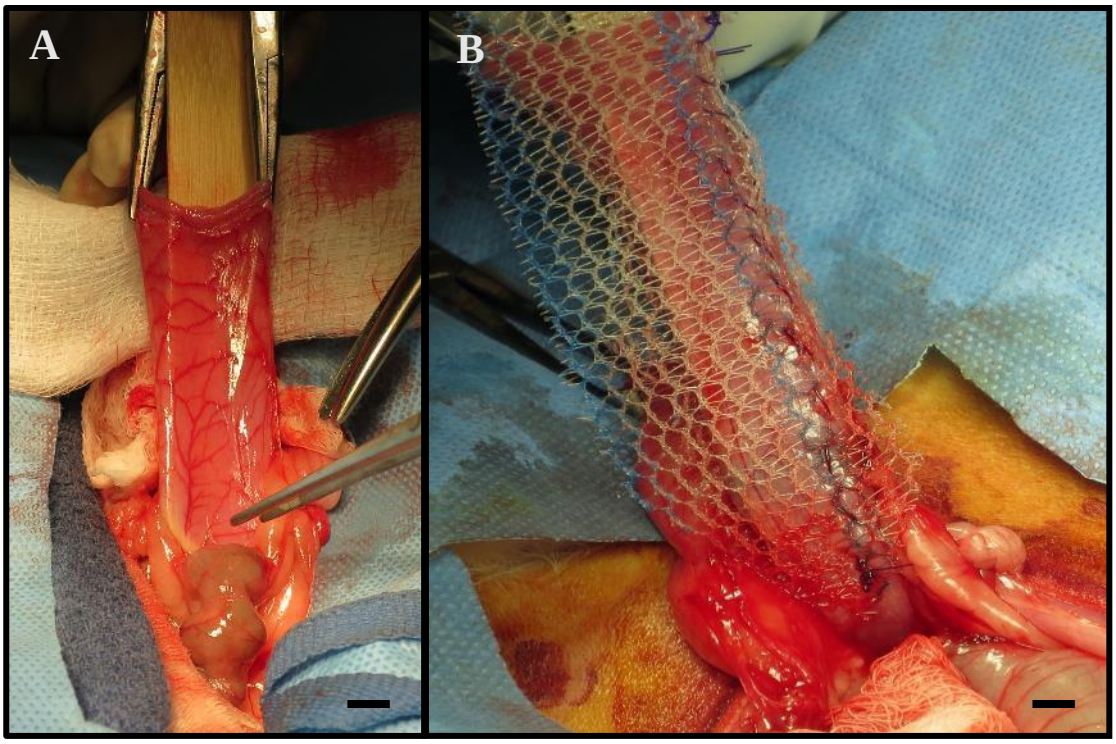

Figure 3: A. Dissection away from rectum and posterior vagina. B. Attachment of mesh along vaginal wall. All scale bars indicate 0.5 cm.

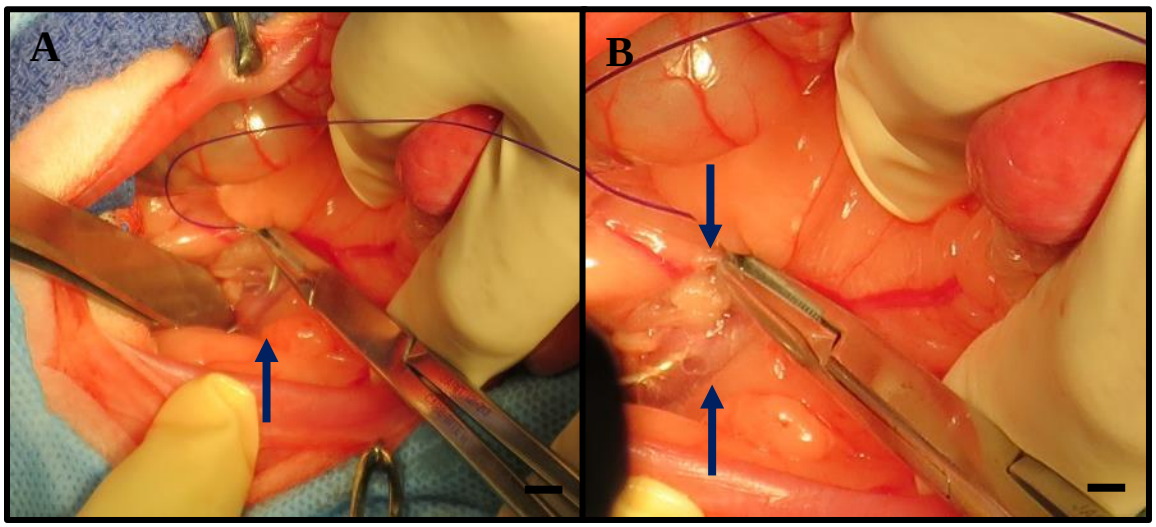

Figure 4: A. Suturing through ligament in lumbar space for proximal attachment B. Attaching suture through ligament for anchoring at lumbar (Blue arrows indicate suture needle through ligament). All scale bars indicate 0.5 cm.

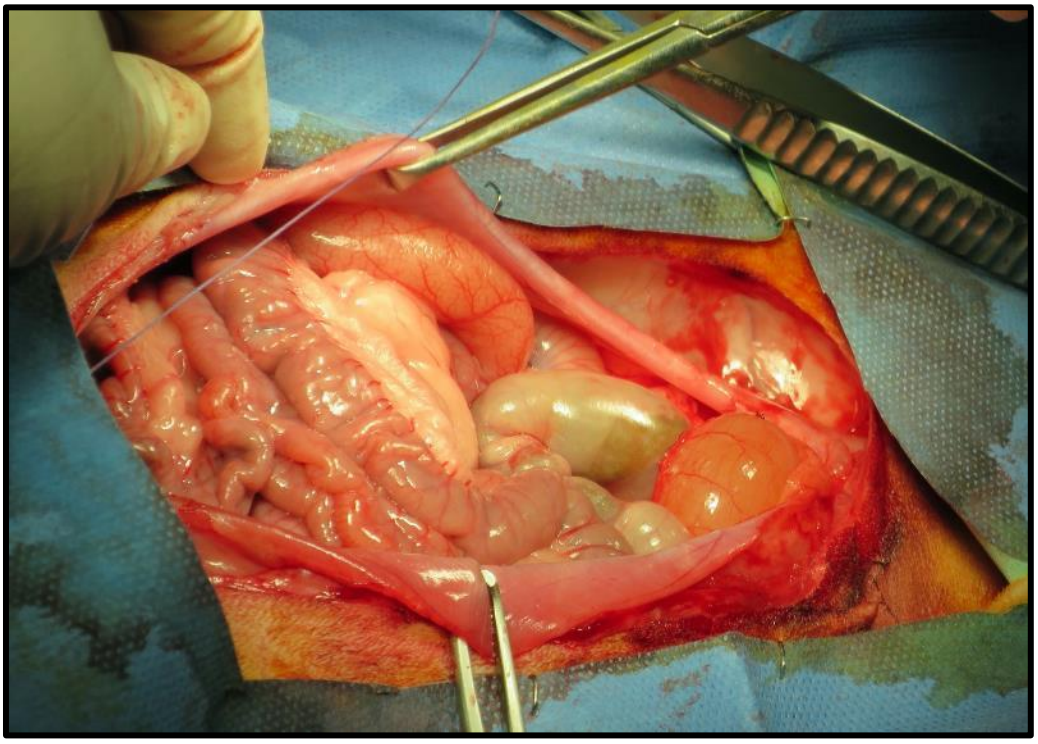

Figure 5: Ensuring peritoneal space is adequately hydrated and unpacking bowels prior to subcutaneous procedure

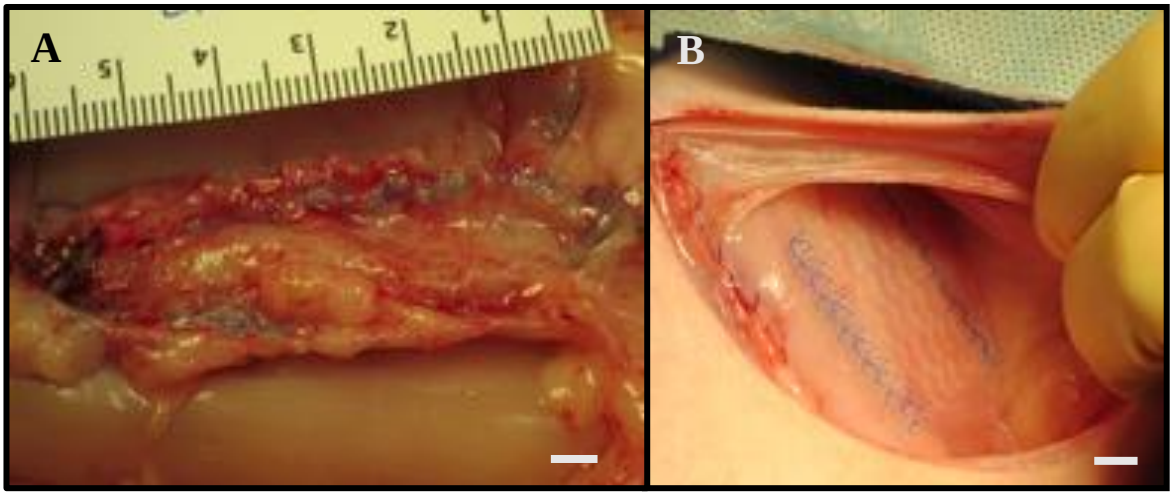

Figure 6: A. Mesh attached to vaginal wall and secured to ligaments completing lumbar colpopexy procedure B. Mesh implanted in the subcutaneous space. All scale bars indicate 0.5 cm.

6.2.3 Post-operative Care

Animals were carefully monitored for signs of discomfort (as evidenced by failure to eat, drink, or resume normal ambulation and activity). Cefazolin (25 mg/kg), Buprenex (0.02 mg/kg), and Ketoprofen (2 mg/kg twice daily as needed) was given via subcutaneous injection for pain for 3 days postoperative. At the veterinarian's discretion, the animals were given Ranitidine (2 mg/kg) as an antacid in cases of a decreased appetite until normal activity resumed.

6.2.4 Tissue Explants and Tissue Processing

At 14 days and 90 days post-implantation, the animals were sedated with acepromazine (1 mg/kg) and injected intravenously with sodium pentobarbital (100 mg/kg) for euthanasia. The

mesh and surrounding tissue were extracted from the rabbit and immediately processed. One portion of a representative mesh-tissue explant (Figure 7A & 7B) was fixed in formalin for at least 48 hours before paraffin embedding. 7 μm sections were used for histological analysis. Another portion of the explant was flash frozen and kept in -80°C for biochemical evaluations. A 3x3 cm^2 piece of vaginal-mesh tissue was carefully wrapped in gauze and kept in sterile saline at -20°C for biomechanical testing.

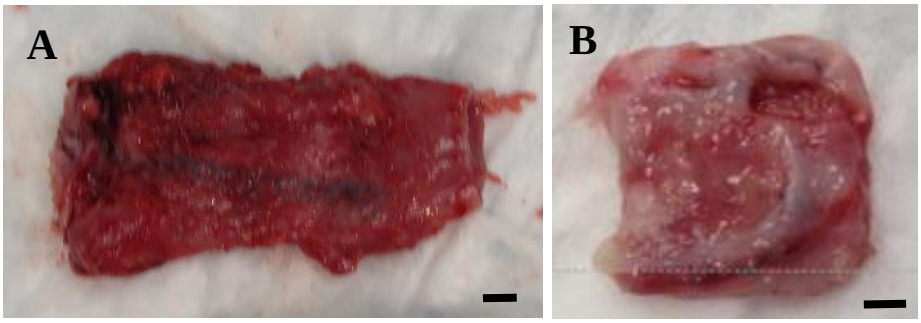

Figure 7: A. Representative image of excised vaginal tissue B. Representative image of excised subcutaneous tissue. All scale bars indicate 0.5 cm.

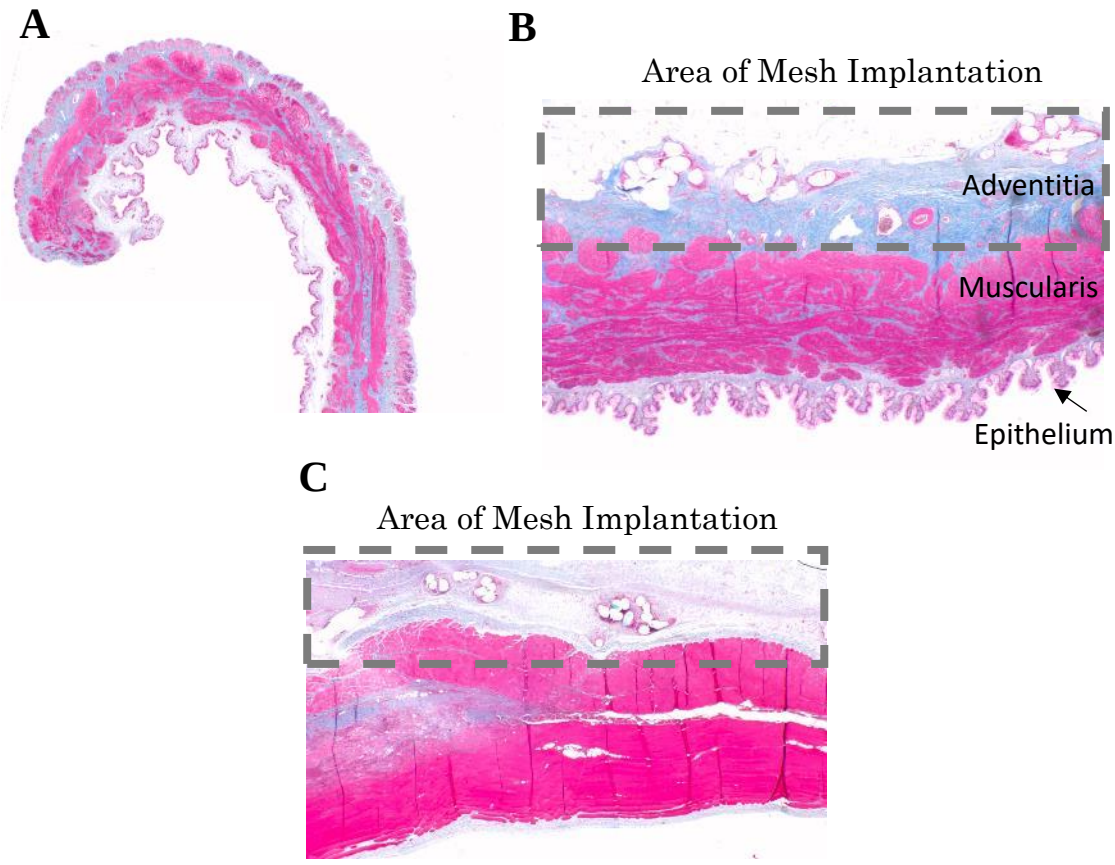

Figure 8: Histological Representation of Explanted Tissue A. Control vaginal tissue extracted during hysterectomy procedure. B. Representative vaginal-mesh tissue cross-section depicting tissue layers C. Representative subcutaneous-mesh tissue cross-section

6.2.5 Histology (H&E) Tissue Morphology and Characteristics

Tissue sections were stained with hematoxylin and eosin to observe key aspects of the host response to mesh including tissue organization, degradation and encapsulation. Specifically, tissue sections were analyzed with an emphasis regarding mononuclear cellular infiltration near mesh fibers, the presence of foreign body giant cells and potential angiogenesis. Cellularity analysis

was based on 5 to 7 single mesh fibers imaged per sample at a 40X objective on Nikon Eclipse 50i (Nikon, Tokyo, Japan) and using Fiji image processing software (National Institutes of Health, Bethesda, MD).

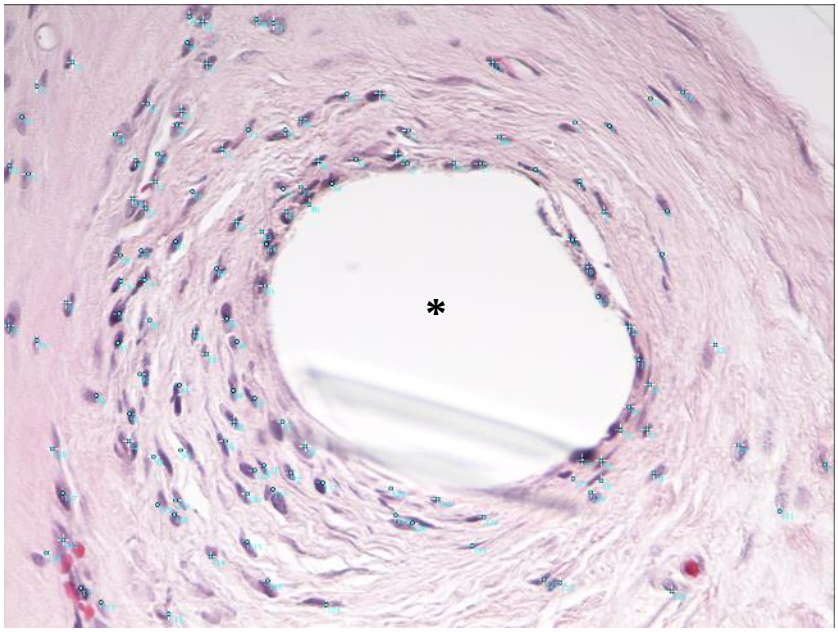

Figure 9: Representative image of mesh fiber at 40X objective (shown by *) and utilization of Fiji software for cellularity counts shown in blue

6.2.6 Collagen Staining & Quantitative Analysis

6.2.6.1 Masson's Trichrome

Tissue sections stained with Masson's trichrome were imaged to observe the collagen deposition within the implantation site. Briefly, sections were immersed in Bouin's solution at 56°C for 15 minutes, with subsequent washing steps. Sections were then stained with Weigert's Iron Hematoxylin Working Solution for 5 minutes and lastly immersed in Trichrome AB solution

(Sigma, St. Louis, MO) for 5 minutes. All analysis of collagen area surrounding mesh fibers was based on 5 to 7 single mesh fibers per sample imaged at 20X objective on Nikon Eclipse 50i (Nikon, Tokyo, Japan). Fiji image processing software (National Institutes of Health, Bethesda, MD) provided a quantitative assessment of the fibrous capsule thickness surrounding the mesh fibers.

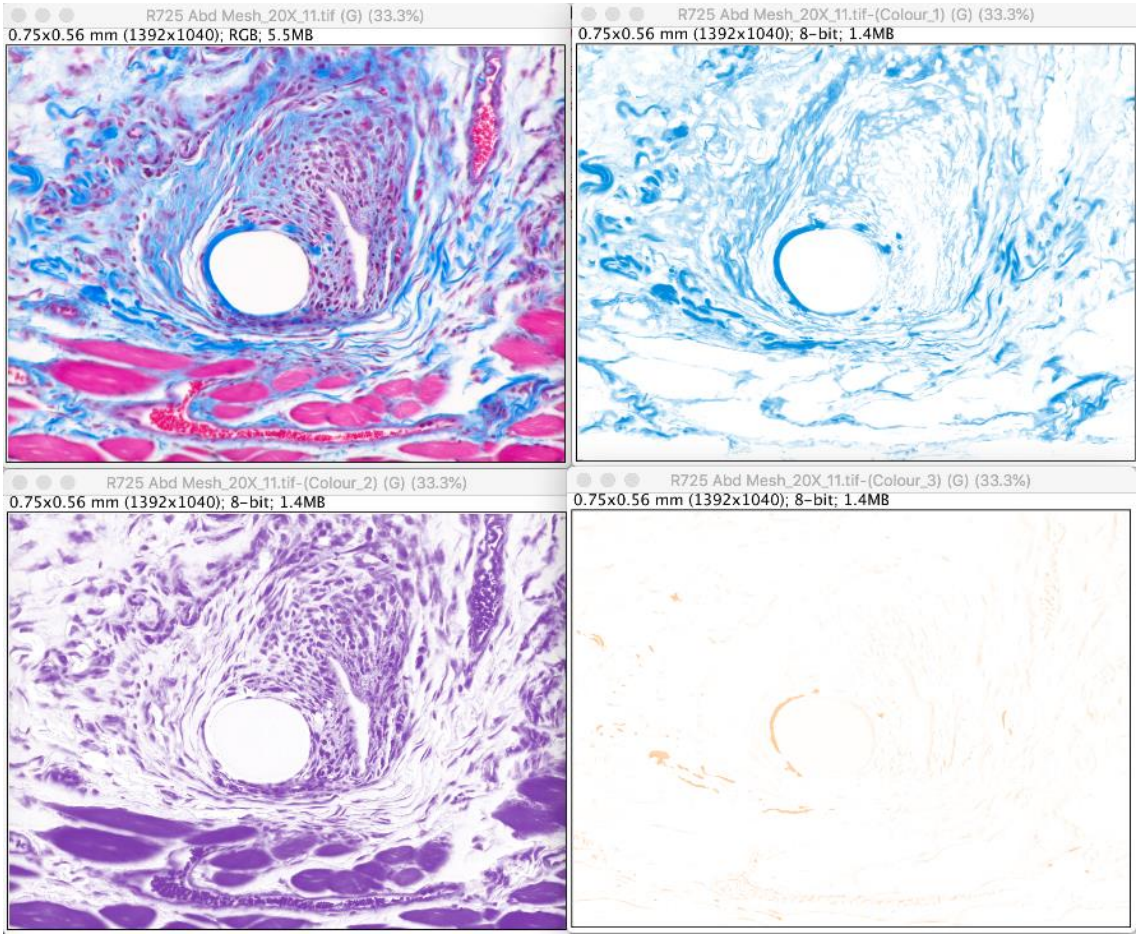

Figure 10: Example of color deconvolution algorithm for quantification of fibrous collagen capsule thickness distinguishable in blue channel. Images shown are 20X magnification.

6.2.6.2 Picrosirius Red

Sections were immersed in Weigert's Hematoxylin for 8 minutes, followed by washing steps and incubation in Picrosirius Red for 1 hour. Picrosirius red staining of the mesh and surrounding tissue can demonstrate the size and maturity of the surrounding collagen fibers inside the fibrous capsule surrounding the implanted mesh. A custom algorithm in Matlab (MathWorks, Natick, MA) was used to quantify the fibers based on thickness and type of collagen, through polarized light in red (thickest fibers), orange, yellow and green (thinnest fibers). Analysis was also based on imaging 5 to 7 single mesh fibers per sample taken at 20X field on TE-2000-E inverted Nikon through polarized light (Nikon, Tokyo, Japan).

6.2.7 Macrophage Immunohistochemistry (Peroxidase)

Sections were deparaffinized and rehydrated in a graded series of alcohols followed by antigen retrieval in citric acid buffer (pH 6.0) for 20 minutes at 95°C. Sections were then incubated in 3% hydrogen peroxide in methanol for 30 minutes at RT to block endogenous peroxidases. Tissue sections were blocked in a blocking solution of 5% Donkey Serum, 2 % Bovine Serum Albumin, 0.1% Tween-20, 0.1% Triton-X-100 for 2 hours at RT in a humidity chamber. Slides were immunolabeled using either monoclonal mouse anti-rabbit RAM11 (1:200) (Dako North America, Inc., Carpinteria, CA), a pan-macrophage marker, overnight at 4°C. After PBS washes, sections were incubated in a secondary biotinylated anti-mouse IgG (1:200) (Vector, Burlingame, CA) for 30 minutes at RT followed by incubation in Vectastain Elite Avidin/Biotin Complex (ABC) Reagent (Vector, Burlingame, CA) for 30 minutes at RT. Tissue section were then incubated with DAB (3,3'-diaminobenzidine) HRP substrate until dark brown reaction was visible.

Vector Hematoxylin QS was used to counterstain the nuclei followed by a dehydrated series of alcohols and mounting coverslips for imaging. Images of 5 to 7 single mesh fibers per sample were taken at 40X objective for RAM11+ on Nikon Eclipse 50i (Nikon, Tokyo, Japan) and using Fiji image processing software (National Institutes of Health, Bethesda, MD).

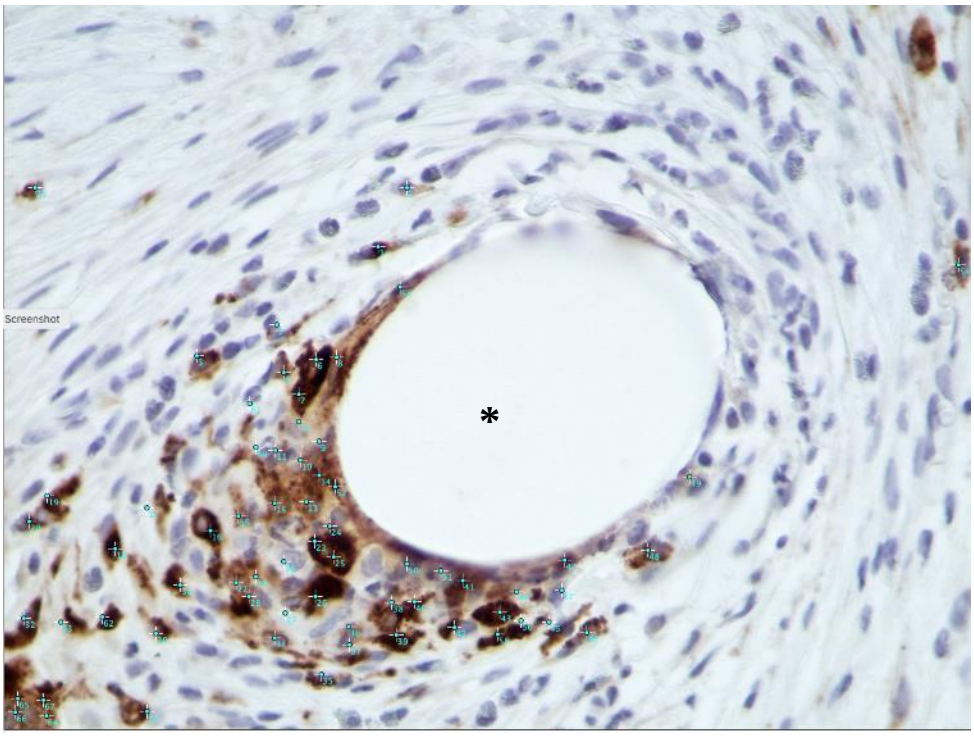

Figure 11: Representative image of mesh fiber shown at 40X objective (shown with *) and RAM11 immunolabeling followed by the utilization of image processing software for RAM11+ counts shown in blue.

6.2.8 CD31 Immunohistochemistry & Vessel Analysis

Sections were deparaffinized and rehydrated in a graded series of alcohols followed by antigen retrieval in citric acid buffer (pH 6.0) for 20 minutes at 95°C. Sections were then incubated in 3% hydrogen peroxide in methanol for 30 minutes at RT to block endogenous peroxidases.

Tissue sections were blocked in a blocking solution of 5% Donkey Serum, 2 % Bovine Serum Albumin, 0.1% Tween-20, 0.1% Triton-X-100 for 2 hours at RT in a humidity chamber. Slides were immunolabeled using monoclonal mouse anti-rabbit CD31 (1:50) (Thermo Fisher Scientific, Waltham, MA), an indicator for angiogenesis via endothelial cells overnight at 4°C. After PBS washes, sections were incubated in a secondary biotinylated anti-mouse IgG (1:200) (Vector, Burlingame, CA) for 30 minutes at RT followed by incubation in Vectastain Elite Avidin/Biotin Complex (ABC) Reagent (Vector, Burlingame, CA) for 30 minutes at RT. Tissue section were then incubated with DAB (3,3'-diaminobenzidine) HRP substrate until dark brown reaction was visible. Vector Hematoxylin QS was used to counterstain the nuclei followed by a dehydrated series of alcohols and mounting coverslips for imaging. Images of 5 to 7 single mesh fibers per sample were taken at 40X objective for CD31+ immunolabeling on Nikon Eclipse 50i (Nikon, Tokyo, Japan).

Blood vessels were identified as positively immunolabeled endothelial cells morphologically representing a lumen and vessel counts were measured based on an adapted Weidner's method [78]. Each image was overlaid with a 19x14 grid (650 um^2 with 266 total points) in Fiji image processing software (National Institutes of Health, Bethesda, MD) (Figure 12). The intersection of the superimposed grid points with a blood vessel was counted and allowed to take vessel size into consideration into the final result. Using this count and the total tissue area measured as the area of the 20X field subtracted by the area of the mesh fiber, a vessels/area value was calculated for each image. The mean and standard error of the mean was respectively calculated for each sample.

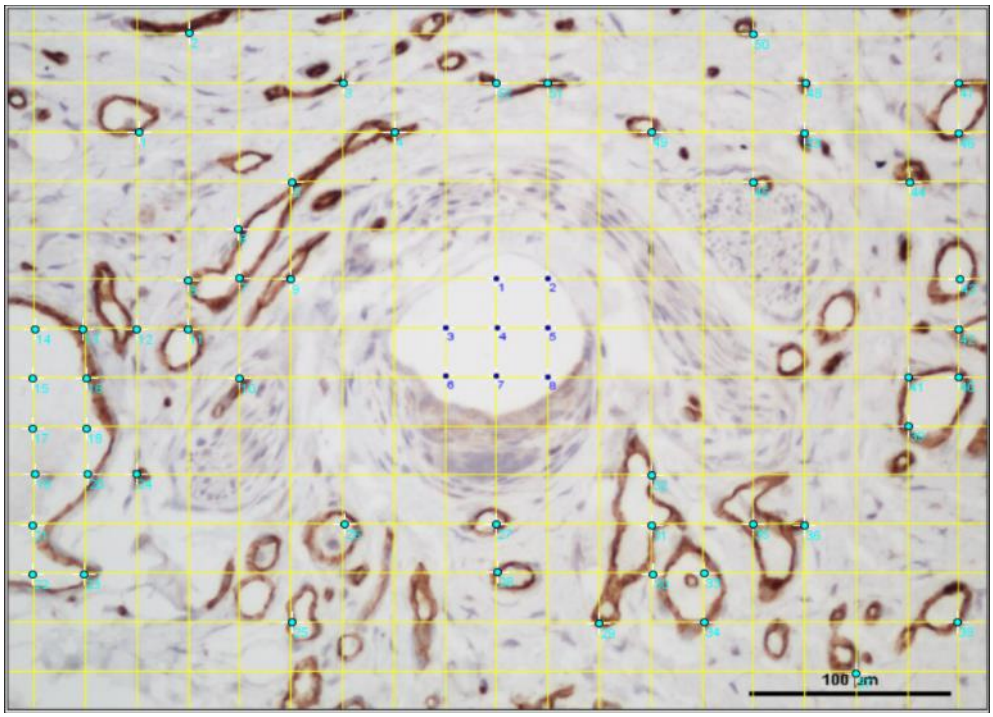

Figure 12: Example of a mesh fiber labeled with CD31 and utilizing Fiji image processing software to display a counted image shown with grid overlay

6.2.9 Verhoeff's Van Gieson (Elastin)

Vaginal tissue sections were stained with Verhoeff's van Gieson Elastic Stain kit (Sigma Aldrich, St. Louis, MO) to observe the appearance of elastic fibers throughout vaginal tissue. Sections were submerged in a Working Elastic Stain Solution for 10 minutes, with subsequent rinsing, followed by differentiating steps in Ferric Chloride solution for 1 minute. Sections were immersed in a Van Gieson counterstain for 2 minutes. Representative images per sample were taken at 20X and 40X field to observe the presence and type of fragmentation of elastic fibers throughout tissues on Nikon Eclipse 50i (Nikon, Tokyo Japan).

6.2.10 Biochemical Components (MMP Activity, Elastin, Collagen, sGAG)

6.2.10.1 Protein Extractions

All tissue samples were homogenized in a High Salt Buffer (pH 7.5, 50 mM Tris base, 150 mM NaCl, 5 M CaCl2, 1% Triton-X-100, 0.01 % Halt protease inhibitor cocktail, Pierce Biotechnology, Rockford, IL). Protein concentrations were quantified using the BCA Protein Assay Kit (Pierce Biotechnology, Rockford, IL) following the manufacturer's instructions.

6.2.10.2 MMP Activity Assay

MMP assay was adapted from the EnzChek Gelatinase/Collagenase protocol (Molecular Probes, Inc., Eugene, OR). 10 µg of protein for each sample was used. Samples were incubated with 1X Reaction buffer (diluted from 10X 0.5M Tris-HCl, 1.5 M NaCl, 50 mM $CaCl_2$, 2 mM sodium azide, pH 7.6) followed by addition of DQ gelatin from porcine skin (100 µg/mL) at room temperature. The fluorescence intensity was read at an excitation of 495 nm and an emission at 515 nm after 1 hour of incubation and 16 hours of incubation. MMP values are calculated using Type IV collagenase/gelatinase standards where one unit of gelatinase A is defined as the amount that can hydrolyze 1 mg of type IV collagen within one hour at 37C, pH 7.5. The 16-hour incubation time point was optimized for use due to the increased sensitivity in measurements.

6.2.10.3 Ninhydrin Assay (Insoluble Elastin Quantification)

Vaginal control and vaginal mesh protein extracts were hydrolyzed in 0.1 M NaOH at 98°C for 1 hour. This was then followed by centrifugation and washing steps that separated the insoluble elastin. Samples were incubated in 6N HCl at 110°C for 24 hours followed by a 2-hour cycle in a speed vacuum until samples were completely dry. In order to run the Ninhydrin assay, samples

were incubated with a working reagent consisting of stannous chloride and Ninhydrin reagent for 1 hour at 56°C in a water bath. The optical density was determined at a wavelength of 570 nm. Elastin content was quantified through the calculations from a known standard curve.

6.2.10.4 Hydroxyproline Assay (Collagen Quantification)

10 mg of each frozen sample was digested in a papain solution (0.01 M L-cysteine (Sigma, St. Louis, MO), 0.125 mg/mL Papain Type III from papaya latex (Sigma, St. Louis, MO), Phosphate Buffer (0.1 M Na_2HPO_4, 0.01 M Na_2EDTA, pH 6.5) at 60°C in a water bath for 16 hours. Samples were further hydrolyzed in 2N NaOH at 100°C on a heating block for 12 hours. This was followed by the addition of 5N HCl, 0.01 M $CuSO_4$, 2.5 N NaOH, and 6% H_2O_2. Samples were then placed on a heat block at 80°C for 5 minutes and cooled. 3N H2SO4 was added to each sample as well as 5% p-dimethylaminobenzyladehyde in n-propanol followed by incubation at 70°C on a heat block for 15 minutes. The absorbance was read at 540 nm. Collagen content was quantified with the knowledge that hydroxyproline is estimated to consist of 13 – 14% of total collagen [79, 80].

6.2.10.5 Glycosaminoglycan Assay (GAG Quantification)

10 mg of each frozen sample was digested in a papain solution (0.01 M L-cysteine (Sigma, St. Louis, MO), 0.125 mg/mL Papain Type III from papaya latex (Sigma, St. Louis, MO), Phosphate Buffer (0.1 M Na_2HPO_4, 0.01 M Na_2EDTA, pH 6.5) at 60°C in a water bath for 16 hours. Samples and a Chondroitin-6-sulfate from shark cartilage (Sigma, St. Louis, MO) serially diluted standard were incubated with a 1,9-Dimethylmethylene Blue dye and the optical density was read at a wavelength of 525 nm.

6.2.11 Ball Burst Mechanical Testing

Vaginal mesh samples preserved in saline were used for ball burst testing to determine structural properties of the vaginal tissue post-implantation. Polypropylene mesh (n = 5) was tested alone to allow for comparison of mesh properties and for later calculations on determining tissue contributions. Mesh was placed between two metal clamps that was screwed into the apparatus setup on an Instron TM 4502 (Instron, Norwood, MA) (Figure 13). At the top was a stainless-steel ball rod designed to push through a hole in the clamps. The ball rod diameter measured to be 9.52 mm with a surface area of 216 mm^2 as scaled previously using the American Society of Testing and Materials (ASTM) standards [81]. This ball was attached to a load cell, which can produce up to 5 kN of load.

The ball rod was centered and lowered against each clamped sample at a constant rate of 10 mm/min to a 0.5 N pre-load. Then, each sample was loaded to failure at a rate of 10 mm/min.

The failure load (N) and elongation (mm) data are then utilized to create load-elongation curves to determine the structural properties. Stiffness (N/mm) was calculated as the maximum slope of the over 20% of the failure elongation. Energy absorbed was calculated as the area underneath the curve until failure.

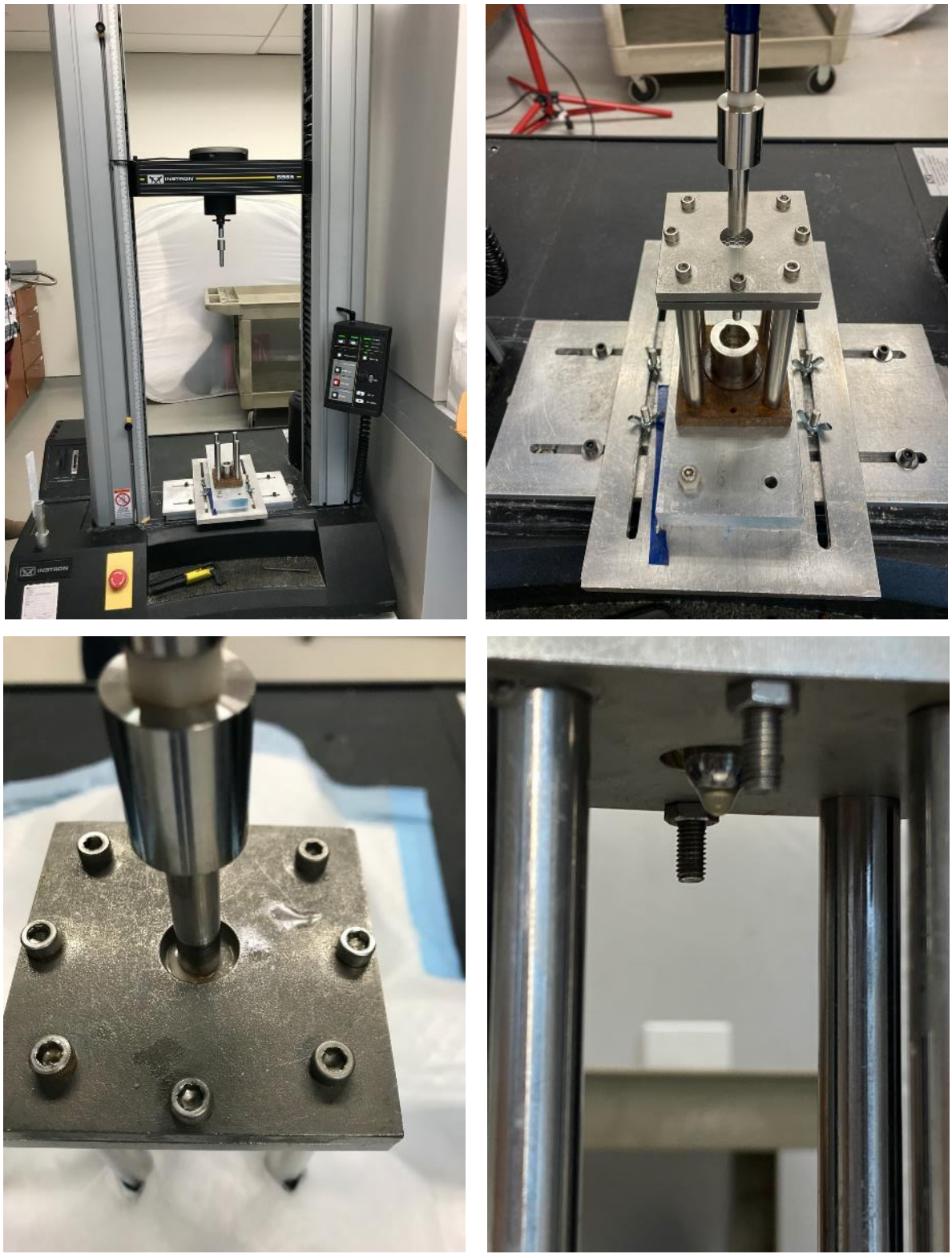

Figure 13: Instron Set up for Ball Burst Testing

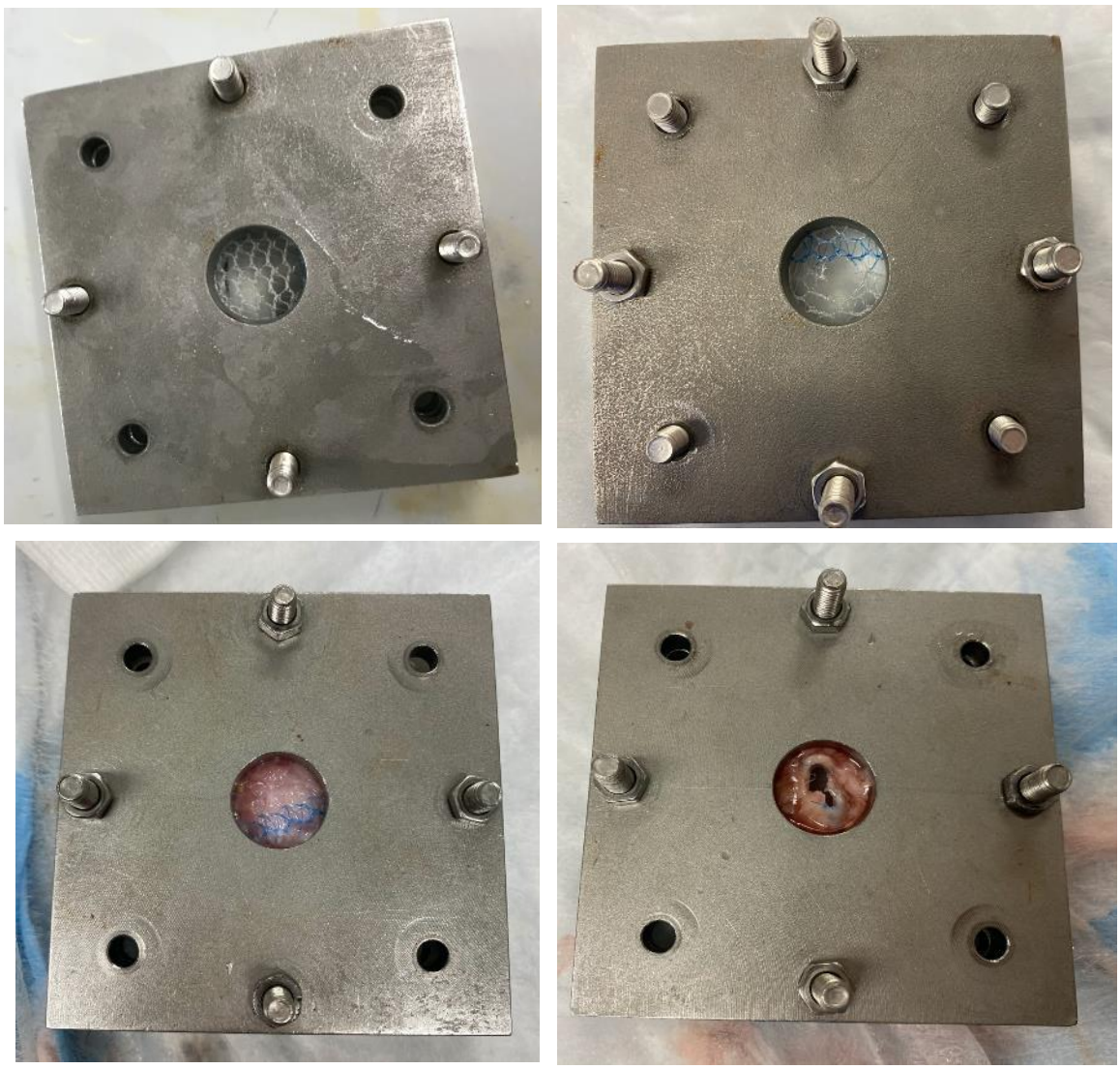

Figure 14: Example of mesh and mesh-tissue complexes before (shown left) and after (shown right) mechanical testing

6.2.12 Statistical Analysis

Based on previous studies, a sample size of 5 animals were deemed sufficient for determining statistical differences between groups in the analysis [73]. Descriptive statistical

analysis was done to determine normality using Kolmogorov-Smirnov and Shapiro-Wilk tests with alpha = 0.05. Immunolabeling data for each anatomical location at both acute and chronic time points were assessed using one-way analysis of variance with Tukey post hoc test with $p<0.05$ used to determine significance. Independent samples t-tests were used to determine differences based solely on anatomical location.

6.3 Results & Discussions

6.3.1 Surgical Outcomes

A total of 12 nulliparous New Zealand White Rabbits were used in this study. Rabbits were randomly assigned to be split into two groups (n = 7 for 14 days and n = 5 for 90 days). One animal in the study experienced an abdominal hernia where a portion of the intestinal tract pushed through the abdominal muscle wall. However, the hernia was repaired and the overall animal health was not impacted. Two other animals in the study experienced dehiscence of the skin, but those were also immediately repaired and were far from implant location.

At the time of necropsy, all rabbits were observed for presence of adhesions or any internal deviations. At both 14 and 90 days, there was noticeable scar tissue surrounding the subcutaneous implant location that is characteristic of a normal response to a material. Upon opening inside the peritoneal cavity, there were adhesions formed by the peritoneal mesothelium between the internal organs, indicative of an active response to the mesh and the surgery itself [82]. The 14-day implants were easier to dissect away from the surrounding tissues than the 90-day implants. This aligns with

the expected differences upon comparing the acute and chronic responses, where stronger adhesions indicate increased time for the fibrinous gel matrix to develop [82].

6.3.2 Histological Analysis Tissue Morphology

Post-implantation evaluation showed all animals elicited an immune response at 14 days which persisted at 90 days. This is consistent with the host response to mesh seen in other animal models observing multiple time points[44, 50, 62, 75, 77]. Histological analysis revealed a mononuclear cell population surrounding mesh fibers followed by the presence of a few foreign body giant cells in some cases (Figure 16). Interestingly, there was an increased presence of eosinophils (Figure 15) found distributed throughout both the subcutaneous and vaginal tissues. Eosinophils are known to be present in the process of wound healing and allergic inflammation, however there is little known on the significance of eosinophil presence long-term. Nevertheless, researchers have previously found a relationship between eosinophils and the metabolism of collagen [83]. Eosinophils can be identified by the purple nucleus and perfectly round cytoplasmic granule appearance. They are 12 – 16 μm in diameter, thus slightly larger than a heterophil[83, 84].

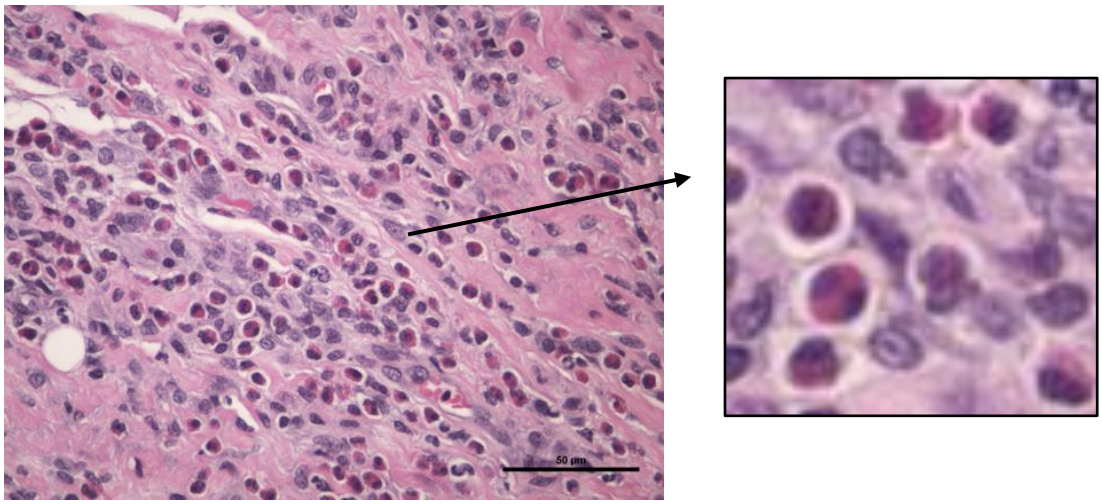

Figure 15: Distribution of eosinophils observed throughout the tissues in mesh host response. Scale bar shown as 50 µm.

Overall, a foreign body response to mesh indicative of inflammation both at acute and chronic time points was observed both in the subcutaneous and vaginal implants, but heightened for the vaginal implants as observed through quantification and analyses. This corresponds to previous work in discovering tissue degradation and chronic inflammation with the implantation of mesh[33, 34, 50, 69]. The distinct biological processes of the cell response, collagen deposition, immune cell presence, vascularity, elastic fiber presence, and other factors will be discussed in detail in further sections.

6.3.3 Cellularity Quantitative Analysis

Total cell response showed differences based on anatomical location at 90 days with subcutaneous implantation showing a 22 % increase compared to vaginal implants ($p = 0.0030$) (Figure 17). However, vaginal implants showed 46 % less in cellularity from 14 days of

implantation to 90 days of implantation ($p = 0.0043$) (Figure 17). This indicates that the subcutaneous implants encouraged a higher cellular infiltration count when compared to the vaginal implants. While cellular infiltration is the beginning of understanding the host response, further analysis on the characteristics of these cells provides more information on how the response has developed.

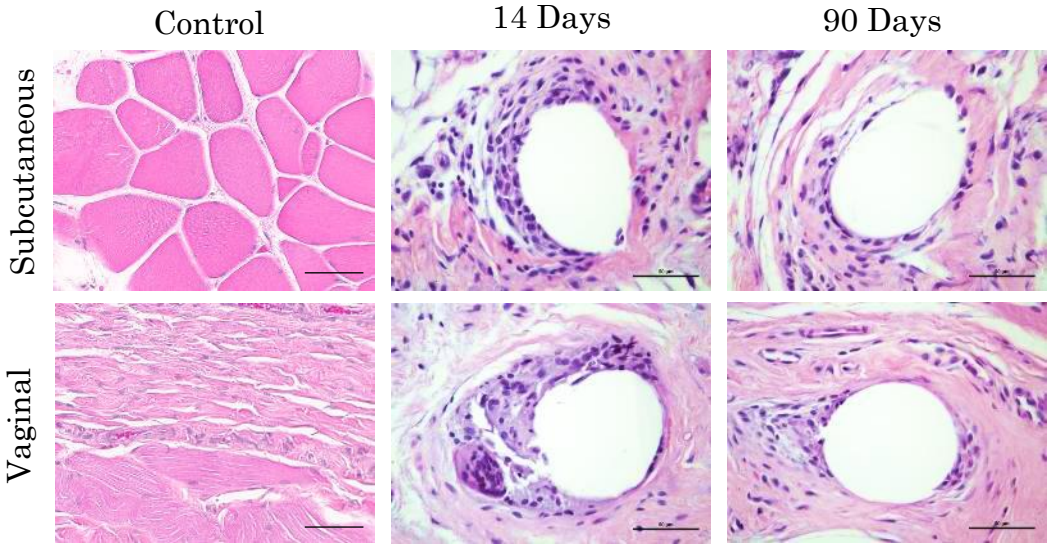

Figure 16: H&E Analysis. Representative hematoxylin and eosin stained images of single mesh fibers implanted both subcutaneously and vaginally at 14 and 90 days. Control tissues refer to native abdominal muscle and native vaginal tissue. All scale bars indicate

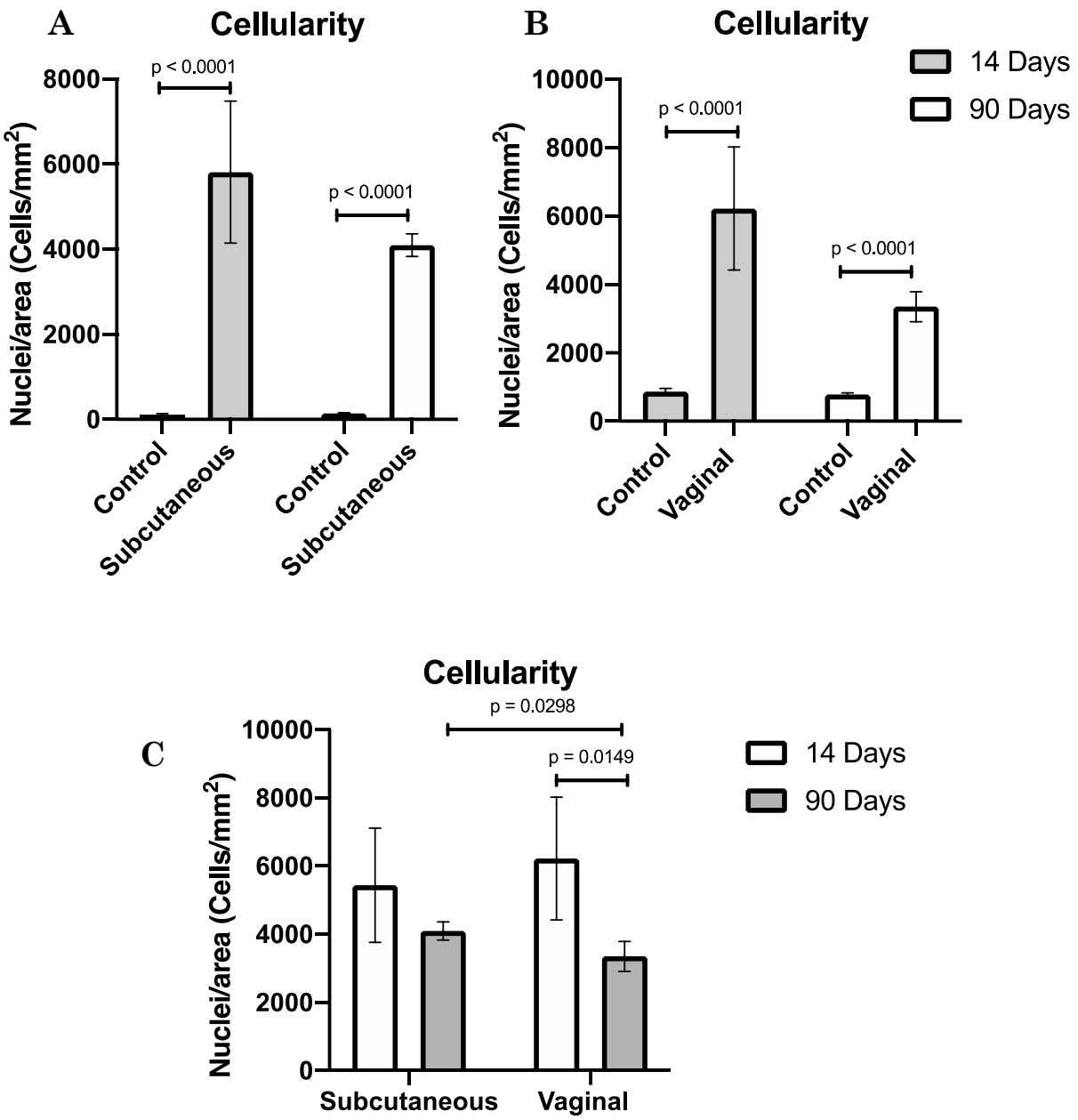

Figure 17: Cellularity analysis of subcutaneous and vaginal tissues at both 14- and 90-days post-implantation of mesh [C]. Comparisons are made to control tissues consisting of native vaginal tissue [A] and native abdominal muscle tissue [B]. Data is represented

6.3.4 Collagen Quantitative Analysis

Both subcutaneous and vaginal implants formed fibrotic capsules surrounding mesh fibers, however, both showed significant differences in collagen formation between 14- and 90-days indicative of scar tissue. At 14-days post-implantation, loose collagen fibers were observed to be dispersed in the fibrous connective tissue (Figure 18) considered to be typical during the early host response. At 90-days post-implantation, however, both implants depicted denser collagen fibers surrounding the implants (Figure 19) with the presence of looser fibers farther distances away from mesh fibers. Subcutaneous implants showed a 1.6- fold increase in % collagen from 14 days to the 90-day mesh implants ($p = 0.0171$). Vaginal implants increased 1.91-fold in % collagen area at 90 days as compared to the early response ($p = 0.0028$). At both locations, marked thicker collagen fibers were observed surrounding mesh fibers by 90 days as compared to 14 days. Picrosirius staining depicted changes in collagen fiber thickness surrounding mesh implants, with both locations increasing in thicker collagen fibers ($p < 0.0001$) by 90 days (Figure 20). Overall, increased collagen deposition in vaginal explants further supports that the vaginal explants have a significantly higher inflammatory reaction overall. The increased collagen suggests processes of fibrotic development as time progresses, which is observed with the shifts in the two time points of implantation.

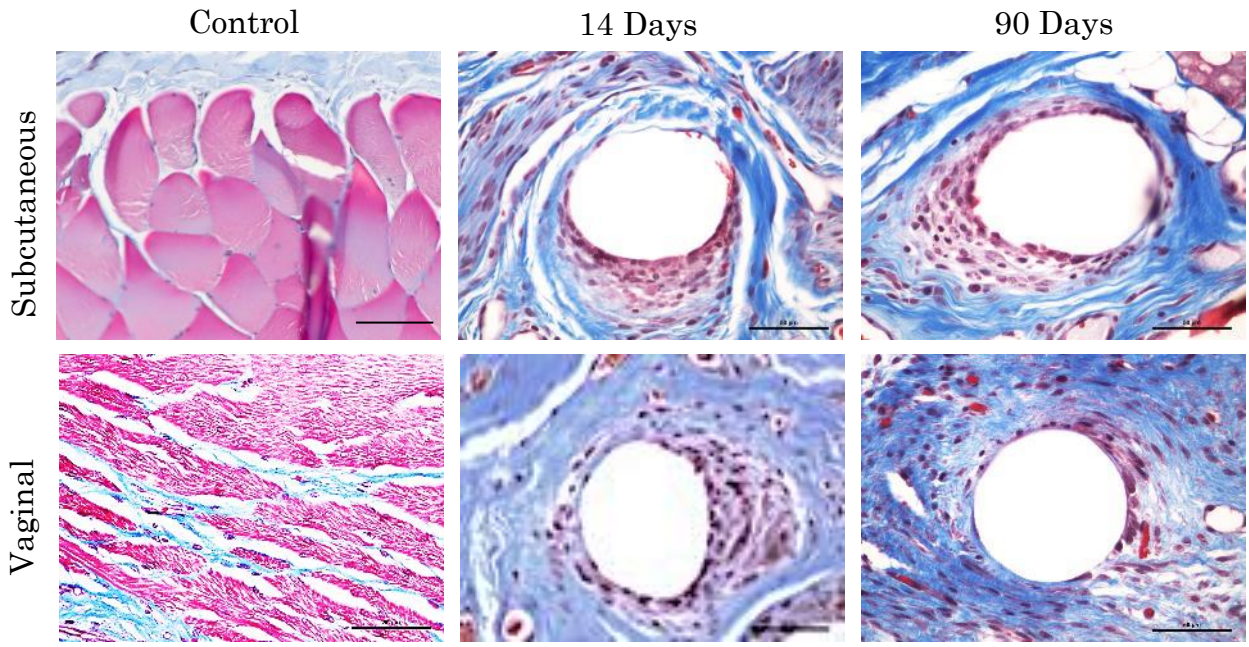

Figure 18: Representative Masson's Trichrome stained images of single mesh fibers implanted both subcutaneously and vaginally at 14 and 90 days compared to native vaginal tissues and native abdominal muscle controls. Collagen is depicted in blue; Muscle is shown

The results of this study presented an interesting trend with increased collagen deposition around vaginal explants, most significantly at 90 days post-implantation. Increased collagen deposition in vaginal explants further supports that the vaginal explants have a significantly higher inflammatory reaction overall. The increased collagen suggests processes of fibrotic development as time progresses, which is observed with the shifts in the two time points of implantation.

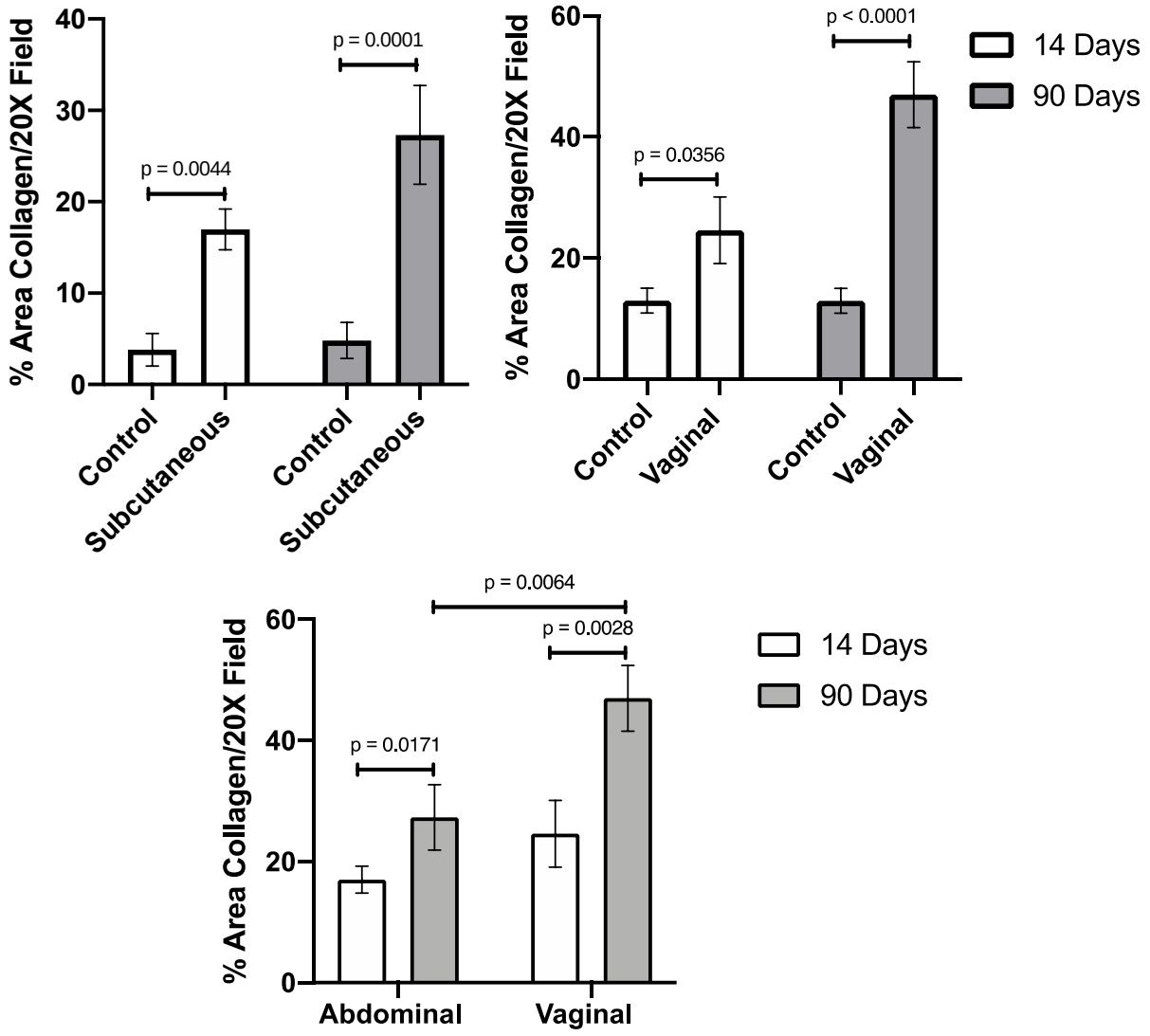

Figure 19: Trichrome analysis of subcutaneous and vaginal tissues at both 14- and 90-days post-implantation of mesh. Comparisons are made to control tissues consisting of native vaginal tissue and native abdominal muscle tissue. Data is represented as values ± SE

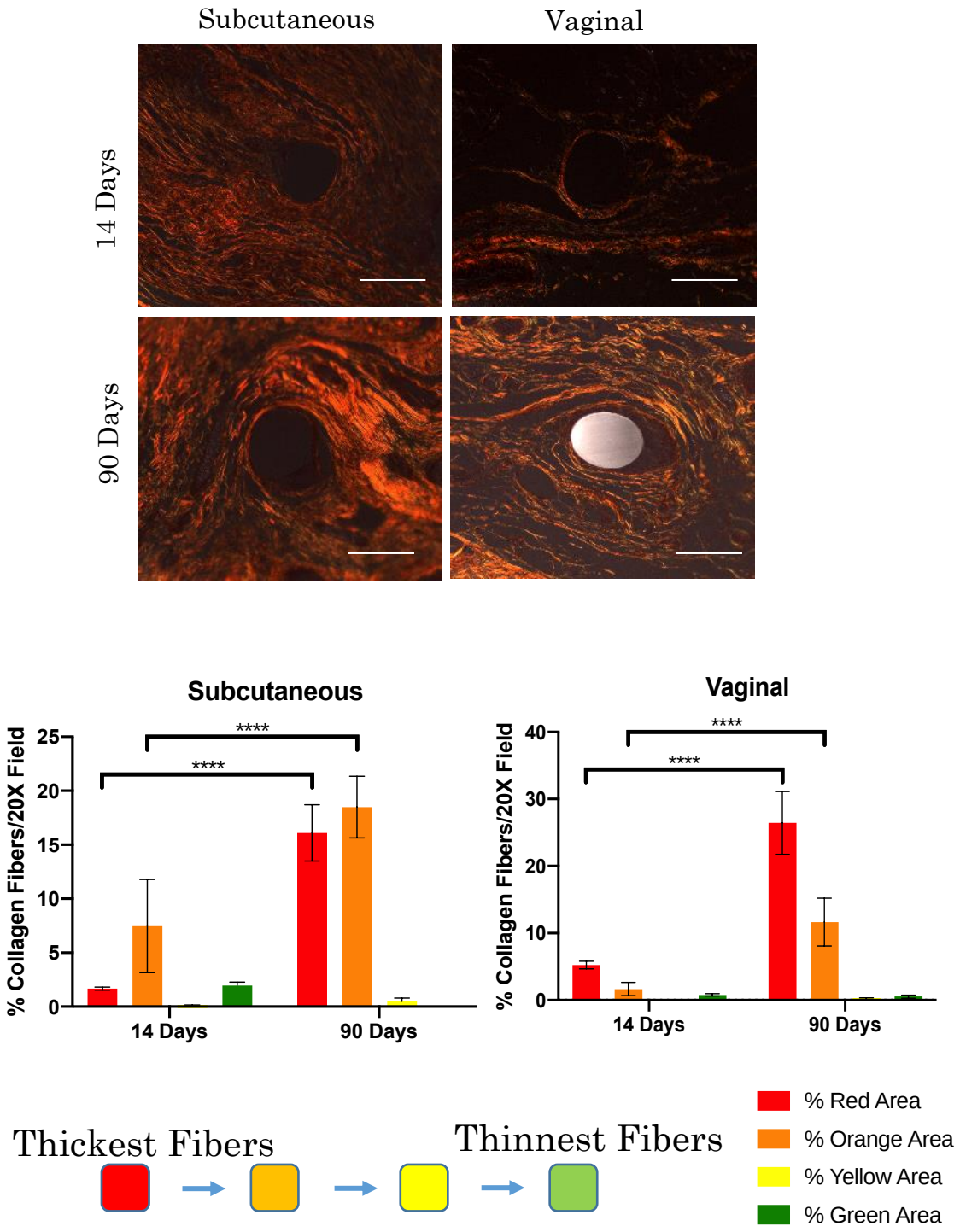

Figure 20: Picrosirius Red Analysis: Representative Picrosirius Red stained images of single mesh fibers implanted both subcutaneously and vaginally at 14 and 90 days shown under polarized light. All scale bars indicate 50 µm. Data shown as values ± SEM.

6.3.5 Elastin Qualitative Analysis

The appearance of elastic fibers changed drastically from the control tissue (native vagina) to tissue with mesh implanted. Histologically, native vaginal tissue depicts thick black continuous elastic fibers (Figure 21A & 21B). However, the changes in appearance at 14 days post-implantation of mesh are distinctive as the elastic fibers completely fragment or appear to remodel. There are noticeable differences in the context of the surrounding connective tissue alignment with these elastic fibers and mesh fibers. At 14 days post-implantation, single layers of fragmented elastic fibers (Figure 21C & 21D) were observed in the same area of tissue remodeling surround mesh fibers. Conversely, the vaginal implants at 90 days post-implantation had limited, if any elastin that could be found throughout the tissues (Figure 22).

A unique finding in this study was the appearance of elastic fibers at 14 days post-implantation in the vaginal explants. In the native vagina, elastin composes 13 % of the total organ, mostly in the muscularis along the vaginal wall [68, 85]. Elastin is a key structural component, responsible for the resilience and elasticity of tissues [86]. Little is known of elastic remodeling in the vagina compared to other organs in the body, however, it has previously been found that elastin metabolism is altered in the vagina in rodent models of prolapse and as opposed to other organs in the body is capable of remodeling over the reproductive lifespan [85]. A recent study demonstrated that polypropylene mesh negatively impacts rabbit vaginal morphology and function, specifically in the context of smooth muscle degradation[87]. Other studies have shown that degradation of the vaginal wall occurs as a result of a decreased mechanical load with the use of mesh, otherwise known as stress shielding [35, 79]. Verhoeff's van Gieson staining allows for demonstration in changes of elastic fibers, such as thinning and loss related to the atrophy of elastic tissue. The

findings at 90 days indicate that the elastin may have degraded completely or become so fragmented that it was not feasible to observe via histologic methods.

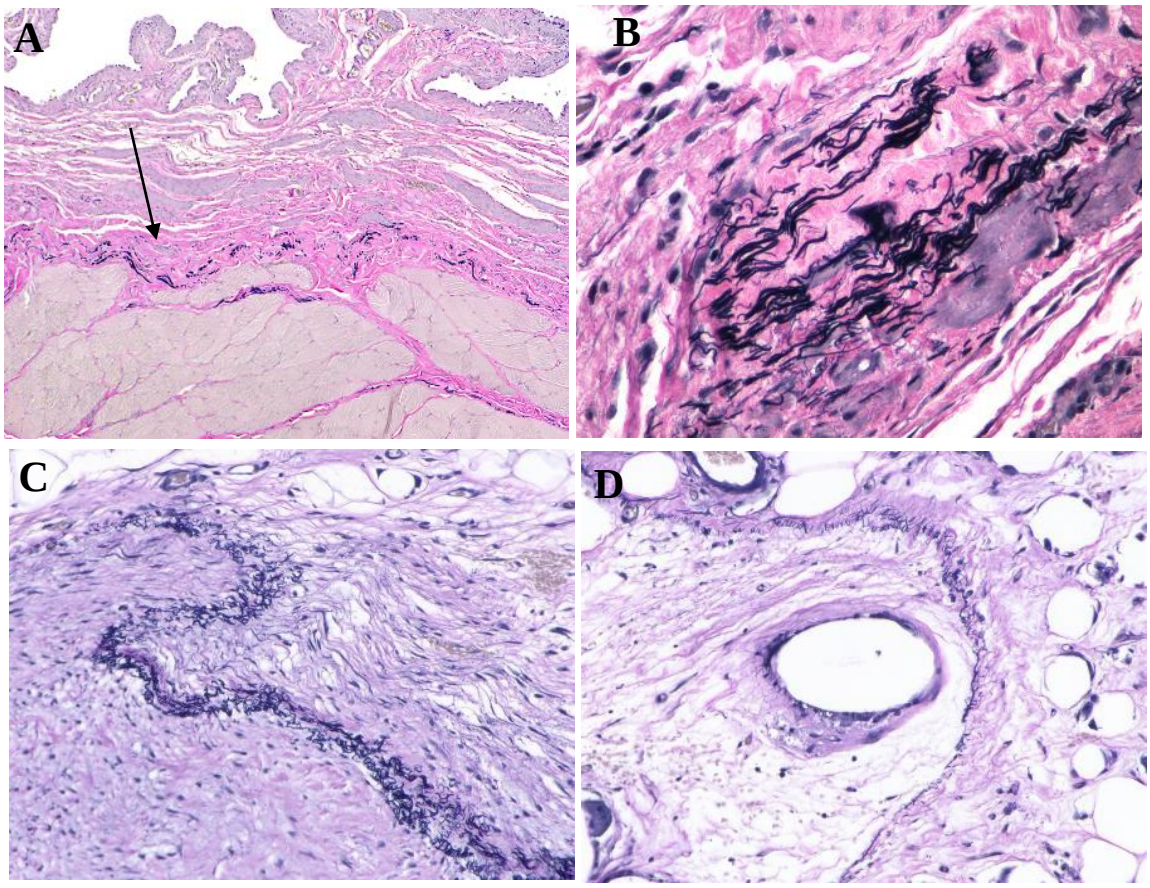

Figure 21: Elastin in the Native Vagina vs. Elastin implanted via Lumbar Colpopexy at 14 Days. A. Native vaginal tissue in a 10X field stained with Verhoeff's van Gieson. Arrow indicates elastic fibers in tissue. B. Representation of elastic fibers in a 40X field

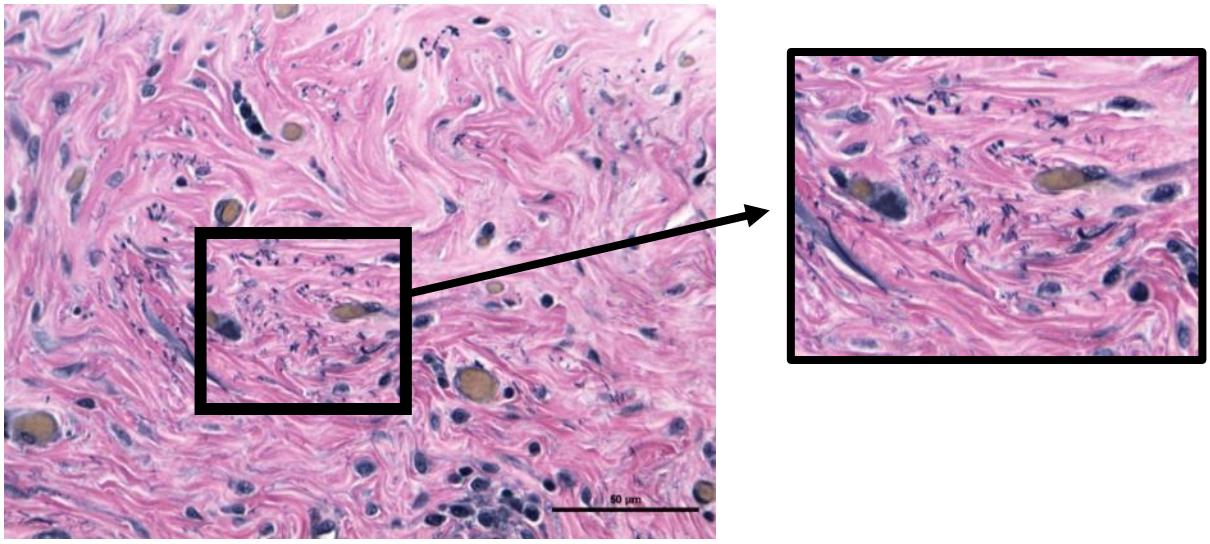

Figure 22: Representative image of vaginal tissue stained with Verhoeff's van Gieson at 90 Days depicting fragmented elastic fibers

6.3.6 Angiogenic Analysis

At 14 days post-implantation, both subcutaneous and vaginal explants histologically showed the presence of blood vessels surrounding individual mesh fibers (Figure 23). Utilizing an endothelial cell marker (monoclonal mouse anti-CD31) widely used to label cells lining blood vessels, the subcutaneous implants did not depict any significant differences in the number of vessels observed per area surrounding each fiber. However, the vaginal implants increased by almost two-fold in the number of vessels per area by 90 days of implantation from 14 days ($p = 0.0134$) (Figure 23). This is consistent with the immune response related to cases where the tissue is considered hypoxic and angiogenic factors are increased, thus the presence of blood vessels overall is found to be increased. However, the vaginal tissue is complex and there can be a variety

of factors related to the vaginal microenvironment, such as macrophage cues, that may have resulted in this increase in vascularity.

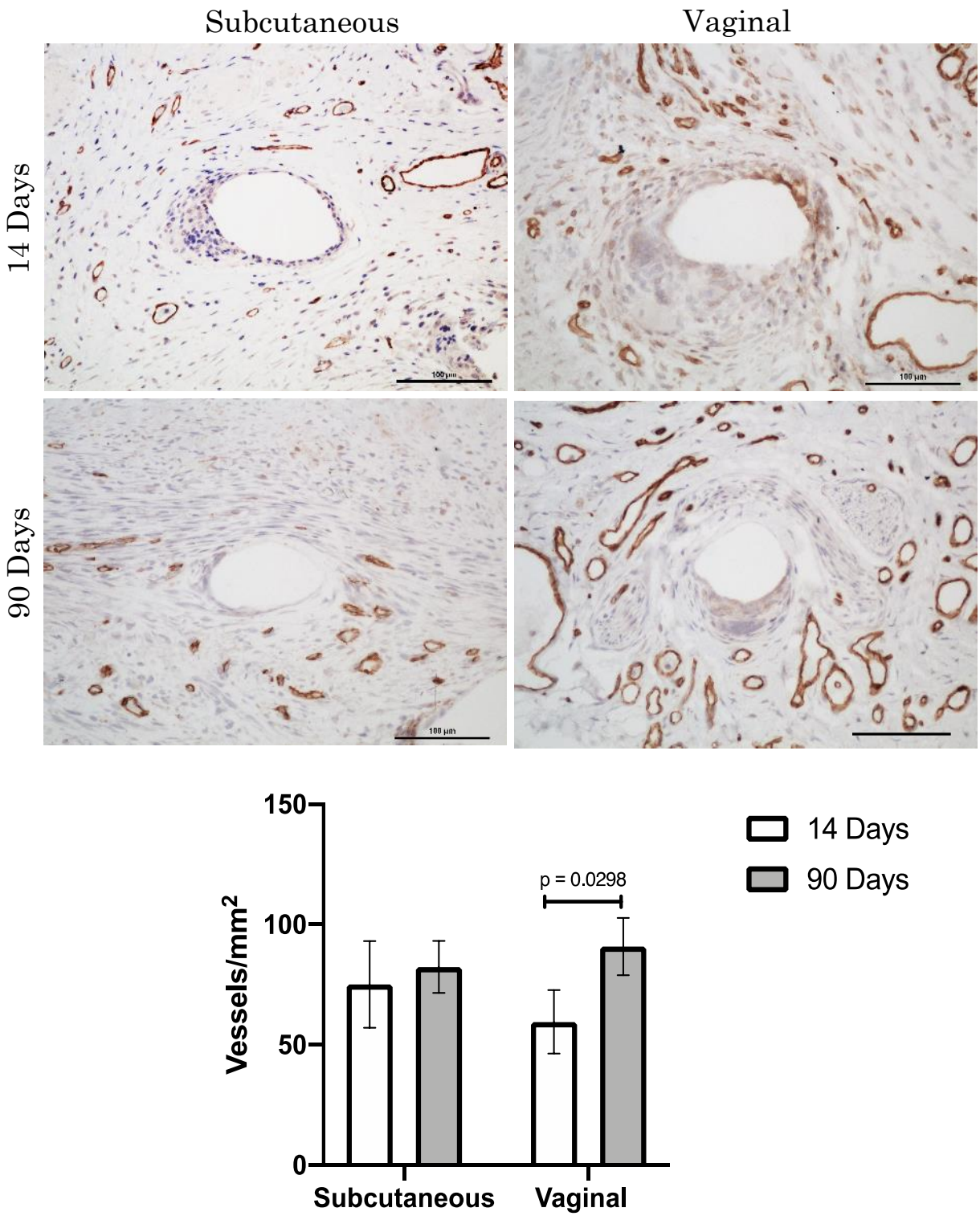

Figure 23: Representative images of CD31+ immunolabeling of mesh fibers both subcutaneous and vaginal at 14 and 90 days post-implantation. All scale bars are 100 µm. Data is shown as values ± SEM.

6.3.7 Macrophage Analysis

Vaginal implants elicited an overall increased host inflammatory response as compared to the subcutaneous implants (Figure 24). Interestingly, 37% of the total cell population was positive for macrophages at 14 days, with the macrophage response persisting at 90 days consisting of 53% of the total cell population ($p = 0.0057$). Comparatively, at 14 days post-implantation, 14% of the total cell population consisted of macrophages in the subcutaneous implants with a persistent response at 90 days comprising of 24 % of the total cell population ($p = 0.35$) (Figure 24).

It is especially interesting to consider the increased host macrophage response observed in vaginal implants as the total cellular response to mesh remained consistent across anatomical location. There was an initial increase at 14 days observed in both sites of implantation followed by a decrease at the later time point of 90 days. However, the macrophage presence was not proportional to the cellular density. This suggests that the increased macrophage presence in the vaginal mesh-tissue explants was due to an increased inflammatory response, where majority of the cell population were macrophages surrounding mesh fibers as opposed to an increased proportion due to a change in location of implantation. In fact, there was even a decrease in cellularity observed at 90 days in the vaginal implants as compared to the subcutaneous implants at 90 days.

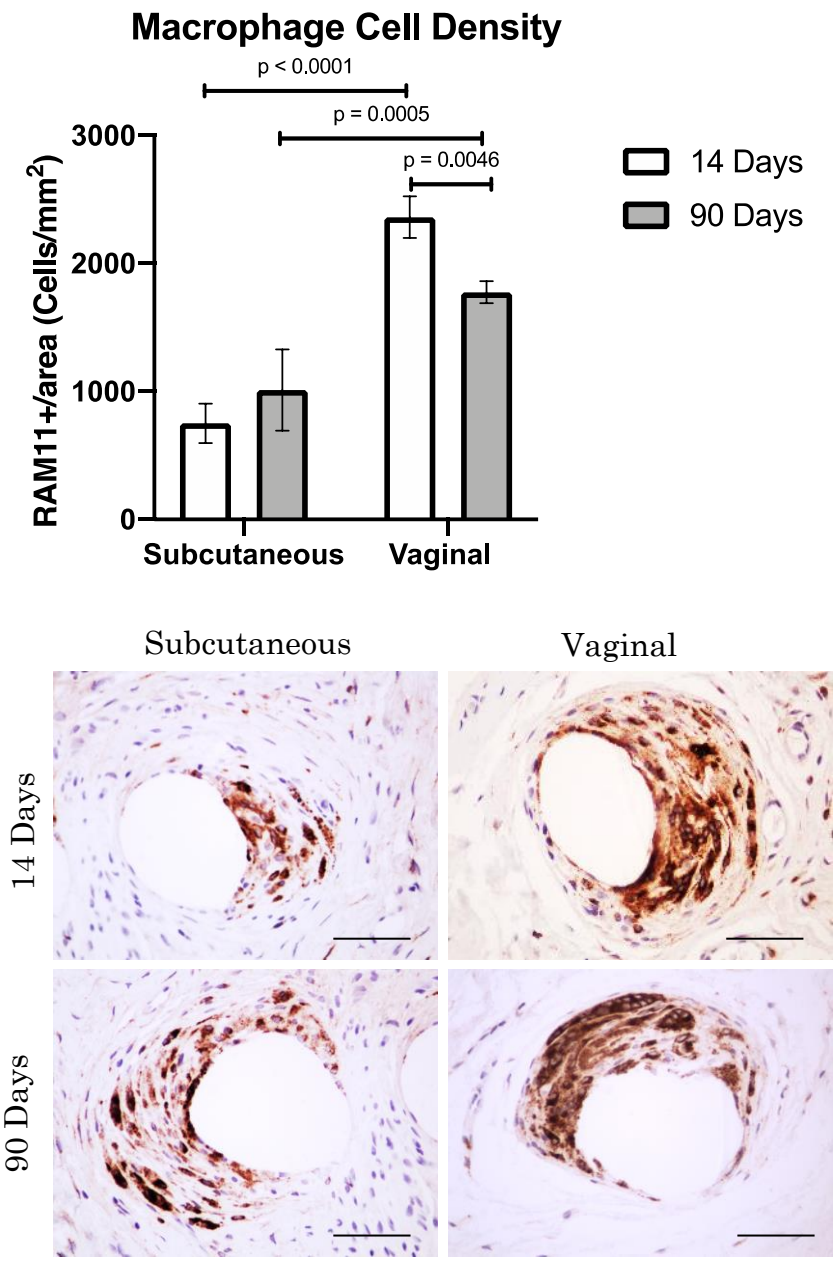

Figure 24: Macrophage Analysis: Representative images of RAM11+ immunolabeling of mesh fibers both subcutaneous and vaginal at 14- and 90-days post-implantation. All scale bars are 50 µm. Data is shown as values ± SEM.

Most interestingly, the vaginal mesh-tissue implants elicited an inflammatory response at 14 days post-implantation that persisted at 90 days as noted by the macrophage presence surrounding mesh fibers. By contrast, the subcutaneous tissue implants showed a decreased macrophage presence, although a mild reaction was observed. However, the trend of an initial acute foreign body response observed at 14 days post-implantation followed by a reduced, but persistent inflammatory response observed at 90 days post-implantation for all mesh-tissue implants is a consistent trend with the implantation of any synthetic material. This is similar to what is seen in other animal models implanted with mesh including mice implanted subcutaneously [50] and rhesus macaques implanted via sacrocolpopexy[33, 88].

6.3.8 Biochemical Components

In order to assess the matrix-metalloproteinase (MMP) levels in vaginal tissues, a gelatinase substrate degradation assay was performed to measure gelatinase activity. It is well known that MMPs are associated with tissue matrix degradation and has even been found to be upregulated in the vagina in women with prolapse [89]. Interestingly, we found no significant differences in MMP activity between the vaginal control (3.06 ± 1.41 units/mg protein) and vaginal implants at 14 days after implantation (3.67 ± 1.72 units/mg protein). However, there was a significant increase in activity at 90 days post-implantation (18.96 ± 5.60 units/mg protein, $p < 0.0001$). This indicates the MMP activity was upregulated at chronic points of implantation.

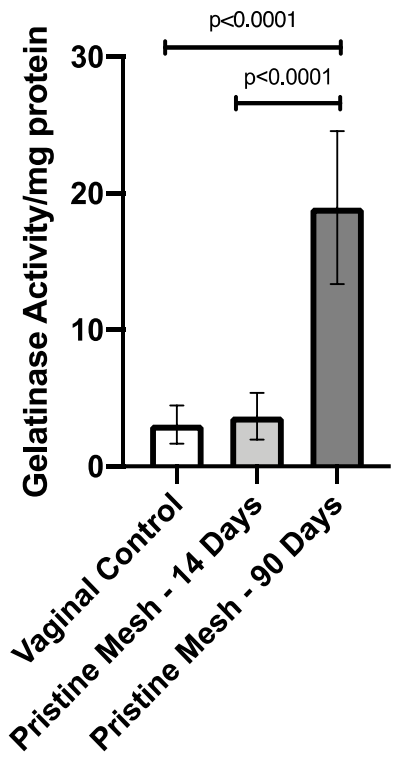

Figure 25: Gelatinase Activity comparing pristine mesh vaginal implants at 14 days and 90 days post implantation with native vaginal control tissues. Data shown as values ± SEM.

In order to further assess the elastin content in the vaginal tissues, a ninhydrin assay was performed using protein extracts. Interestingly, we found a high amount of elastin in the vaginal control samples (73.22 ± 7.07 elastin percentage (µg elastin/mg total protein)). However, after 14 days post-implantation, samples had significantly decreased amount of elastin (28.26 ± 11.36 elastin percentage (µg elastin/mg total protein), $p = 0.0019$) compared to the vaginal control samples. Additionally, after 90 days post-implantation, vaginal implants were not significantly different in elastin percentage than at 14 days but still significantly different than the vaginal control (25.35 ± 6.34 elastin percentage (µg elastin/mg total protein), $p = 0.0002$). This provides for an interesting case of characterizing changes in elastin observed histologically and now in protein biochemistry.

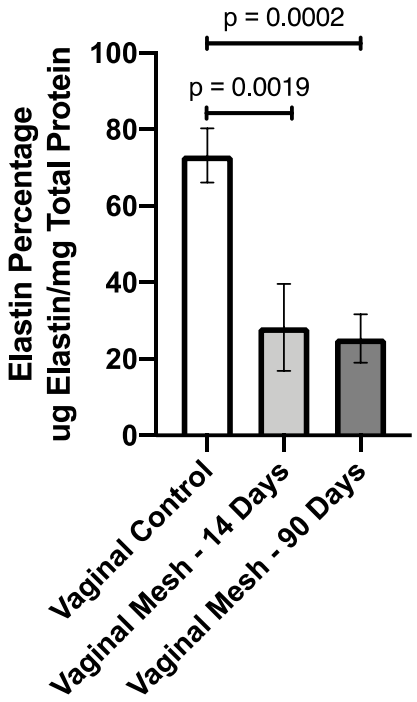

Figure 26: Elastin Content comparing pristine mesh vaginal implants at 14 days and 90 days post-implantation with native vaginal tissues. Data shown as values ± SEM.

In order to further quantify the hydroxyproline content found in the explanted tissues, a hydroxyproline assay was performed. While there was an overall increase in concentration for the vaginal samples compared to the subcutaneous samples, there were no significant differences found between groups that were found between the 14 day and 90-day times of implantation. Additionally, a glycosaminoglycan assay was performed, however, the concentrations were found to be relatively low and thus difficult to observe differences between groups.

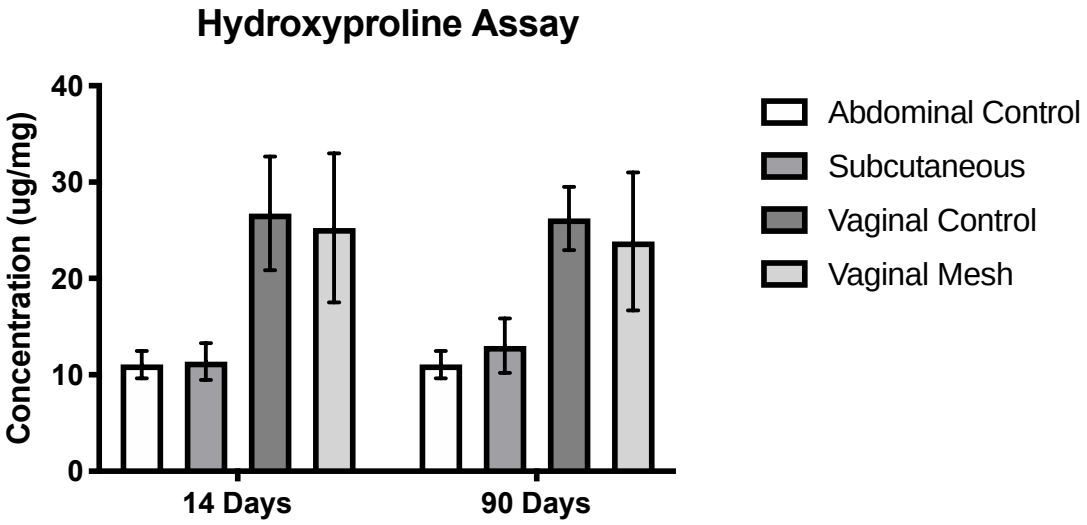

Figure 27: Hydroxyproline content comparing native abdominal muscle control and native vaginal control to pristine mesh implants both subcutaneously and vaginally at both 14 and 90 days

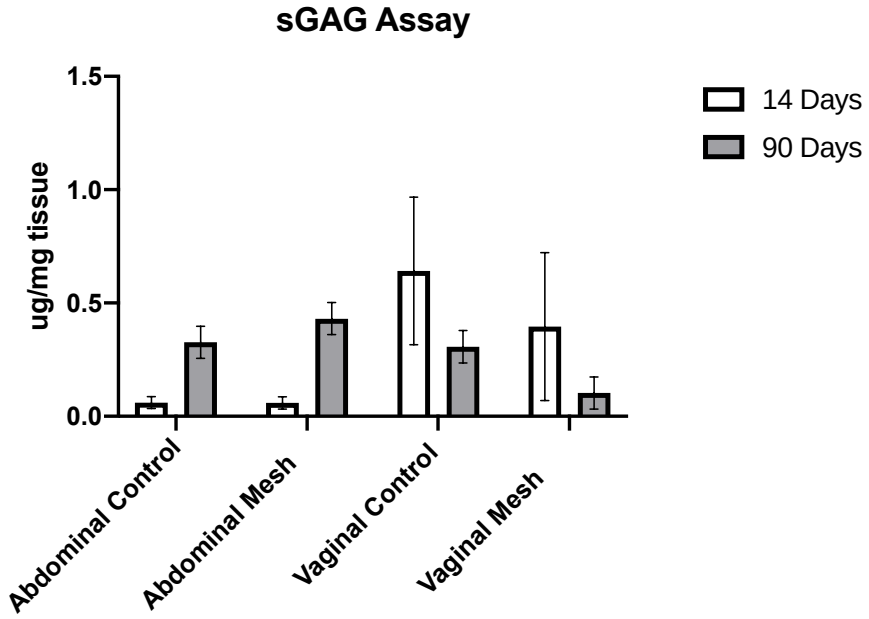

Figure 28: Glycosaminoglycan content comparing native abdominal muscle control and native vaginal control to pristine mesh implants both subcutaneously and vaginally at both 14 and 90 days

6.3.9 Ball Burst Mechanical Testing Outcomes

In order to estimate the individual vaginal mechanical properties, specifically related to structural integrity, we performed ball-burst mechanical tests on the mesh-tissue complexes both at 14- and 90-days post-implantation. This is then followed with the assumption that by calculating the stiffness of the mesh by itself, we can subtract that value from the determined stiffness of the complex to estimate the vaginal tissue stiffness. It has been previously shown that the innate structural properties of polypropylene mesh remain stable over time [81]. Thus, by determining the structural properties of the mesh and the structural properties of the mesh-tissue complexes will allow for us to determine the structural properties of the tissue by assuming that the stiffness of the mesh plus the stiffness of the tissue totals the stiffness of the mesh-tissue complex. There were no significant differences observed in the estimated vaginal tissue contribution calculated at 14 days post-implantation and 90 days post-implantation. However, in both cases, the estimated stiffness was very low as compared to what has been previously seen in other animals implanted with Gynemesh [90].

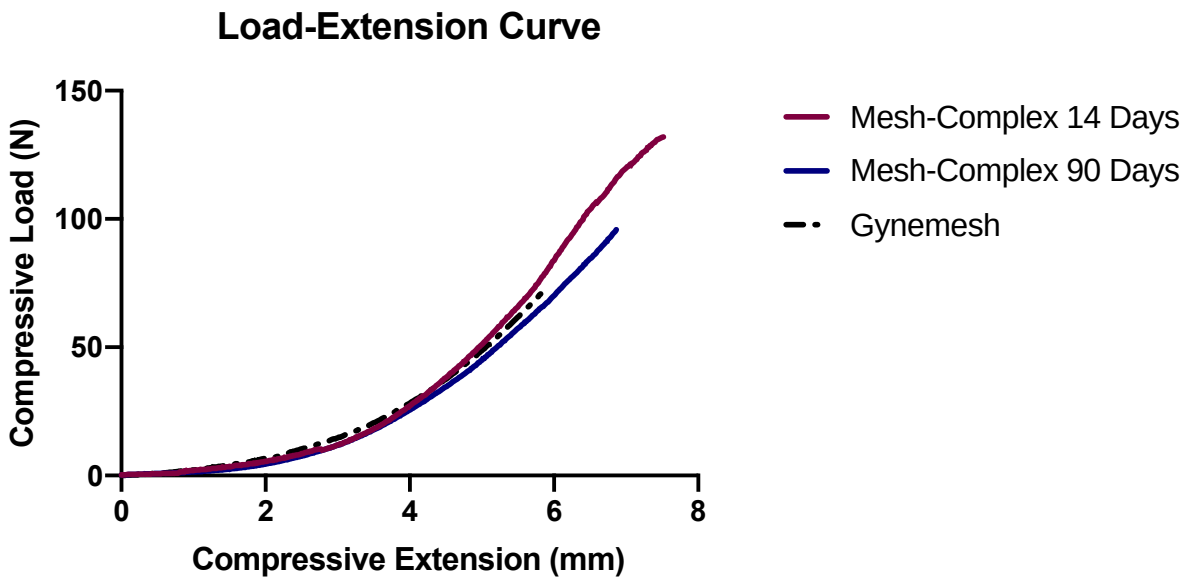

Figure 29: Representative Load-Extension curves from Ball-Burst tests of Gynemesh, Vaginal mesh-tissue complex at 14 days post-implantation, and Vaginal mesh-tissue complex at 90 days post-implantation

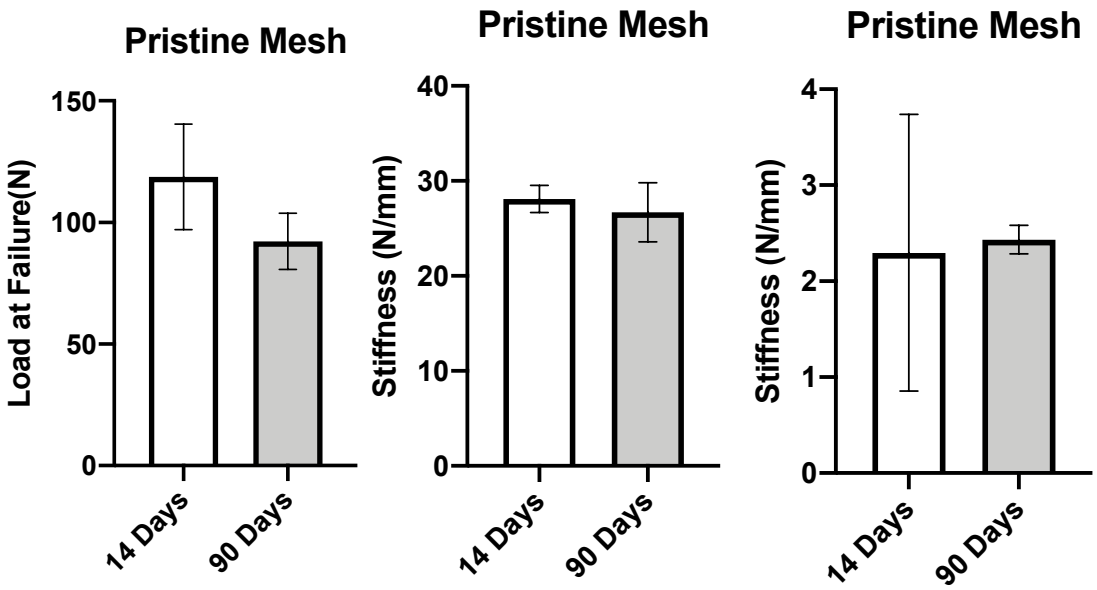

Figure 30: A. Load at Failure for pristine mesh implants at 14- and 90-days post-implantation B. Stiffness of mesh-tissue complex at 14- and 90-days post-implantation C. Estimated stiffness of vaginal contribution for pristine mesh implants at 14- and 90-days pos

Table 4: Ball-Burst Mechanical Testing Data

SAMPLE TYPE	ESTIMATED VAGINAL CONTRIBUTION (N/MM)	STIFFNESS (N/MM)	ULTIMATE LOAD (N)	ULTIMATE ELONGATION (MM)	ENERGY ABSORBED (JOULES (N*MM))
GYNEMESH	0	25.82 ± 1.81	70.77 ± 6.22	5.81 ± 1.01	122.77 ± 23.38
14 DAY MESH-TISSUE COMPLEX	2.29± 1.44	28.12 ± 1.44	118.78 ± 21.70	8.98 ± 2.06	223.55 ± 124.71
90 DAY MESH-TISSUE COMPLEX	2.43 ± 0.15	27.37 ± 3.11	97.03 ± 11.60	7.99 ± 1.31	193.11 ± 31.54

6.4 Conclusions

A rabbit model of pelvic reconstruction provides the ability to implant mesh via lumbar colpopexy and to examine the host inflammatory and remodeling response at acute and chronic time points. The overall purpose of this aim was to identify significant differences in the immune and tissue remodeling response dependent upon anatomical location of implantation, suggesting that results of subcutaneous implantation studies are not a reliable predictor of performance when implanted into the vagina. This underscores the importance of developing a full understanding of the tissue-specific microenvironment of pelvic floor repair. Results from this aim contribute to the overarching data previously reported following the implantation of mesh in a variety of animal models and anatomical locations. Overall, this suggests that the rabbit may offer a more cost-effective alternative while still allowing a clinically relevant implantation.

We found distinct host responses to polypropylene mesh implanted in two different anatomical locations. In a model of pelvic reconstructive surgery, mesh was implanted onto the vagina and tensioned to the spine via lumbar colpopexy. A common surgical model of

subcutaneous implantation of mesh was used for comparison as an assessment of the host response to mesh in the abdominal wall. The overall aim of the study was to describe the host response to mesh post-implantation in each of these locations with the distinct perspective of understanding the response at early and late time points. We found significant differences in the development of the inflammatory response to polypropylene prolapse mesh, with respect to the presence of macrophages, the collagen fibrotic capsule formation, elastic fiber changes, and vascularity. Overall the host response to the same material implanted vaginally versus subcutaneously was heightened in vaginally implanted meshes.

7.0 Aim 2: To Scale Up the Controlled Release of IL-4 from a Layer-by-layer Coating Immunomodulatory Strategy to Improve Downstream Outcomes Following Mesh Implantation

7.1 Introduction

The findings from the previous aim confirm the presence of an inflammatory response to mesh at both acute and chronic time points, with indications of tissue degradation, poor remodeling outcomes, and unresolved inflammation. As a consequence, the purpose of this study involves the scale up of an immunomodulatory strategy to directly affect the response to mesh in a clinically relevant model at both acute and chronic time points.

There has been much work in the field of immunomodulation that demonstrates improved tissue remodeling outcomes associated with a shift from a pro-inflammatory profile to a more anti-inflammatory profile [44, 50, 52, 55]. This is particularly evident when this shift occurs during the earlier stages of the inflammatory response to a biomaterial. Specifically, an IL-4 eluting coated mesh developed previously for a mouse subcutaneous model of implantation has shown great success in promoting a dominant M2 anti-inflammatory macrophage response and was found to be associated with decreased fibrotic capsule deposition while showcasing improved mesh-tissue integration [50]. However, the success of this work has been limited to utilizing mesh proportional to the size of the rodent model along with a limited mode of implantation. In order to contribute to the field and further the knowledge on modulating the host response, the second aim focuses on scaling the IL-4 eluting coating to a larger animal model and utilizing a clinically significant surgical model. Thus, paired with the development and utilization of the clinically relevant model

of lumbar colpopexy from Aim 1, this subsequent aim intends to incorporate a cytokine release system onto the polypropylene mesh with the goal of promoting a positive regenerative outcome.

7.2 Materials & Methods

7.2.1 Plasma Irradiation Treatment

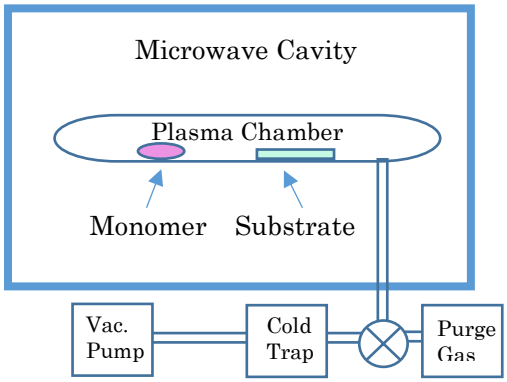

Figure 31: Schematic of the plasma irradiation process

The surface of polypropylene mesh was exposed to an adapted radio frequency glow discharge method to create a stable negative charge preparing for further coating procedures. Large (3 x 12 cm^2) and small (1x1 cm^2) pieces of mesh were cleaned by immersion into a 1:1 solution of isopropanol and acetone followed by sonication for 1 minute and air dried. Mesh was then exposed to one minute of Argon plasma at a flow rate of 35 mL/min, 600 W (2.45 GHz frequency) and steady state pressure (250 – 285 mTorr) in an Ion 40 Gas Plasma System (PVA TePla America, Inc, Corona, CA). Utilizing a monomer to react with the plasma, 1.5 g of maleic

anhydride was crushed into a powder via mortar and pestle and carefully distributed in a glass dish. The glass dish with the maleic anhydride and mesh pieces spaced 8 – 8.5 cm apart were placed into the Ion 40 Gas Plasma chamber on a tray with electrodes connected to the ground (Figure 33).

a. Argon gas flow rate: **35 mL/min**
b. RF Power Generator: **600 W (2.45 Ghz frequency)**
c. Steady State Pressure: **250 – 285 mTorr**
d. Time: **(1 minute)**

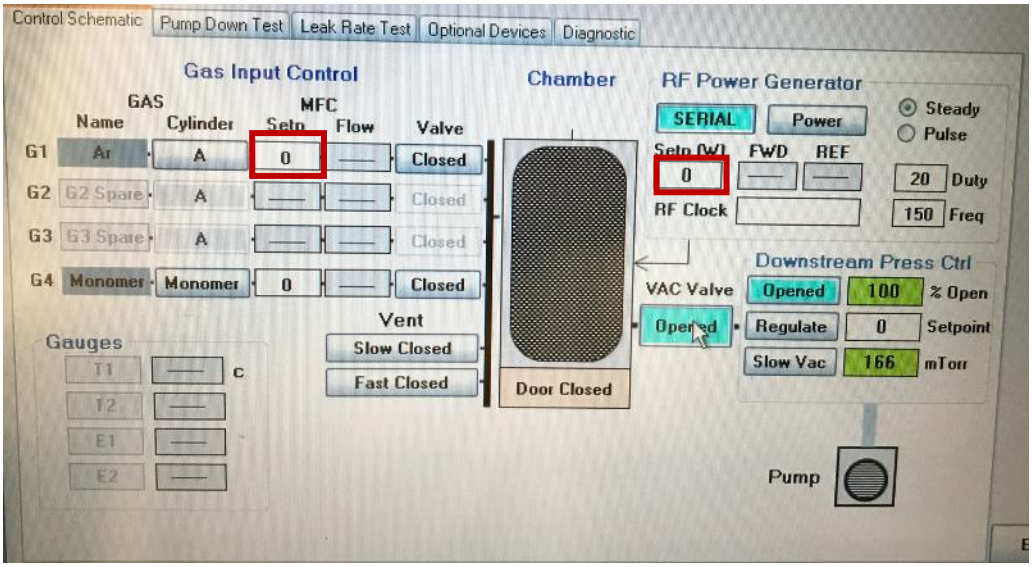

Figure 32: Ion Gas Plasma System Machine interface

3 Tray Run		
Tray 1		Power (+) Right Side
Tray 2		
Tray 3	Ground (-) Left Side	
Tray 4		
Tray 5		Power (+) Right Side

5 Tray Run		
Tray 1		Power (+) Right Side
Tray 2	Ground (-) Left Side	
Tray 3		Power (+) Right Side
Tray 4	Ground (-) Left Side	
Tray 5		Power (+) Right Side

Figure 33: Set up of tray orientation inside plasma chamber

A vacuum was created inside the chamber by reaching a pressure of 50 mTorr or lower, followed by exposure to plasma irradiation for 1 minute at an Argon gas flow of 35 mL/min, 600W (2.45 GHz frequency), and a steady state pressure (250 – 285 mTorr). Mesh was then hydrolyzed in Type I H_2O for 30 minutes and boiled for 20 minutes.

7.2.2 Scale Up of Layer-by-Layer Coating

The polypropylene mesh was immersed in alternating polycationic and polyanionic solutions to create 50 bilayers in total, with one bilayer being defined as one set of consequential polycationic and polyanionic dips. This was achieved utilizing a custom MTI SILAR Automated Dip Coated machine (Figure 34) (8 – position SILAR coating system, PTL-SC-6A, MTI Corporation, Richmond, CA). Chitosan (Sigma, St. Louis, MO) was dissolved in 0.5 % acetic acid at a concentration of 2 mg/mL and used for each polycationic layer. Dermatan sulfate (Sigma, St. Louis, MO) was dissolved in Type I water at a concentration of 2 mg/mL and used for each polyanionic layer. For each alternating polycationic polymer and polyanionic polymer solution, the mesh was immersed for 10 minutes each, interspersed with a brief air-drying period. After each bilayer was formed, the mesh was washed three times in Type I water for one minute and air dried before the next immersion step. A core coating consisting of 10 bilayers of each polymer was formed on each piece of mesh. In order to incorporate cytokine release, recombinant rabbit IL-4 (R&D Systems, Minneapolis, MN) at a concentration of 1.5 µg/mL was complexed with a 2 mg/mL solution of dermatan sulfate for at least 18 hours at 4°C. Mesh was subsequently dipped in chitosan and IL-4 complexed dermatan sulfate solutions for 40 bilayers total. Once completed, mesh was terminally sterilized using ethylene oxide and stored at -20°C.

Figure 34: MTI SILAR Automated Dip Coating machine used for layer-by-layer coating

7.2.3 Scale Up Cytokine Bioactivity

A controlled release assay was used to determine the release profile of the IL-4. Briefly, 5 different 1x1 cm^2 pieces of coated mesh were sampled from different locations on a large 3x12 cm^2 piece (See schematic) Each mesh was submerged in release media (1X phosphate buffered saline consisting of 0.05 U/mL chitosanase (Sigma, St. Louis, MO) and 0.05 U/mL chondroitinase ABC (Sigma, St. Louis, MO) at 37°C. The solution was sampled and replaced with fresh release media at periodic intervals until IL-4 had finished eluting. Each sampled solution was measured via enzyme linked immunosorbent assay (ELISA) for quantification of IL-4 concentration (Rabbit IL-4 ELISA, R&D Systems, Minneapolis, MN).

7.2.4 Isolation of Rabbit Peripheral Blood-Derived Macrophages

Peripheral blood was collected from the New Zealand White Rabbit ear vein and placed directly into heparinized blood tubes for further processing. Each sample was diluted 1:1 in Hank's balanced salt buffer no calcium, no magnesium (Thermofisher, Waltham, MA) followed by the addition of Ficoll-Paque PLUS solution according to manufacturer's instructions on proportions (Fisher Scientific, Hampton, NH). The mononuclear cell layer (Figure 35) was isolated and cells were resuspended in macrophage culture media (RPMI 1640, 10% FBS, 1% PenStrep, 1% HEPES Buffer, 2 % Non-essential Amino Acids, and 20 ng/mL Rabbit GM-CSF).

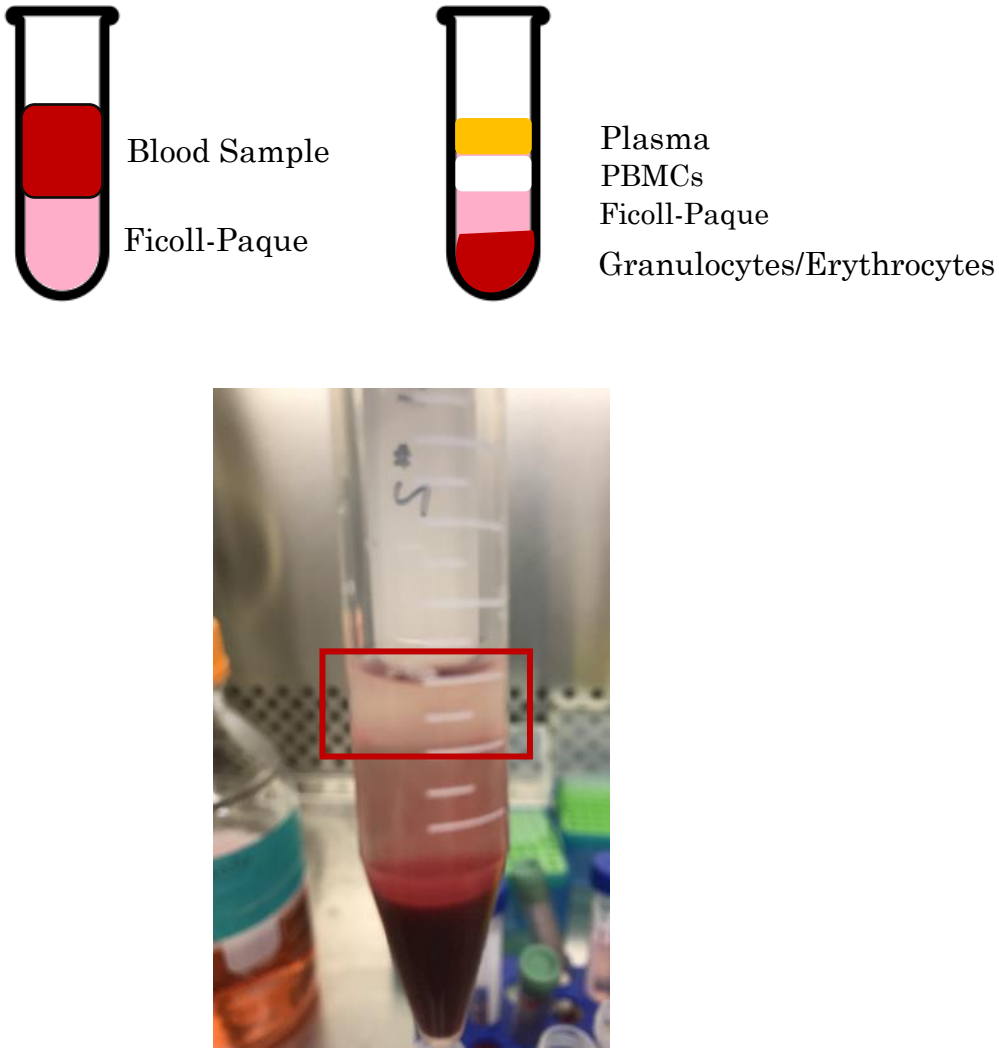

Figure 35: Isolation of mononuclear cell layer using Ficoll-Paque separation technique

7.2.5 Isolation of Rabbit Bone Marrow-Derived Macrophages

Bone marrow-derived macrophages were collected from the femurs and tibia of New Zealand white rabbits at the time of necropsy. The skin, muscle, and connective tissue was removed to isolate the femur and tibia of each rabbit. Bones were then moved into a sterile environment where each end was cut using bone cutting forceps (See diagram). The bone marrow

cavity was flushed with a needle and syringe filled with macrophage culture media (RPMI 1640, 10% FBS, 1% PenStrep, 1% HEPES Buffer, 2 % Non-essential Amino Acids, and 20 ng/mL Rabbit GM-CSF). Followed by a series of subsequent centrifugation and filtration steps, bone marrow aspirate was reconstituted in macrophage culture media and ready for plating.

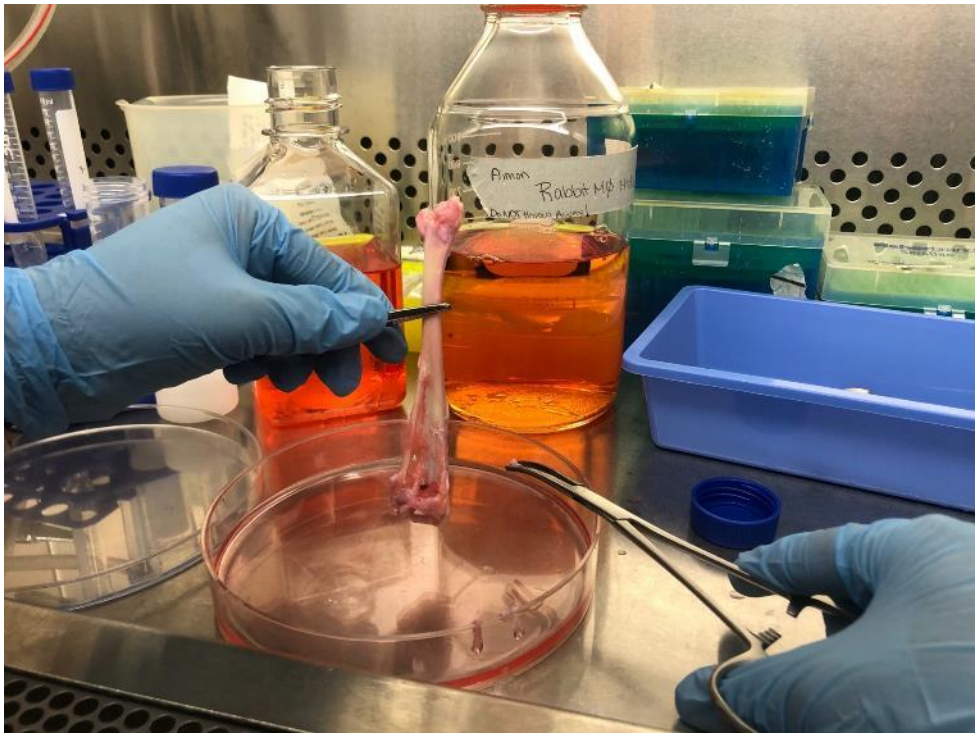

Figure 36: Image of a tibia isolated from the New Zealand White Rabbit

7.2.6 *In vitro* Macrophage Rabbit Macrophage Polarization

Rabbit macrophages obtained from either method of isolation (peripheral blood vs. bone-marrow lysate) were plated at a concentration of 1 x 10^6 cells/mL and cultured for 7 days at 37°C, 5% CO_2 with the addition of macrophage media at 2 intervals. Macrophages were then treated

with polarizing cytokines for 24 hours to culture three distinct phenotypic differentiations. M0 macrophages were cultured in traditional macrophage media and served as naïve controls. M1 pro-inflammatory macrophages were cultured with 20 ng/mL recombinant rabbit interferon gamma (IFN- γ) (Abcam, Cambridge, United Kingdom) and 100 ng/mL lipopolysaccharide (LPS) from *Escherichia coli* supplemented in macrophage media (RPMI 1640, 10% FBS, 1% PenStrep, 1% HEPES Buffer, 2 % Non-essential Amino Acids, and 20 ng/mL Rabbit GM-CSF). M2 anti-inflammatory macrophages were cultured with 20 ng/mL of recombinant rabbit interleukin-4 (R&D Systems, Minneapolis, MN) supplemented in macrophage media (RPMI 1640, 10% FBS, 1% PenStrep, 1% HEPES Buffer, 2 % Non-essential Amino Acids, and 20 ng/mL Rabbit GM-CSF).

7.2.7 Macrophage Immunolabeling

After macrophage polarization, the supernatant was aspirated and saved for other functional assays. Macrophages were then fixed with 2% paraformaldehyde (PFA) for 30 minutes. Macrophages were then washed in 1X phosphate buffered saline followed by incubation in blocking solution (2% donkey serum, 1% bovine serum albumin, 0.1% Tween-20, 0.1% Triton X-100) for 1 hour. Macrophages were immunolabeled with monoclonal mouse anti-rabbit RAM11 (1:200) (Dako North America, Inc. Carpinteria, CA) overnight at 4°C. After washing with 1X phosphate buffered saline, macrophages were then incubated with the secondary antibody, donkey anti-mouse Alexa Fluor 594 (1:200) (Abcam, Cambridge, United Kingdom) for 1 hour. Macrophages were counterstained with 4',6-diamidino-2-phenylindole (DAPI) (BioLegend, San Diego, California) to label nuclei. At least 3 – 5 images of each well were taken in a 10X and 20X field using a Nikon TE-2000-E inverted microscope in TRITC and DAPI channels.

7.2.8 Functional Assays: Nitric Oxide Production

The supernatants collected from the previous macrophage polarization cultures were used for the Nitric Oxide Greiss Reagent System Assay (Promega, Madison, WI). Briefly, supernatants were incubated with 1% sulfanilamide in 5% phosphoric acid in the dark at room temperature for 10 minutes. This was followed by the addition of 0.1% N-1-napthylethylenediamine dihydrochloride in Type I water for 10 minutes at room temperature in the dark. The absorbance was read at a wavelength 540 nm and compared to a sodium nitrite standard curve.

7.2.9 Functional Assays: Arginase Activity

Macrophages following polarization procedure were lysed using a lysis buffer (0.001% Triton X-100, 0.01% Halt Protease Inhibitor in Type I water). An arginase activation solution (10 mM $MnCl_2$, 50 mM Tris-HCl in Type I water, pH 7.5) was added to cell lysates and incubated for 10 minutes at 55°C. An arginine substrate solution (0.5 M L-arginine in Type I water, pH 9.7) was added to the activated samples and incubated at 37°C for 2 hours and 24 hours. At 2 hours and at 24 hours of incubation, 5 uL of each sample and standard was taken into a new 96-well plate followed by the addition of urea detection solution (0.03% Brij35, 2.5 M Sulfuric Acid, 2.5 g/L Boric Acid, 100 mg/L Phthalaldehyde, 513 mg/L Primaquine). The absorbance was measured at a wavelength of 430 nm at 10 minutes and 20 minutes of incubation and compared to a urea standard.

7.2.10 RNA Extraction and Pro-Inflammatory/Anti-Inflammatory Gene Expression

Following manufacturer's instructions, total RNA of polarized macrophages was extracted using RNeasy Miniprep RNA Isolation kit (Qiagen, Valencia, CA). RNA concentration and purity were determined using a NanoDrop Lite Spectrophotometer.

Isolated RNA was reverse-transcribed to create cDNA templates using a High Capacity RNA-to-cDNA kit (ThermoFisher Scientific, Waltham, MA) and following the manufacturer's instructions. Taqman Gene Expression Assays (ThermoFisher Scientific, Waltham, MA) were performed for the following pro-inflammatory and anti-inflammatory panel of markers (See Table 3). Gene expression was normalized to the housekeeping gene, glyceraldehyde 3-phosphate dehydrogenase (GAPDH; Oc03823402_g1). Values were normalized to those obtained from the control group (M0, naïve macrophages).

Table 5: Panel of pro-inflammatory and anti-inflammatory markers

Pro-inflammatory	Anti-inflammatory
iNOS (Oc04096740_g1)	Arg1 (Oc03397217_m1)
IFN G (Oc04096817_m1)	IL10 (Oc03396940_m1)
IL6 (Oc04097053_m1)	TGFB 1 (Oc04176122_u1)
IL1-BETA (Oc03823250_s1)	MRC1 (Oc06778204_m1)

7.2.11 Cytokine Bioactivity Assays

A series of *in vitro* macrophage cultures was also used to test the bioactivity of IL-4 incorporated into the coating on the mesh. Pristine mesh, polymer-only coated mesh, and IL-4 coated mesh were incubated with previously cultured macrophages for 24 hours with culture media (RPMI 1640, 10% FBS, 1% PenStrep, 1% HEPES Buffer, 2 % Non-essential Amino Acids) supplemented with 0.05 U/mL chitosanase (Sigma, St. Louis, MO) and 0.05 U/mL chondroitinase ABC (Sigma, St. Louis, MO). Concurrent cultures of macrophages were treated with polarizing cytokines for 24 hours culture three distinct phenotypic differentiations were used as comparison. M0 macrophages were cultured in traditional macrophage media and served as naïve controls. M1 pro-inflammatory macrophages were cultured with 20 ng/mL recombinant rabbit interferon gamma (IFN- γ) (Abcam, Cambridge, United Kingdom) and 100 ng/mL lipopolysaccharide (LPS) from *Escherichia coli* supplemented in macrophage media (RPMI 1640, 10% FBS, 1% PenStrep, 1% HEPES Buffer, 2 % Non-essential Amino Acids, and 20 ng/mL Rabbit GM-CSF). M2 anti-inflammatory macrophages were cultured with 20 ng/mL of recombinant rabbit interleukin-4 (R&D Systems, Minneapolis, MN) supplemented in macrophage media (RPMI 1640, 10% FBS, 1% PenStrep, 1% HEPES Buffer, 2 % Non-essential Amino Acids, and 20 ng/mL Rabbit GM-CSF).

After 24 hours, all treatment groups were processed identically for macrophage immunolabeling, functional assays (nitric oxide assay and arginase activity assay), and gene expression as described earlier.

7.2.12 Animal Subjects

A total of 10 nulliparous New Zealand White Rabbits aged 4 – 6 months (~4 kg) were used in this study. Animals were obtained from Covance, Inc. (Princeton, NJ). All animals were housed in the Center for Preclinical Studies at the McGowan Institute for Regenerative Medicine (MIRM) for at least 7 days prior to the start of any procedure. All animals were examined by staff veterinarians and determined to be in good health prior to admission into any study. All animals were monitored daily. All procedures were approved by the Institutional Animal Care and Use Committee at the University of Pittsburgh.

Rabbits were kept with fresh bedding and enrichment along with access to food and water as directed by National Institutes of Health Animal Care Guidelines for rabbit care. Extra enrichment was provided in the form of preferential snacks such as blueberries, pineapple, celery, strawberries, grapes and romaine lettuce. The rabbits were exposed to a 12-hour light/dark cycle and monitored for signs of distress throughout the study.

7.2.13 Surgical Design: Lumbar Colpopexy vs. Subcutaneous

Rabbits were sedated with acepromazine (1 mg/kg) followed by intramuscular injection of ketamine/xylazine (35 mg/kg & 5 mg/kg). Animals were then incubated and a surgical plane of anesthesia was achieved via inhalation of 2% isofluorane.

A midline longitudinal incision was performed opening the peritoneal space with the bowels packed away followed by identification of the uterine horn and reproductive organs (Figure 2A). A hysterectomy was performed followed by trimming and collection of the proximal vagina

of the rabbit to serve as a positive control (Figure 2B). Once the uterus was removed, space was dissected along the vaginal wall on both sides between the bladder and the rectum (Figure 3A). Two 3 x 12 cm^2 pieces of Recombinant IL-4 coated Gynemesh PS (Ethicon, Somerville, NJ) were secured with 3-0 PDS suture along the posterior and anterior vaginal walls (Figure 3B). The remaining flaps at the top were then attached to a ligament in the lumbar spine with 2-0 PDS creating support to the pelvic organs (Figure 4A & 4B). The peritoneal cavity was continuously hydrated (Figure 5) and sutured closed with continuous stitching using 3-0 PDS. A 2 x 2 cm^2 piece of mesh was implanted subcutaneously (Figure 6B) onto the abdominal musculature via 3-0 PDS prior to closing the initial abdominal incision in the skin with subcuticular stitches. Post-surgically, all animals were monitored closely to ensure full recovery from anesthesia.

7.2.14 Post-Operative Care

Animals were carefully monitored for signs of discomfort (as evidenced by failure to eat, drink, or resume normal ambulation and activity). Cefazolin (25 mg/kg), Buprenex (0.02 mg/kg), and Ketoprofen (2 mg/kg twice daily as needed) was given via subcutaneous injection for pain for 3 days postoperative. At the veterinarian's discretion, the animals were given Ranitidine (2 mg/kg) as an antacid in cases of a decreased appetite until normal activity resumed.

7.2.15 Tissue Explants and Tissue Processing

At 14 days and 90 days post-implantation, the animals were sedated with acepromazine (1 mg/kg) and injected intravenously with sodium pentobarbital (100 mg/kg) for euthanasia. The mesh and surrounding tissue were extracted from the rabbit and immediately processed. One

portion of a representative mesh-tissue explant (Figure 7A & 7B) was fixed in formalin for at least 48 hours before paraffin embedding. 7 μm sections were used for histological analysis. Another portion of the explant was flash frozen and kept in -80°C for biochemical evaluations. A 3x3 cm^2 piece of vaginal-mesh tissue was carefully wrapped in gauze and kept in sterile saline at -20°C for biomechanical testing.

7.2.16 Histological (H&E) Tissue Morphology and Characteristics

Tissue sections were stained with hematoxylin and eosin to observe key aspects of the host response to mesh including tissue organization, degradation and encapsulation. Specifically, tissue sections were analyzed with an emphasis regarding mononuclear cellular infiltration near mesh fibers, the presence of foreign body giant cells and potential angiogenesis. Cellularity analysis was based on 5 to 7 single mesh fibers imaged per sample at a 40X objective on Nikon Eclipse 50i (Nikon, Tokyo, Japan) and using Fiji image processing software (National Institutes of Health, Bethesda, MD).

7.2.17 Collagen Staining & Quantitative Analysis

7.2.17.1 Masson's Trichrome

Tissue sections stained with Masson's trichrome were imaged to observe the collagen deposition within the implantation site. Briefly, sections were immersed in Bouin's solution at 56°C for 15 minutes, with subsequent washing steps. Sections were then stained with Weigert's Iron Hematoxylin Working Solution for 5 minutes and lastly immersed in Trichrome AB solution (Sigma, St. Louis, MO) for 5 minutes. All analysis of collagen area surrounding mesh fibers was

based on 5 to 7 single mesh fibers per sample imaged at 20X objective on Nikon Eclipse 50i (Nikon, Tokyo, Japan). Fiji image processing software (National Institutes of Health, Bethesda, MD) provided a quantitative assessment of the fibrous capsule thickness surrounding the mesh fibers.

7.2.18 Macrophage Immunohistochemistry (Peroxidase)

Sections were deparaffinized and rehydrated in a graded series of alcohols followed by antigen retrieval in citric acid buffer (pH 6.0) for 20 minutes at 95°C. Sections were then incubated in 3% hydrogen peroxide in methanol for 30 minutes at RT to block endogenous peroxidases. Tissue sections were blocked in a blocking solution of 5% Donkey Serum, 2 % Bovine Serum Albumin, 0.1% Tween-20, 0.1% Triton-X-100 for 2 hours at RT in a humidity chamber. Slides were immunolabeled using either monoclonal mouse anti-rabbit RAM11 (1:200) (Dako North America, Inc., Carpinteria, CA), a pan-macrophage marker, overnight at 4°C. After PBS washes, sections were incubated in a secondary biotinylated anti-mouse IgG (1:200) (Vector, Burlingame, CA) for 30 minutes at RT followed by incubation in Vectastain Elite Avidin/Biotin Complex (ABC) Reagent (Vector, Burlingame, CA) for 30 minutes at RT. Tissue section were then incubated with DAB (3,3'-diaminobenzidine) HRP substrate until dark brown reaction was visible. Vector Hematoxylin QS was used to counterstain the nuclei followed by a dehydrated series of alcohols and mounting coverslips for imaging. Images of 5 to 7 single mesh fibers per sample were taken at 40X objective for RAM11 on Nikon Eclipse 50i (Nikon, Tokyo, Japan) and using Fiji image processing software (National Institutes of Health, Bethesda, MD).

7.2.19 CD31 Immunohistochemistry & Vessel Analysis

Sections were deparaffinized and rehydrated in a graded series of alcohols followed by antigen retrieval in citric acid buffer (pH 6.0) for 20 minutes at 95°C. Sections were then incubated in 3% hydrogen peroxide in methanol for 30 minutes at RT to block endogenous peroxidases. Tissue sections were blocked in a blocking solution of 5% Donkey Serum, 2 % Bovine Serum Albumin, 0.1% Tween-20, 0.1% Triton-X-100 for 2 hours at RT in a humidity chamber. Slides were immunolabeled using monoclonal mouse anti-rabbit CD31 (1:50) (Thermo Fisher Scientific, Waltham, MA), an indicator for angiogenesis via endothelial cells overnight at 4°C. After PBS washes, sections were incubated in a secondary biotinylated anti-mouse IgG (1:200) (Vector, Burlingame, CA) for 30 minutes at RT followed by incubation in Vectastain Elite Avidin/Biotin Complex (ABC) Reagent (Vector, Burlingame, CA) for 30 minutes at RT. Tissue section were then incubated with DAB (3,3'-diaminobenzidine) HRP substrate until dark brown reaction was visible. Vector Hematoxylin QS was used to counterstain the nuclei followed by a dehydrated series of alcohols and mounting coverslips for imaging. Images of 5 to 7 single mesh fibers per sample were taken at 40X objective for CD31+ on Nikon Eclipse 50i (Nikon, Tokyo, Japan).

Blood vessels were identified as positively immunolabeled endothelial cells morphologically representing a lumen and vessel counts were measured based on an adapted Weidner's method.[46] Each image was overlaid with a 19x14 grid (650 um^2 with 266 total points) in Fiji image processing software (National Institutes of Health, Bethesda, MD). The intersection of the superimposed grid points with a blood vessel was counted and allowed to take vessel size into consideration into the final result. Using this count and the total tissue area measured as the area of the 20X field subtracted by the area of the mesh fiber, a vessels/area value was calculated

for each image. The mean and standard error of the mean was respectively calculated for each sample.

7.2.20 Verhoeff's Van Gieson (Elastin)

Vaginal tissue sections were stained with Verhoeff's van Gieson Elastic Stain kit (Sigma Aldrich, St. Louis, MO) to observe the nature of elastic fibers throughout vaginal tissue. Sections were submerged in a Working Elastic Stain Solution for 10 minutes, with subsequent rinsing, followed by differentiating steps in Ferric Chloride solution for 1 minute. Sections were immersed in a Van Gieson counterstain for 2 minutes. Representative images per sample were taken to observe the presence of elastic fibers throughout tissues on Nikon Eclipse 50i (Nikon, Tokyo Japan).

7.2.21 RNA Extraction and Pro-Inflammatory/Anti-Inflammatory Gene Expression

Following manufacturer's instructions, total RNA of frozen tissues was extracted using RNeasy Miniprep RNA Isolation kit (Qiagen, Valencia, CA). RNA concentration and purity were determined using a NanoDrop Lite Spectrophotometer. Isolated RNA was reverse-transcribed to create cDNA templates using a High Capacity RNA-to-cDNA kit (ThermoFisher Scientific, Waltham, MA) and following the manufacturer's instructions. Taqman Gene Expression Assays (ThermoFisher Scientific, Waltham, MA) were performed for the following pro-inflammatory and anti-inflammatory panel of markers and other biochemical components (See Table 5). Gene expression was normalized to the housekeeping gene, glyceraldehyde 3-phosphate dehydrogenase

(GAPDH; Oc03823402_g1). Values were normalized to those obtained from the respective control tissues, native vagina and abdominal muscle.

Table 6: Panel of pro- and anti- inflammatory markers and other relevant extracellular matrix components

Pro-inflammatory	Anti-inflammatory
iNOS (Oc04096740_g1)	Arg1 (Oc03397217_m1)
IFN G (Oc04096817_m1)	IL10 (Oc03396940_m1)
IL6 (Oc04097053_m1)	TGFB 1 (Oc04176122_u1)
IL1-BETA (Oc03823250_s1)	MRC1 (Oc06778204_m1)
Biochemical Components	
Elastin (Oc06720017_g1)	MMP2 (Oc03397553_m1)
	MMP9 (Oc03397520_m1)

7.2.22 Biochemical Components (MMP Activity)

7.2.22.1 Protein Extractions

All tissue samples were homogenized in a High Salt Buffer (pH 7.5, 50 mM Tris base, 150 mM NaCl, 5 M CaCl2, 1% Triton-X-100, 0.01 % Halt protease inhibitor cocktail, Pierce Biotechnology, Rockford, IL). Protein concentrations were quantified using the BCA Protein Assay Kit (Pierce Biotechnology, Rockford, IL) following the manufacturer's instructions.

7.2.22.2 MMP Activity Assay

MMP assay was adapted from the EnzChek Gelatinase/Collagenase protocol (Molecular Probes, Inc., Eugene, OR). 10 µg of protein for each sample was used. Samples were incubated with 1X Reaction buffer (diluted from 10X 0.5M Tris-HCl, 1.5 M NaCl, 50 mM $CaCl_2$, 2 mM sodium azide, pH 7.6) followed by addition of DQ gelatin from porcine skin (100 µg/mL) at room temperature. The fluorescence intensity was read at an excitation of 495 nm and an emission at 515 nm after 1 hour of incubation and 16 hours of incubation. MMP values are calculated using Type IV collagenase/gelatinase standards where one unit of gelatinase A is defined as the amount that can hydrolyze 1 mg of type IV collagen within one hour at 37C, pH 7.5. The 16-hour incubation time point was optimized for use due to the increased sensitivity in measurements.

7.2.23 Ball Burst Mechanical Testing

Vaginal mesh samples preserved in saline were used for ball burst testing to determine structural properties of the vaginal tissue post-implantation. Polypropylene mesh (n = 5) was tested alone to allow for comparison of mesh properties and for later calculations on determining tissue contributions. Mesh was placed between two metal clamps that is screwed into the apparatus setup on an Instron TM 4502 (Instron, Norwood, MA). At the top is a stainless-steel ball rod designed to push through a hole in the clamps. This ball is attached to a load cell, which is capable of up to 5 kN of load.

The ball rod was centered and lowered against each clamped sample at a constant rate of 10 mm/min to a 0.5 N pre-load. Then, each sample was loaded to failure at a rate of 10 mm/min.

The failure load (N) and elongation (mm) data are then utilized to create load-elongation curves to determine the structural properties. Stiffness (N/mm) was calculated as the maximum

slope of the over 20% of the failure elongation. Energy absorbed was calculated as the area underneath the curve until failure.

7.2.24 Statistical Analysis

Based on previous studies, a sample size of 5 animals were deemed sufficient for determining statistical differences between groups in the analysis [73]. Descriptive statistical analysis was done to determine normality using Kolmogorov-Smirnov and Shapiro-Wilk tests with alpha = 0.05. Immunolabeling data for each anatomical location at both acute and chronic time points were assessed using one-way analysis of variance with Tukey post hoc test with $p<0.05$ used to determine significance. Independent samples t-tests were used to determine differences based solely on anatomical location. In the case of data found to be not normally distributed, the comparison of non-parametric data was completed using a Kruskal-Wallis comparison with a Mann-Whitney post hoc.

7.3 Results & Discussion

7.3.1 In Vitro Characterization of Scale-Up Rabbit IL-4 Coating

A scale-up of the layer-by-layer coating onto a larger piece of mesh was developed for a relevant larger animal model of implantation. The protocol was modified to adapt to a 3x12 cm^2 piece of mesh and characterized for uniformity and bioactive functionality. Additionally, rabbit cytokines were incorporated to remain relevant to the change in animal model that was being

utilized. All of these factors combined allowed for testing the scale-up of the coating to a clinically relevant standard. All mesh pieces (large – 3x12 cm^2 and small – 1x1 cm^2) were irradiated via an adapted radio frequency glow discharge method described earlier [91, 92]. Preliminary work has confirmed the presence of a stable negative charge formed by the carboxylic acid groups on the surface of the polypropylene mesh after treatment [50].

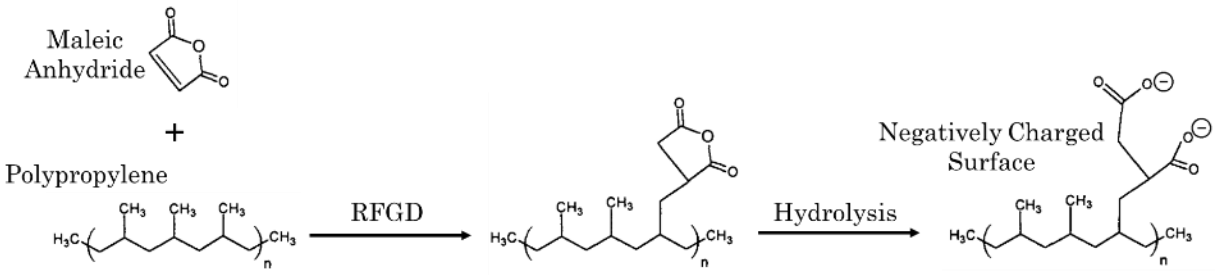

Figure 37: Chemical Overview of Plasma Irradiation

The irradiated mesh was then coated with a series of polycationic and polyanionic polymer solutions utilizing the method of layer-by-layer deposition. These layers differ from physical adsorption in that they attach through the electrostatic interactions of oppositely charged layers. Chitosan was used as the polycation layers due to its nontoxic properties. It is known to be antibacterial, anti-tumoral, and has previously shown *in vivo* to encourage skeletal muscle tissue

growth [57, 93]. Additionally, several researchers have shown that alternatively activated macrophages produce chitinase and other chitinase-like molecules confirming a direct role in degrading chitin or chitin derivatives containing surfaces [94].

For the polyanion layers, dermatan sulfate (also known as chondroitin sulfate B) is known for its role in regulating the extracellular matrix and its ability to enhance the bioactivity of IL-4 *in vivo [53]*. Recombinant rabbit IL-4 was used to incorporate a controlled release mechanism in the polymer coating. The IL-4 cytokine has been shown in previous studies to shift the macrophage phenotype into the M2 pro-inflammatory state (35, 36). This has been associated with improved tissue remodeling outcomes (7, 8). The overall immunomodulatory strategy incorporates multiple components of a complex layered coating and cytokine release to mediate the macrophage response to mesh.

In order to visualize the polymer components of the coating, a quality control using a stain of Alcian Blue was used for each batch of mesh manufactured. This allowed for confirmation of the properties of the coating on the macroscale and detection of uniformity of the coating. Figure 38 depicts pristine mesh and coated mesh stained with Alcian blue. A magnified image of the mesh fibers closely shows the uniformity of the coating even throughout the mesh knots. Conversely, the lack of blue staining indicates that there is no presence of coating on the pristine mesh, serving as the negative control.

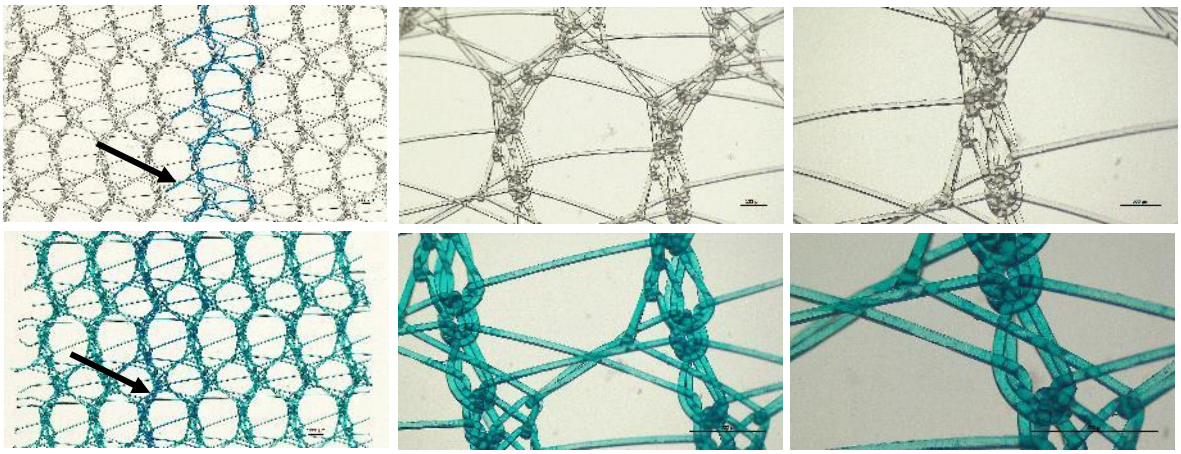

Figure 38: Top Panel: Pristine Mesh stained with Alcian Blue. Bottom Panel: Increasing Magnifications of Coated Mesh stained with Alcian Blue. Black arrow indicates the blue dyed fibers that are characteristic to commercially available Gynemesh and not a part of

7.3.2 Cytokine Functional Assays

Controlled release studies were conducted to determine the release profile of the rabbit IL-4. Obtaining the release profile curve help determined an estimated dosage of IL-4 that would be released once the coating broke down. Quality control for scaling up the larger pieces of mesh was done via sampling 1x1 cm^2 pieces at multiple different locations to determine uniformity of IL-4 being released. The amount of IL-4 released was determined using ELISA assays. Release showed that the amount of IL-4 released in the first week was consistent with a burst release response with approximately 80% of the IL-4 being released. Interestingly, the plateau was consistent up until a non-detectable range of IL-4 was released by approximately 1 month. This aligns with previous kinetics of the coating determined by having 50 bilayers, confirming the ability to control the amount of release over time [50]. Additionally, this information confirms the desired release profile of releasing IL-4 in the early stages post-implantation. This early period of

modulation has the potential to allow for improved downstream outcomes as noted by previous work with an increase in the pro-remodeling M2 macrophage presence [50, 52].

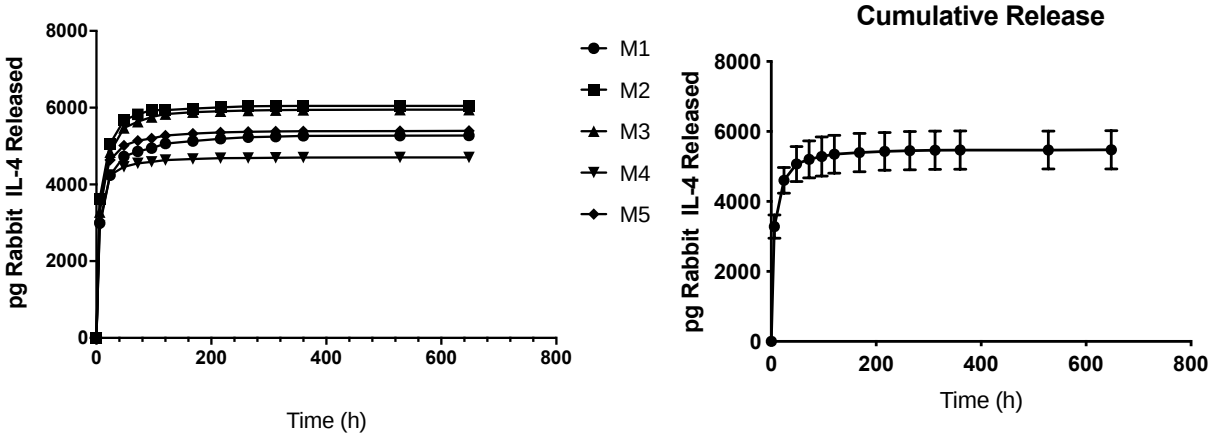

Figure 39: Cumulative Release kinetics of Rabbit IL-4

7.3.3 Macrophage Cultures

Macrophages isolated from the bone marrow had higher cell viability (> 97%) and success during culturing periods than macrophages isolated from peripheral blood. A limiting factor with peripheral blood isolated macrophages was the increased contamination of red blood cells, which may have been alleviated with the use of a red blood cell lysis buffer. Thus, assessment of

macrophage functionality was completed using macrophages isolated from the bone marrow methodology.

Due to the use of rabbit granulocyte-macrophage colony-stimulating factor (GM-CSF), the cells cultured were semi-adhesive in nature and therefore it was important to not complete full media changes during cultures. This allowed for a sustained release of macrophage secretions into the media and characterization of these secretions permitted further information about rabbit macrophages.

7.3.3.1 Immunolabeling with RAM11

In order to initially confirm the culture of macrophages, the cells were fixed and immunolabeled with a pan-macrophage marker, RAM11. This was the first step to confirming the presence of macrophages after isolations from bone marrow. Positively labeled RAM11 cells are shown in TRITC (Red) and counts indicate no significant differences in the number of macrophages cultured for each polarization group. However, it is important to note that approximately 40 – 60 % of the cultured cells were labeled as RAM11+ cells, translating to a 40 – 60% efficiency when isolating from bone marrow. This remaining percentage may correlate to the culture of dendritic cells, red blood cells, and other cell debris coming from the bone marrow. Regardless, RAM11+ cells still indicate the presence of macrophages and further work to determine the macrophage characteristics and functionality is shown.

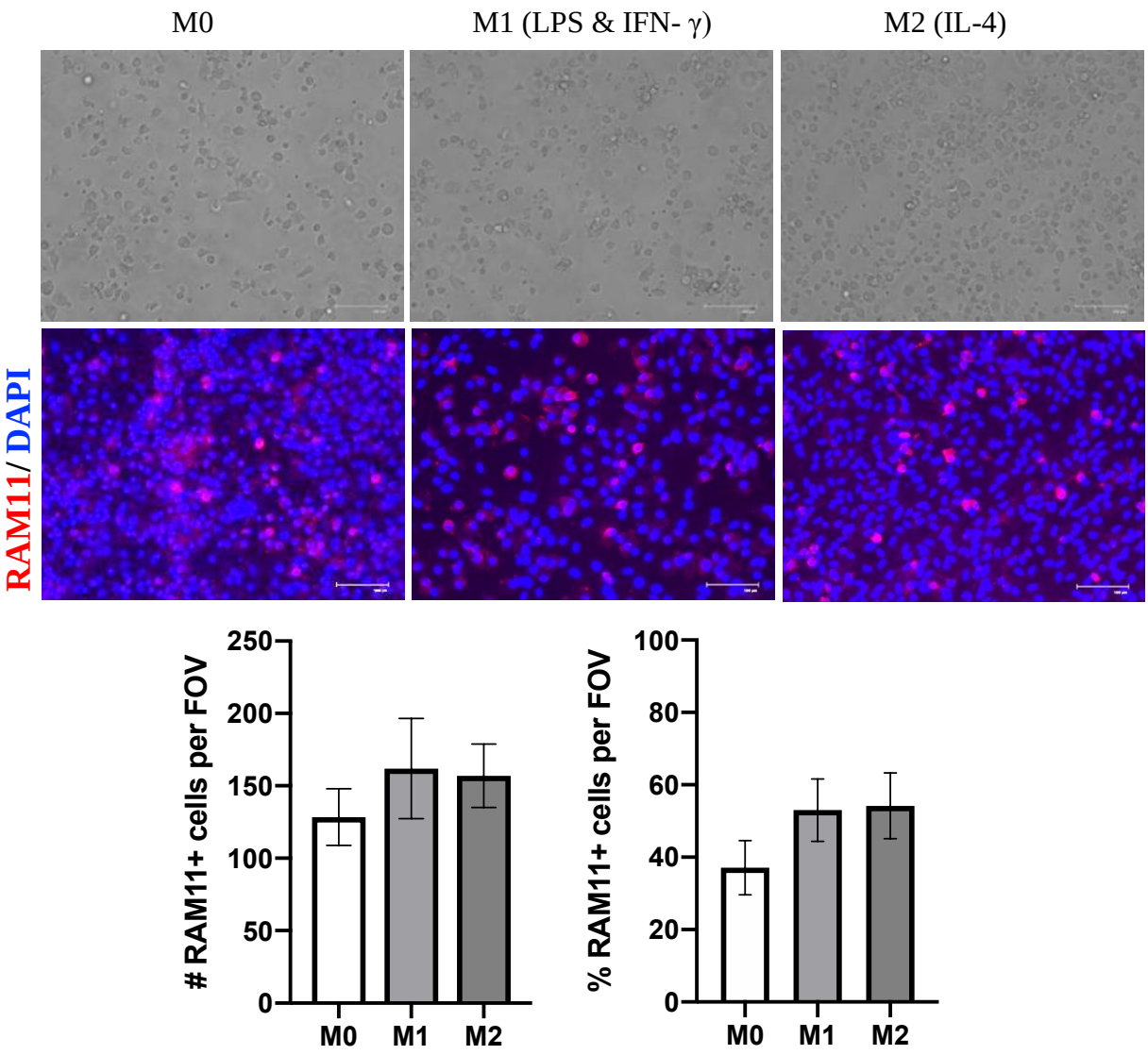

Figure 40: Top Panel: Representative brightfield images of bone marrow-derived macrophages Bottom Panel: Immunolabeling with RAM11 (Repeated in quadruplicate (n = 6)

7.3.3.2 Assessment of Macrophage Polarization

A large component of determining the macrophage phenotypic profile involved utilizing functional assays that are characteristic of macrophages. Specifically, the competing arginine pathways allows for the determination of what can be considered an M1 pro-inflammatory macrophage and what can be considered an M2 anti-inflammatory macrophage. It is widely known that M1 macrophages express the enzyme, nitric oxide synthase, that follows the pathway of metabolizing arginine into nitric oxide and citrulline. Alternatively, M2 macrophages are typically branded by the expression of the enzyme, arginase, that follows the pathway of hydrolysis of arginine into urea and ornithine.

The nitric oxide Griess reagent system assay measured the production of nitric oxide in all groups of macrophage cultures. The assays showed that cells polarized with the pro-inflammatory cytokines (IFN- γ and LPS) significantly produced the highest amount of nitrite concentration (22.01 ± 3.53 µM) as compared to the other groups (M0 vs. M1, $p = 0.0011$ and M1 vs. M2, $p = 0.0002$). This confirms the ability of rabbit macrophages isolated from the bone marrow to be capable of polarizing to the pro-inflammatory phenotype. Interestingly, the control M0 group also produced (7.39 ± 2.57 µM) nitrite concentrations and the M2 group produced very little (2.31 ± 0.98 µM). This further confirms the concept of macrophages existing on a spectrum and exhibiting levels of plasticity depending on certain signaling cues, as done based on the culture assays.

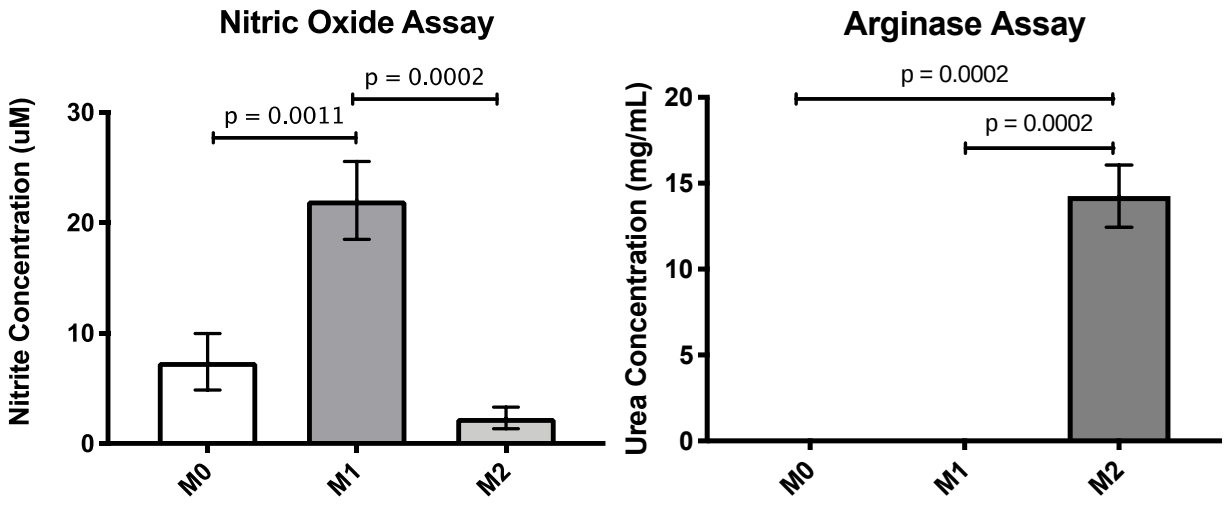

Figure 41: Functional assays to characterize in vitro macrophage polarization. Arginase and Nitric Oxide activity detected ± SEM for three independent assays performed (n = 6) is shown

An arginase activity assay was used to measure the urea production in all groups of macrophage cultures. Arginase activity was measured as the µg of urea per µL of lysate. Results from the assays showed that macrophages polarized with rabbit IL-4 expressed a significant increase in urea concentration in the lysates as compared to the other treatment groups (14.25 ± 1.81 µg Urea per µL lysate, p = 0.0002).

A panel of pro-inflammatory and anti-inflammatory markers were used to determine the relative gene expression in further assessing the phenotypic profile of the macrophages cultured with either the M1-inducing cues (LPS and IFN- γ) or M2 cues (IL-4). All A_{260}/A_{280} ratios were found above or at 2.0, which confirms purity and well-solubilization of RNA. M1 polarized macrophages expressed increased levels of pro-inflammatory markers (IFN-γ, IL-6, and IL-1β) as compared to the control (M0) and M2 polarized macrophages (Figure 42, top panel). There was an increased

expression in the levels of anti-inflammatory markers (Arg1, IL-10, TGF- β, and Mrc1) in the M2 polarized macrophages as compared to the control (M0) and M1 polarized macrophages (Figure 42, bottom panel). The increased expression in each respective pro-inflammatory and anti-inflammatory marker further confirms the representative traits on the polarization spectrum for macrophage phenotypes.

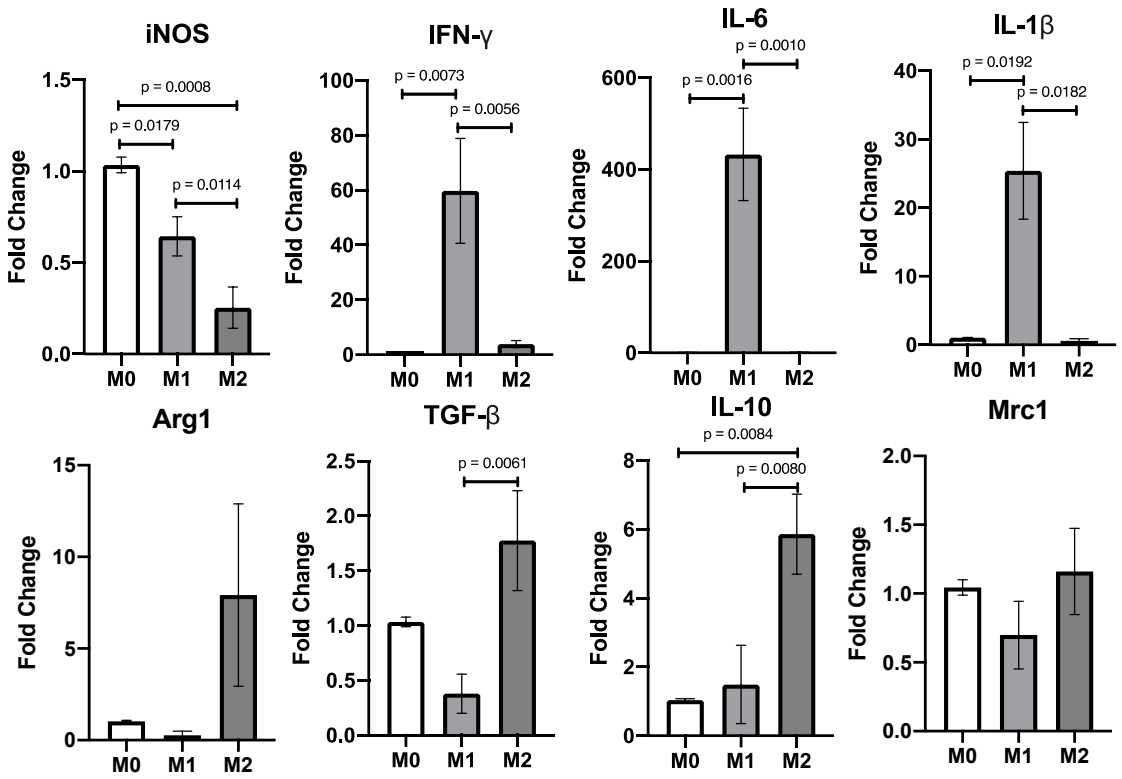

Figure 42: Relative Gene Expression of Pro-inflammatory and Anti-inflammatory markers. Data is normalized to M0 control and represented from 3 biological replicates and (n = 3) technical replicates. Values are shown as Mean Fold Change ± SEM

7.3.4 Cytokine Bioactivity Assays

A set of *in vitro* assays were completed to characterize the effect of mesh on macrophages as well as the bioactivity of the IL-4 loaded onto the coated mesh. Three different groups (Pristine, Polymer-only, IL-4 coated) of mesh were incubated with macrophages. The macrophages were immunolabeled with RAM11, assessed for nitric oxide production, arginase activity, and gene expression for pro-inflammatory/anti-inflammatory markers. At the end of cultures, both coated mesh groups did not inhibit the ability for macrophages to grow. However, there was an overall decrease in the number of RAM11+ cells observed in the cultures with mesh as opposed to the cultures treated with cytokines.

The nitric oxide Griess reagent system assay measured the production of nitric oxide in all groups of macrophage cultures. The assays showed that cells exposed to the pristine mesh group produced a significantly high amount of nitrite concentration compared to the other groups (M0, $p < 0.0001$; IL-4 Coated Mesh, $p < 0.001$; Polymer only coated mesh, $p < 0.001$) (Figure 45). This indicates that the cells activated towards the M1 pro-inflammatory phenotype when cultured with pristine mesh. However, when cells were cultured with IL-4 coated mesh or the polymer-only coated mesh, there was significantly less nitrite production when compared between mesh group and the M1 polarized (IFN- γ and LPS) group. These findings indicate that the IL-4 mesh and the polymer-coated mesh are capable of preventing the activation of a pro-inflammatory M1 response during *in vitro* cultures.

An arginase activity assay was used to measure the urea production in all groups of macrophage cultures. Arginase activity was measured as the μg of urea per μL of lysate. Results from the assays showed that macrophages cultured with the IL-4 coated mesh and the polymer-only coated mesh expressed an increase in urea concentration when compared to the pristine mesh

groups and the other cell culture groups M0 and M1 (Figure 45). While the activity was not as high as M2 polarized (IL-4) macrophages, this still indicates the possibility of both the IL-4 coated mesh and the polymer-only coated mesh to activate the anti-inflammatory M2 phenotype during *in vitro* cultures.

A panel of pro-inflammatory and anti-inflammatory markers were used to determine the relative gene expression in further assessing the phenotypic profile of the macrophages cultured with all mesh groups (Pristine mesh, IL-4 Coated mesh, Polymer-only Coated mesh). All A_{260}/A_{280} ratios were found above or at 2.0, which confirms purity and well-solubilization of RNA. The pristine mesh and polymer-only coated mesh expressed an overall increase in the pro-inflammatory markers (iNOS, IFN-γ, IL-6, and IL-1β) when compared with the IL-4 coated mesh. Upon observing the expression of the anti-inflammatory markers (Arg1, IL-10, TGF- β, and Mrc1), the IL-4 coated mesh showed an increase in expression when compared to the pristine mesh cultures. Interestingly, in the case of IL-10 and Mrc1 expression, the polymer-only coated mesh cultures were found to have expressed even higher in these markers than the IL-4 coated mesh or the pristine mesh. This indicates that the coating itself may have anti-inflammatory effects, as seen through these *in vitro* cultures.

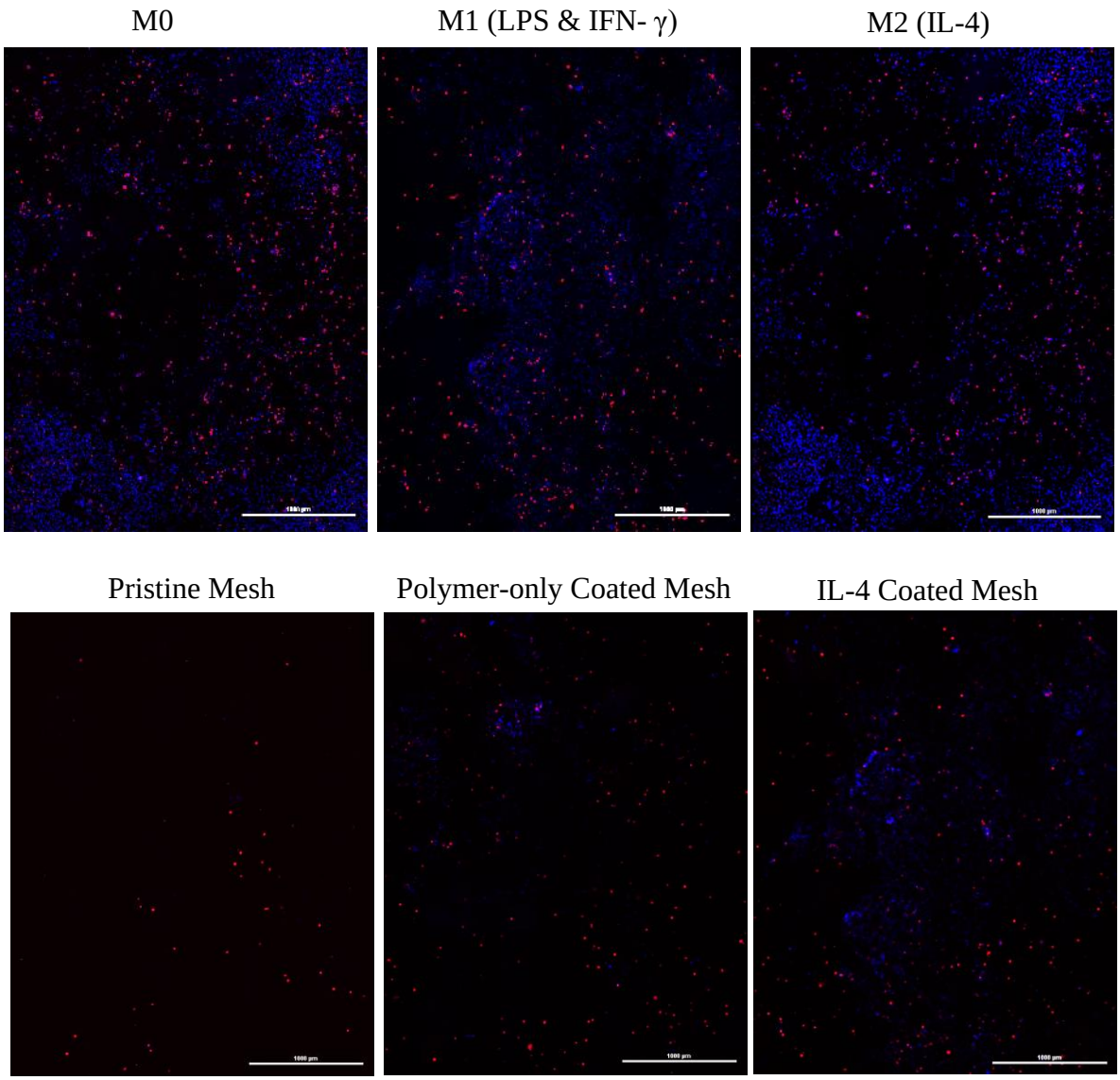

Figure 43: RAM11+ cells shown in red for all groups. Nuclei are stained with DAPI shown in blue. Scale bar is 1000 µm.

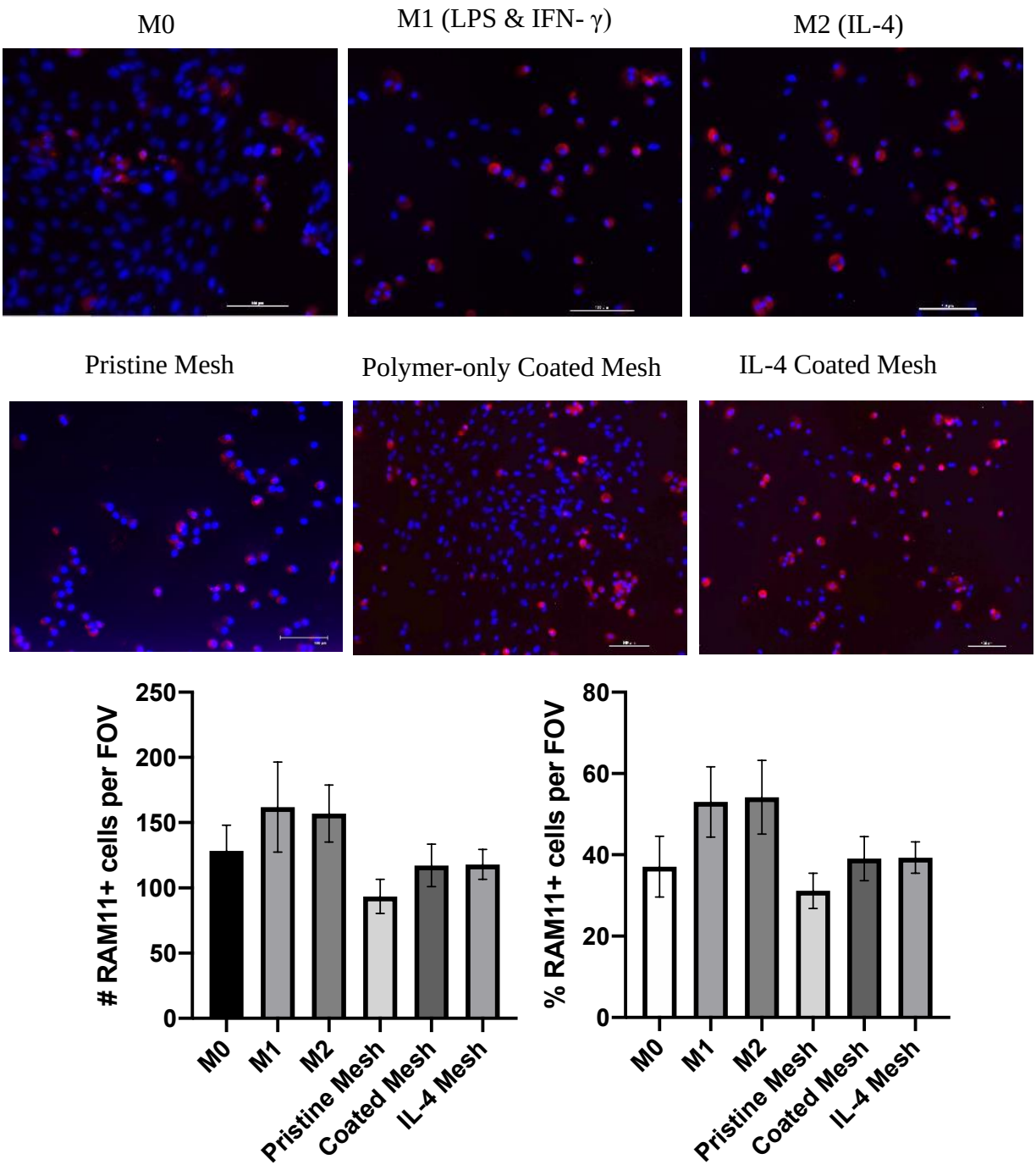

Figure 44: Magnified images of each treatment group. RAM11+ cells are shown in red, nuclei are shown in blue.

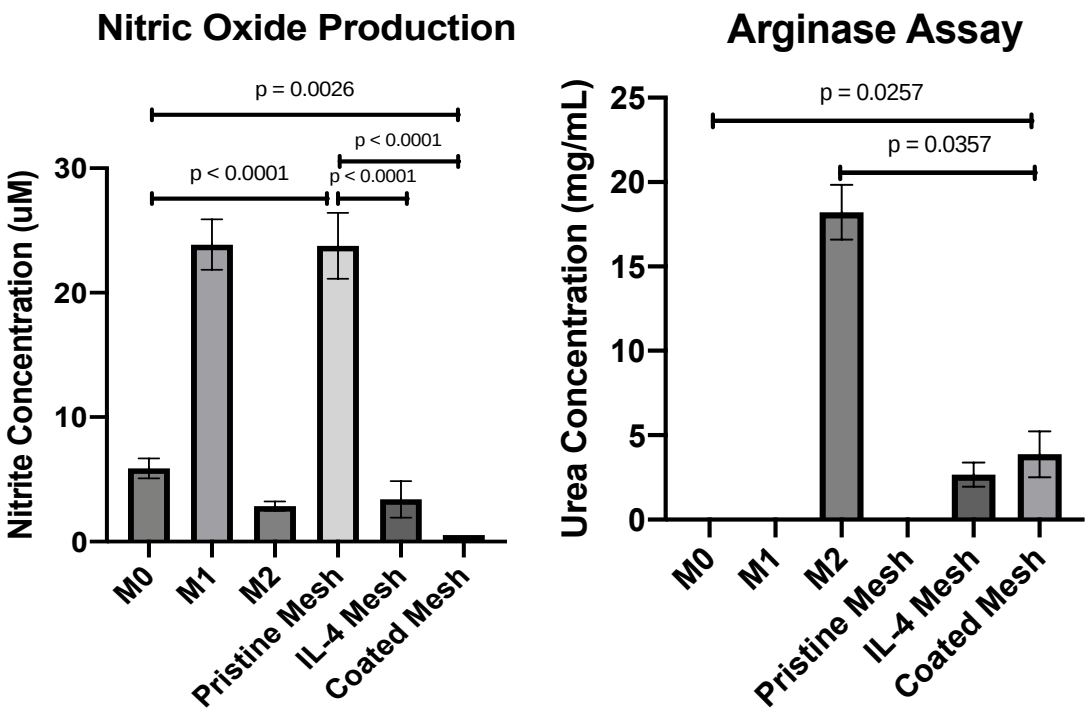

Figure 45: Functional assays with the mesh cultures. Left graph depicts nitric oxide production between groups. Right graph depicts results from arginase assay between groups. All values are shown as mean ± SEM.

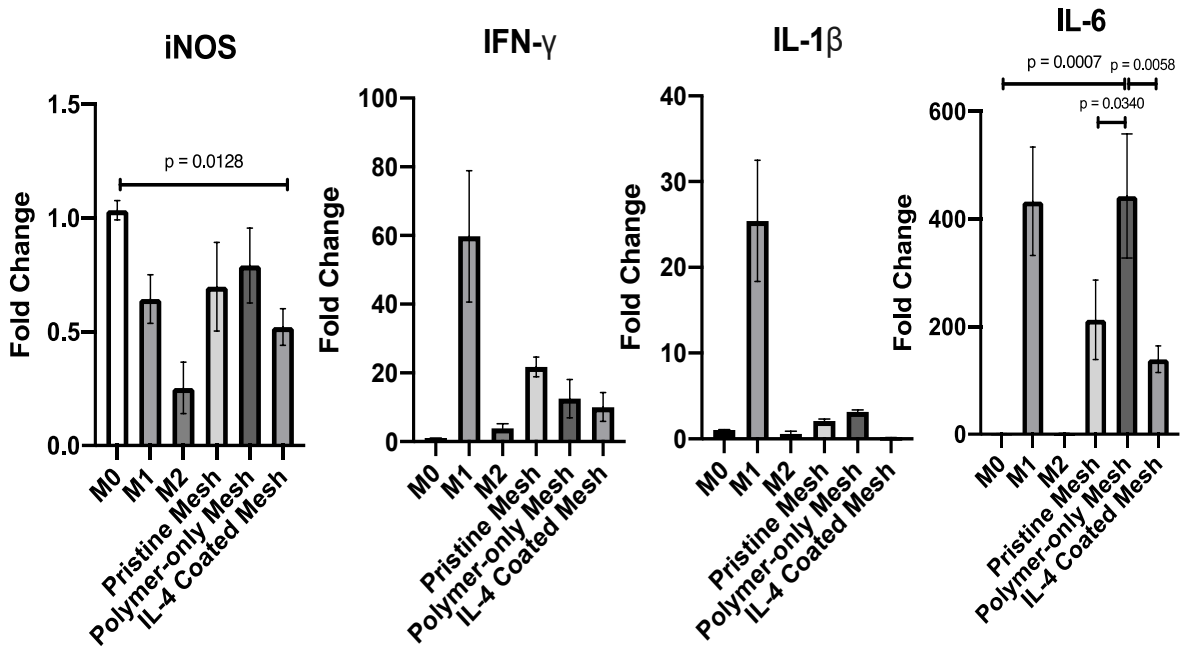

Figure 46: Relative Gene Expression of Pro-inflammatory markers from bioactivity assays. Data is normalized to M0 controls and represented from 3 biological replicates and (n = 3) technical replicates. Values are shown as Mean Fold Change ± SEM

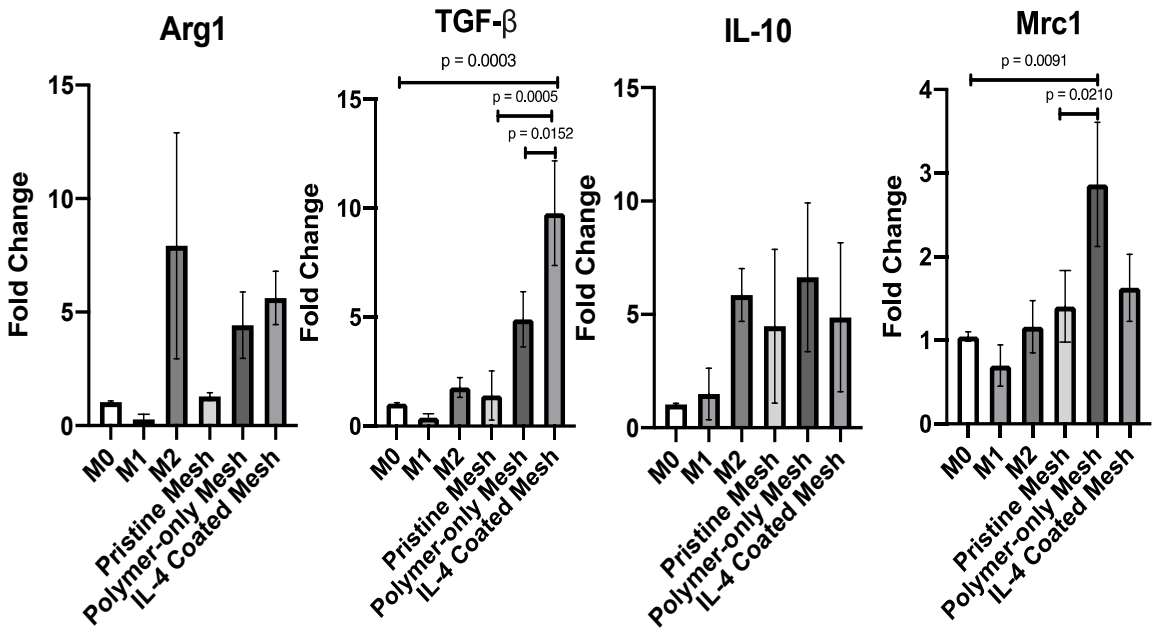

Figure 47: Relative Gene Expression of Anti-inflammatory markers from bioactivity assays. Data is normalized to M0 controls and represented from 3 biological replicates and (n = 3) technical replicates. Values are shown as Mean Fold Change ± SEM

7.3.5 Surgical Outcomes and Gross Morphologic Findings

All animals implanted with IL-4 coated mesh were closely monitored and survived until their respective time points. At the time of necropsy, all rabbits were carefully observed for the presence of adhesions and characteristics were noted according to the Mazuji classification (Table 6) of rating peritoneal adhesions [95, 96]. At both 14 and 90 days, there was noticeable scar tissue surrounding the subcutaneous implant location that is characteristic of a normal response to a material. Intra-abdominally, there were adhesions between the omentum and the internal organs, indicative of an active response to the mesh and the surgery itself. Adhesions are defined as fibrous scar tissue that connect formerly unconnected serosal exteriors of intraabdominal organs either to each other or the abdominal wall. However, at 14 days post-implantation, the adhesions observed

in the peritoneal cavity can be described as Grade 2, as in very easily separable with limited attachment at all between internal organs (Figure 48). During isolation of the vaginal implant, there was some limited attachment of bowels to the implant that was easily detached through blunt dissection. Additionally, there was no presence of any vascularized adhesion development, indicative of a severe response. At 90 days post-implantation, there was a very limited presence of adhesions in the peritoneal cavity when compared to the peritoneal space of a rabbit implanted with pristine mesh (Figure 49). The level of adhesions observed can be categorized as existing both in Grade 1 and Grade 2. Similar to the 14-day implants, it was possible to separate the adhesions that were present through simple blunt dissection, though was rarely needed. This can also be evidenced by the lack of connective tissue surrounding the vaginal implants (Figure 53) where it was easier to isolate compared to pristine mesh implants. Based on these findings, the 90-day IL-4 mesh implants were found to have the most reduced rate of peritoneal adhesion as noted by the adhesion scale and by ease of isolation of each implant.

Table 7: Adhesion grading according to Mazuji classification [95, 96]

Grade	Description of Grade
0	No adhesion
1	Very small, irregular adhesion
2	Easily separable medium intensity adhesion
3	Intense, not easily separable regular adhesion
4	Very intense, not easily separable, homogenous adhesion

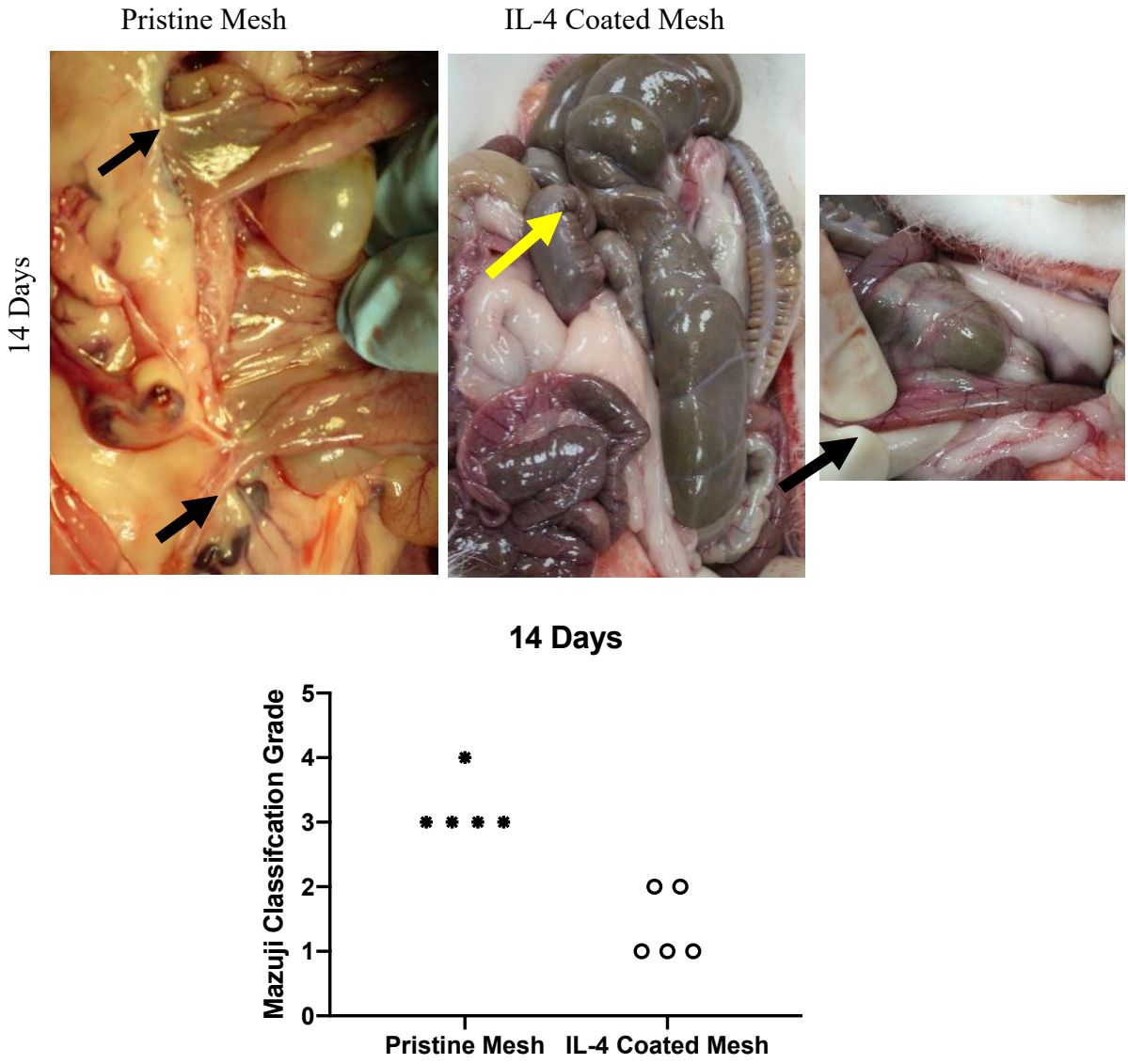

Figure 48: Representative images from 14 days post-implantation of pristine mesh (Left) and IL-4 coated mesh (both Right) indicating levels of adhesions observed at time of necropsy in the peritoneal space. Rightmost image is showcasing how easily bowels were free from adhesions.

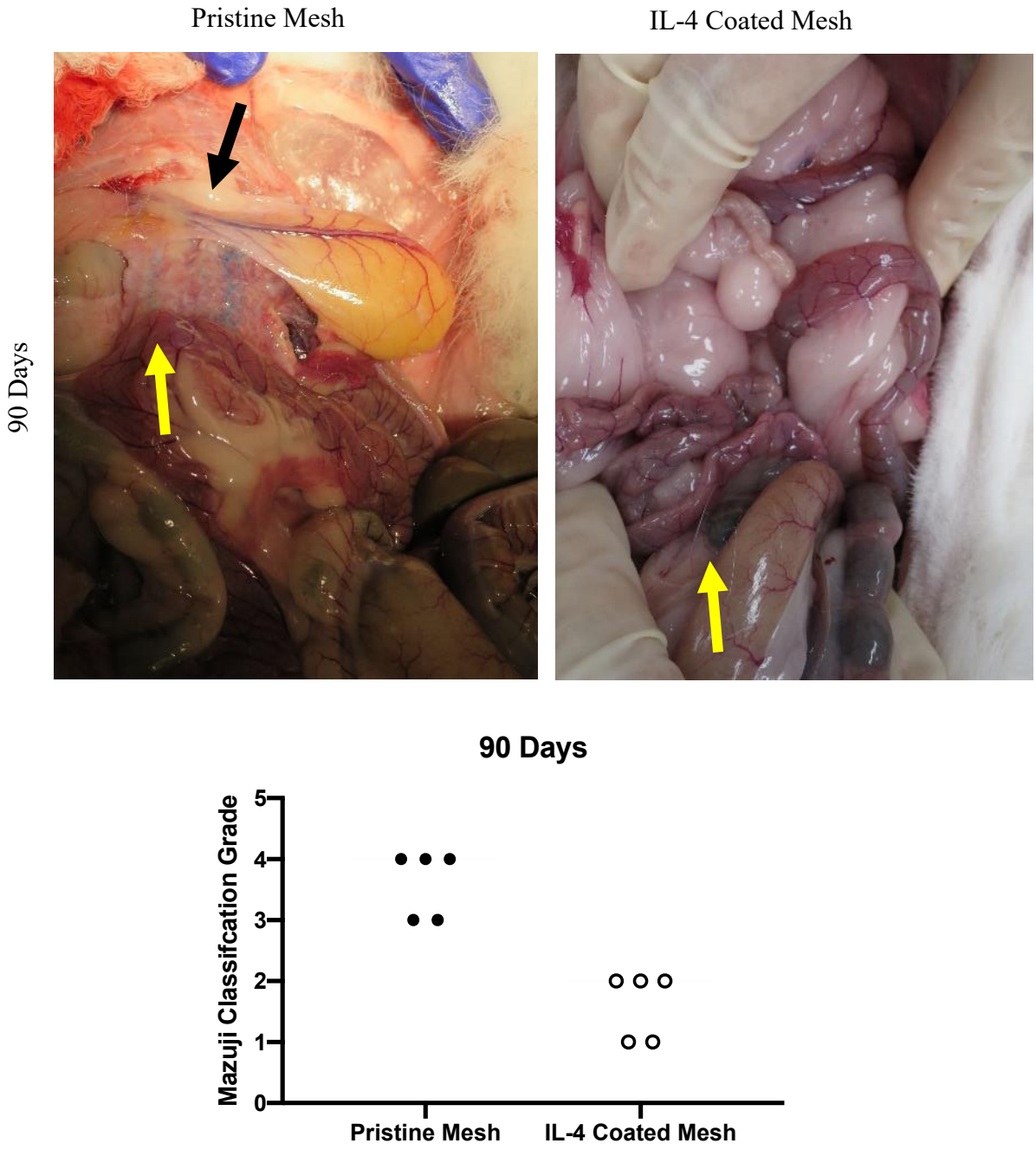

Figure 49: Representative images from 90 days post-implantation of pristine mesh (Left) and IL-4 coated mesh (Right) showcasing levels of adhesions observed during necropsy in the peritoneal body.

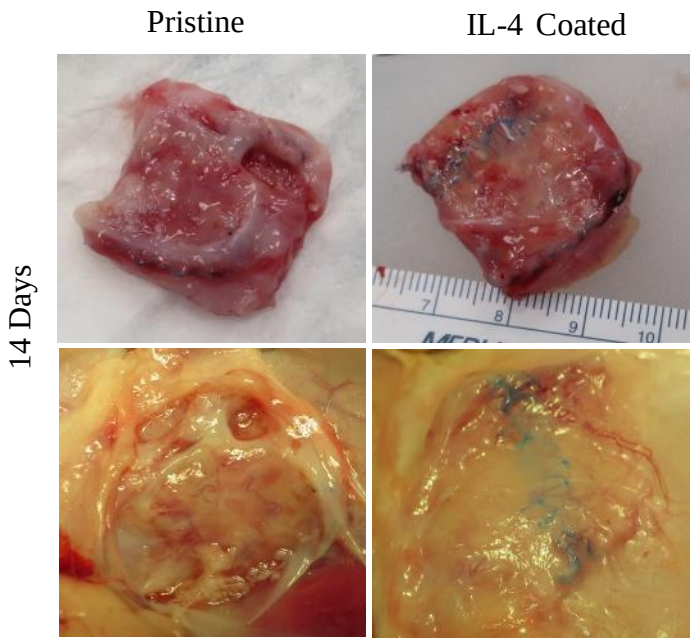

Figure 50: Subcutaneous mesh-tissue explants at 14 days post-implantation for pristine mesh and IL-4 coated mesh

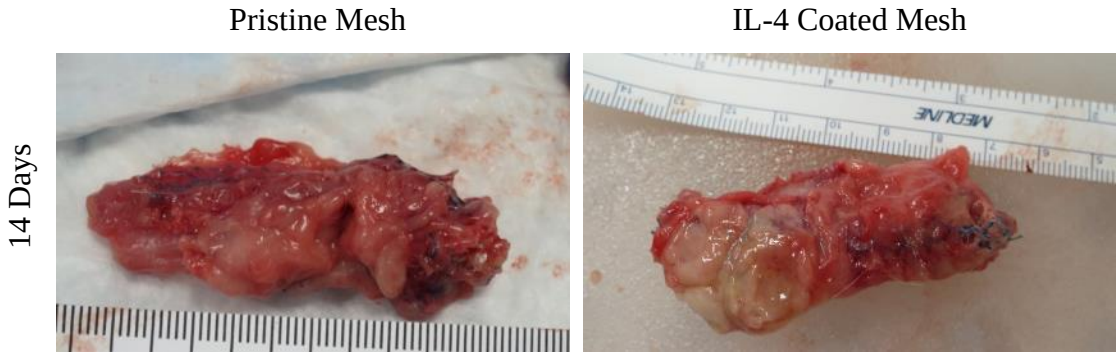

Figure 51: Vaginal mesh-tissue explants at 14 days post-implantation for pristine mesh and IL-4 coated mesh

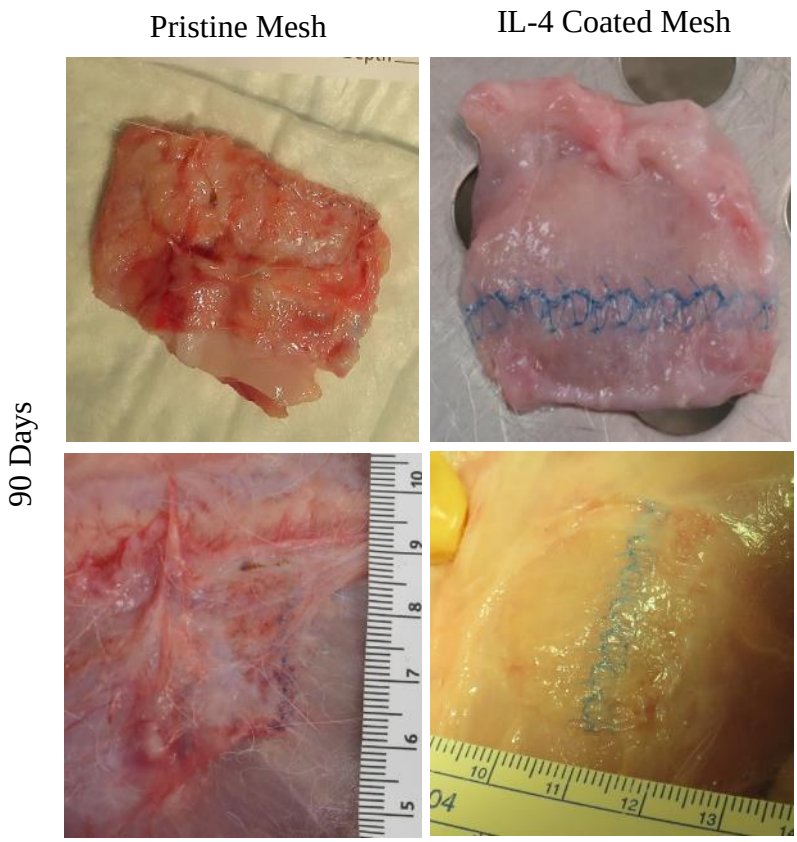

Figure 52: Subcutaneous mesh-tissue explants at 90 days post-implantation for pristine mesh and IL-4 coated mesh

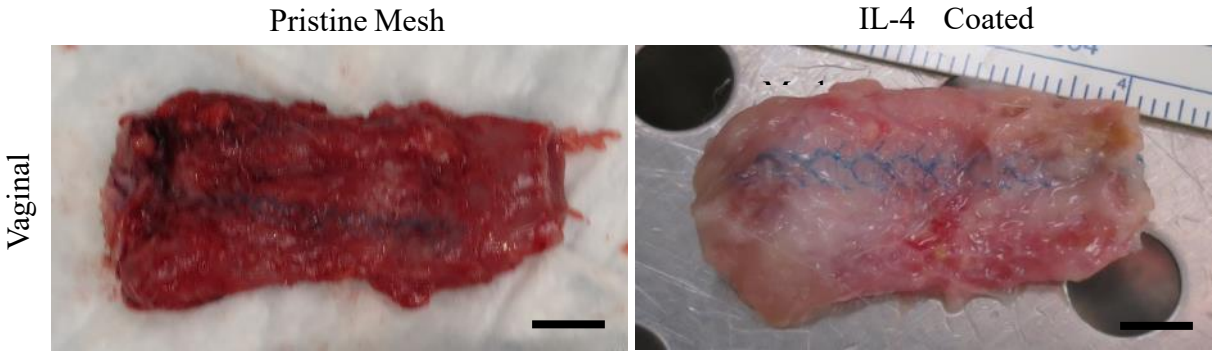

Figure 53: Vaginal mesh-tissue explants 90 days post-implantation for pristine mesh and IL-4 coated mesh

7.3.6 Histological Analysis Tissue Morphology

Histological analysis using hematoxylin and eosin staining was performed to observe the basic tissue morphology and overall architecture along with cellular characteristics and infiltration near the implants. All implants revealed a mononuclear cell population surrounding mesh fibers followed by the presence of a few foreign body giant cells. Total cellular response at 14 days post-implantation of IL-4 coated mesh implants in the vagina was increased by 21.5 % than cellular response of IL-4 coated mesh implants subcutaneously ($p = 0.0005$). Additionally, the subcutaneous IL-4 coated mesh implants had significantly higher cellularity at 14 days post-implantation compared to 90 days (42.4 % decrease at 90 days, $p < 0.0001$). Vaginal IL-4 coated mesh implants followed a similar trend with a 58.4 % decrease in cellularity surrounding mesh fibers at 90 days when compared to cellularity at 14 days post-implantation ($p < 0.0001$). There were no differences observed at 14 days post-implantation in cellularity for subcutaneous implants. However, at 14 days post-implantation, the vaginal IL-4 coated mesh implants were 32.6 % significantly higher in the total cellular response than vaginal pristine mesh implants ($p = 0.0273$). Interestingly, there were no significant differences in the total cell response to mesh fibers at 90 days regardless of the type of mesh or the anatomical location of implantation.

All mesh fibers were surrounded with an increased cluster of mononuclear cells, representative of a response to the implant itself. There were many distinct differences noted between the pristine mesh implants and the IL-4 coated mesh implants at both anatomical locations, with the most striking being the presence of organized connective tissue surrounding the IL-4 coated mesh fibers at both 14- and 90-days post-implantation. This is in addition to variations in the connective tissue architecture surrounding the implants as well. As noted in Figure 54, a distinct direction of the fibrous tissue can be characterized in both subcutaneous and vaginal IL-4

mesh implants whereas the pristine mesh implants mostly have disorganized connective tissue. However, it is important to note that not all mesh fibers in the IL-4 mesh implants displayed a straight alignment, but instead the appearance of denser connective tissue overall was observed as compared to the looser connective tissue observed in pristine mesh implants.

The dense connective tissue response can be further described as either regular or irregular, based on the orientation of fibers. The distinct alignment of the fibers in a single direction noted in Figure 54 is defined as regular connective tissue, as seen in other tissue types like tendons, etc [97]. This is commonly associated with increased tensile strength in that direction. However, in the case of irregular connective tissue, the fibers are arranged randomly in all directions. Interestingly, the fibers surrounding the IL-4 coated mesh implants remain dense and follow the fiber circumferentially, suggesting an integration into the tissue. The connective tissue fibers surrounding the pristine mesh implants are loose and do not follow a distinct pattern, and thus can suggest irregularity, such as what is observed in the skin.

Another important observation was the presence of blood vessels in a wider field of view when imaging mesh fibers. The vascularity surrounding mesh implants will be discussed in a later section, but histologically, there was a notable presence of blood vessels that appeared equidistant from the fibers all around (Figure 54 Subcutaneous IL-4 Coated Mesh implant black arrows). These were only qualitatively observed in the IL-4 mesh implants at 14- and 90-days post-implantation and not in the pristine mesh implants.

There was also the presence of eosinophils observed similarly to the pristine mesh implants, but noticeably a farther distance away from the mesh fibers. However, these were mostly observed at 14 days post-implantation. Additionally, after 14 days, in a few fibers, it was possible

to still see remnants of the coating (Figure 58, black arrows). This is especially interesting because it indicates that the *in vitro* assays are difficult to correlate directly to *in vivo* profiles.

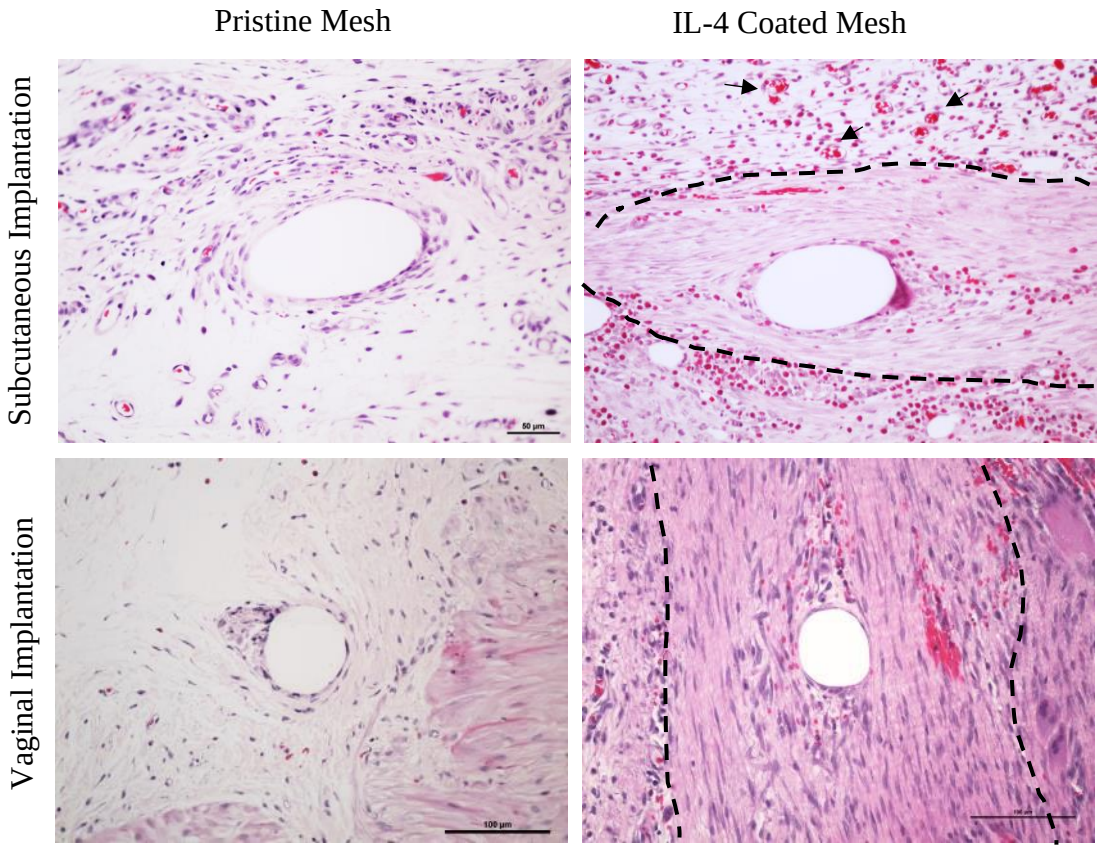

Figure 54: Representative histological hematoxylin and eosin images of pristine mesh and IL-4 coated mesh implants at 14 days post implantation. Black dashes indicate differences in aligned connective tissue observed that was not present in pristine mesh implants

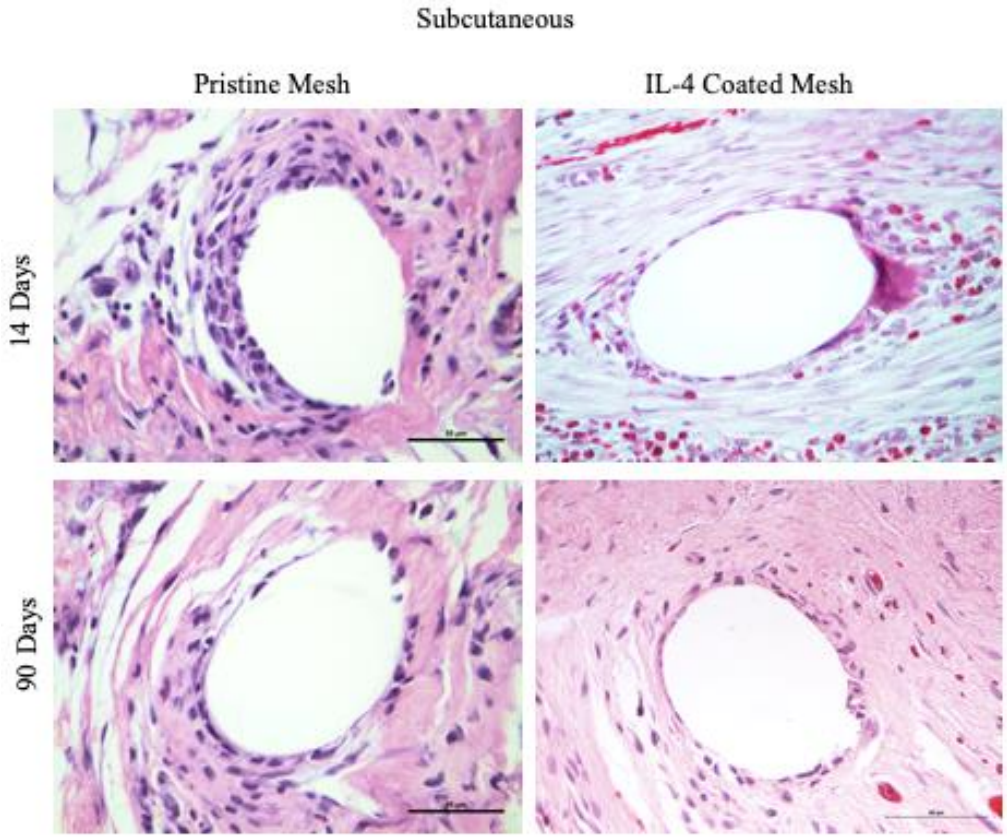

Figure 55: Representative H&E images of Pristine Mesh and IL-4 Coated Mesh subcutaneous implants at 14- and 90-days post-implantation. ***All scale bars are 50 µm.***

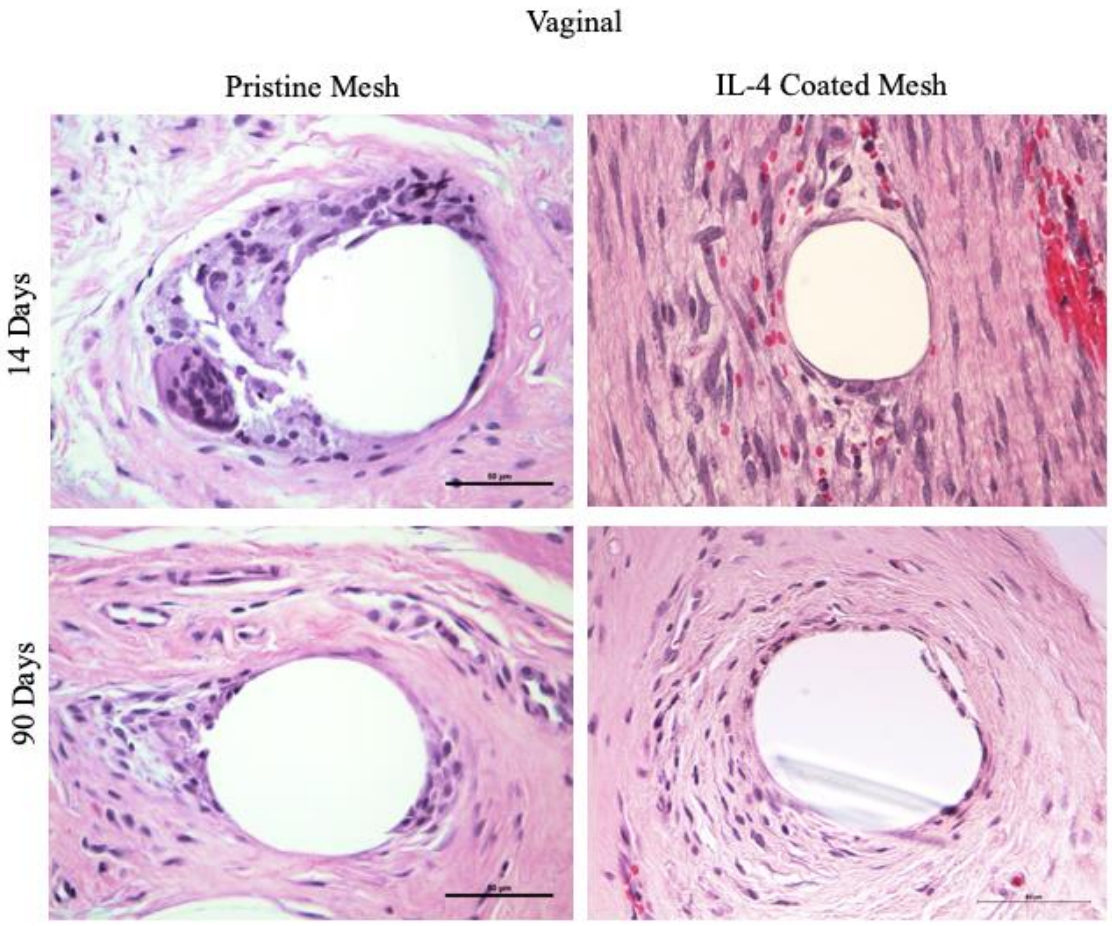

Figure 56: Representative H&E images of Pristine Mesh and IL-4 Coated Mesh vaginal implants at 14- and 90-days post-implantation. ***All scale bars are 50 µm.***

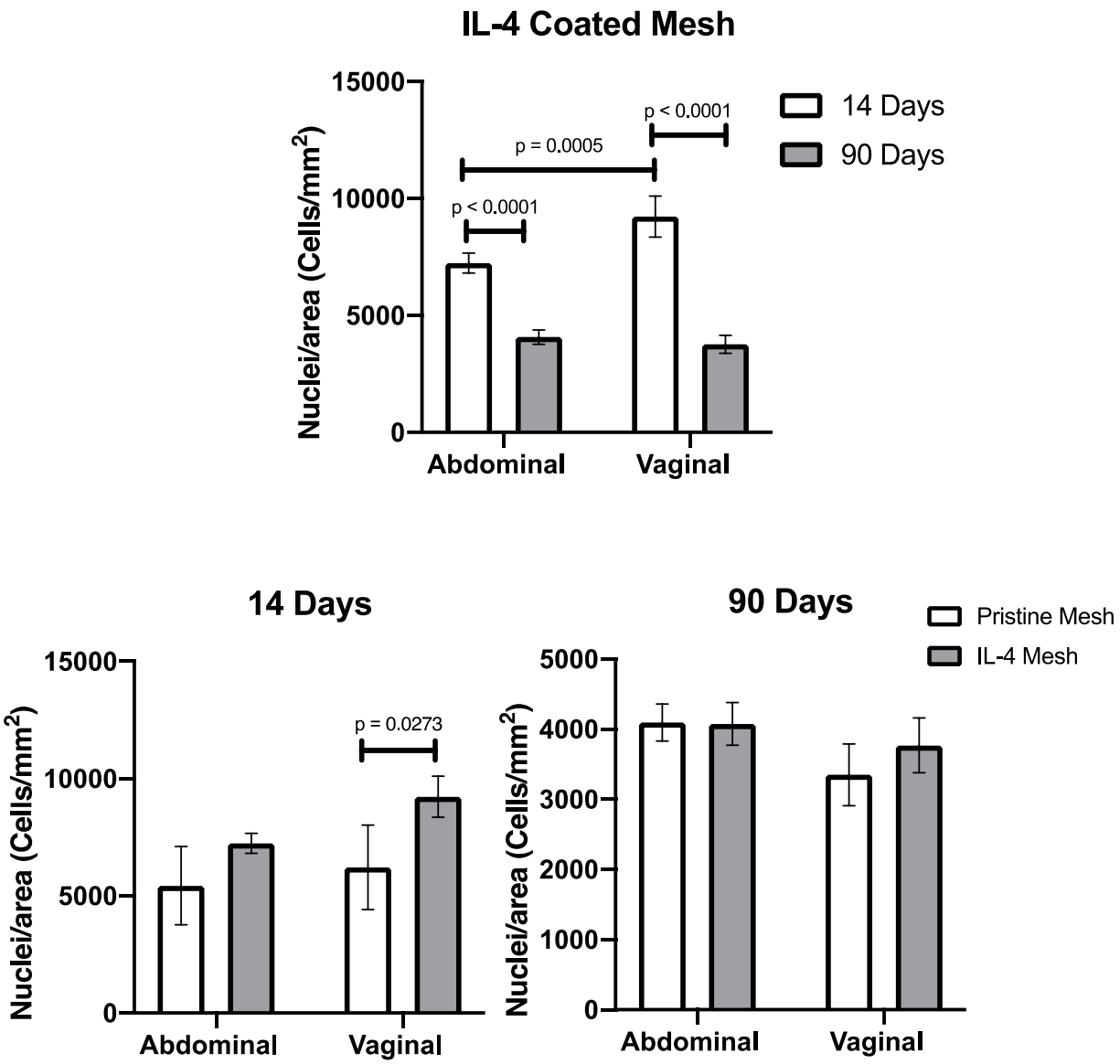

Figure 57: Quantified cellular response of host response to pristine mesh and iL-4 coated mesh. Data shown as mean ± SEM consisting of biological replicates (n = 5) with 5 – 7 fibers imaged per slide.

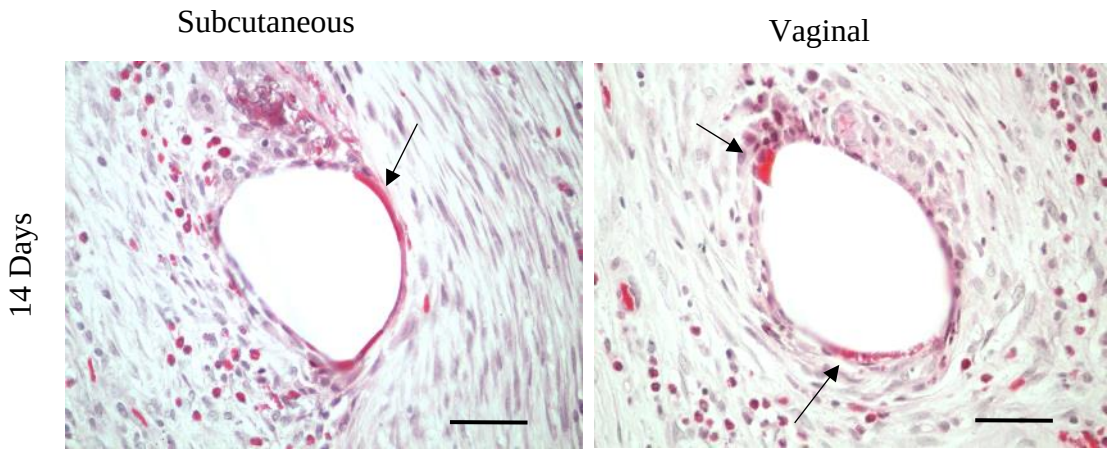

Figure 58: IL-4 coated mesh fibers with remnants of the coating present after 14 days of implantation. Indicated by the black arrows. All scale bars are 50 µm

7.3.7 Collagen Quantitative Analysis

Masson's trichrome staining revealed the presence of a collagen capsule surrounding all mesh fibers in both subcutaneous and vaginal IL-4 coated mesh implants. The subcutaneous IL-4 coated mesh implants showed a 14.6 % increase in the % collagen area surrounding mesh fibers from 14 days to 90 days post-implantation ($p = 0.0263$, Figure 60). Additionally, there were significant differences in collagen formation at 14 days between the subcutaneous and vaginal implants with vaginal implants showing on average 15.5 % more collagen area surrounding mesh fibers than the subcutaneous implants ($p = 0.0241$, Figure 60). Interestingly, there were no significant differences found in % collagen area surrounding IL-4 coated mesh fibers in vaginal implants between 14- and 90-days post-implantation. However, upon comparison to the pristine mesh implants, both subcutaneous and vaginal implants significantly showed higher % collagen

at 14 days in the IL-4 coated mesh (subcutaneous, $p = 0.0001$; vaginal, $p = 0.0001$, Figure 60). The same trend was observed for subcutaneous implants at 90 days post-implantation, where the IL-4 coated mesh implants were found to have significantly higher % collagen than the pristine mesh implants ($p < 0.0001$). However, there were no significant differences determined at 90 days between the pristine mesh and the IL-4 coated mesh for the vaginal implants.

An interesting observation in the IL-4 coated mesh implants was the presence of dense collagen fibers surrounding individual mesh fibers (Figure 59). As mentioned previously, this characteristic is unique to the IL-4 coated mesh implants and observed with a distinct aligned tissue in one direction. In some cases, the collagen fibers had densely formed circumferentially around the mesh fibers, almost as though everything was being incorporated into the tissue. Other research involving the implantation of extracellular matrix scaffolds have shown similar findings consistent with a constructive remodeling response, specifically with an increase in the pro-regenerative activated M2 macrophage behavior[44, 51, 98, 99].

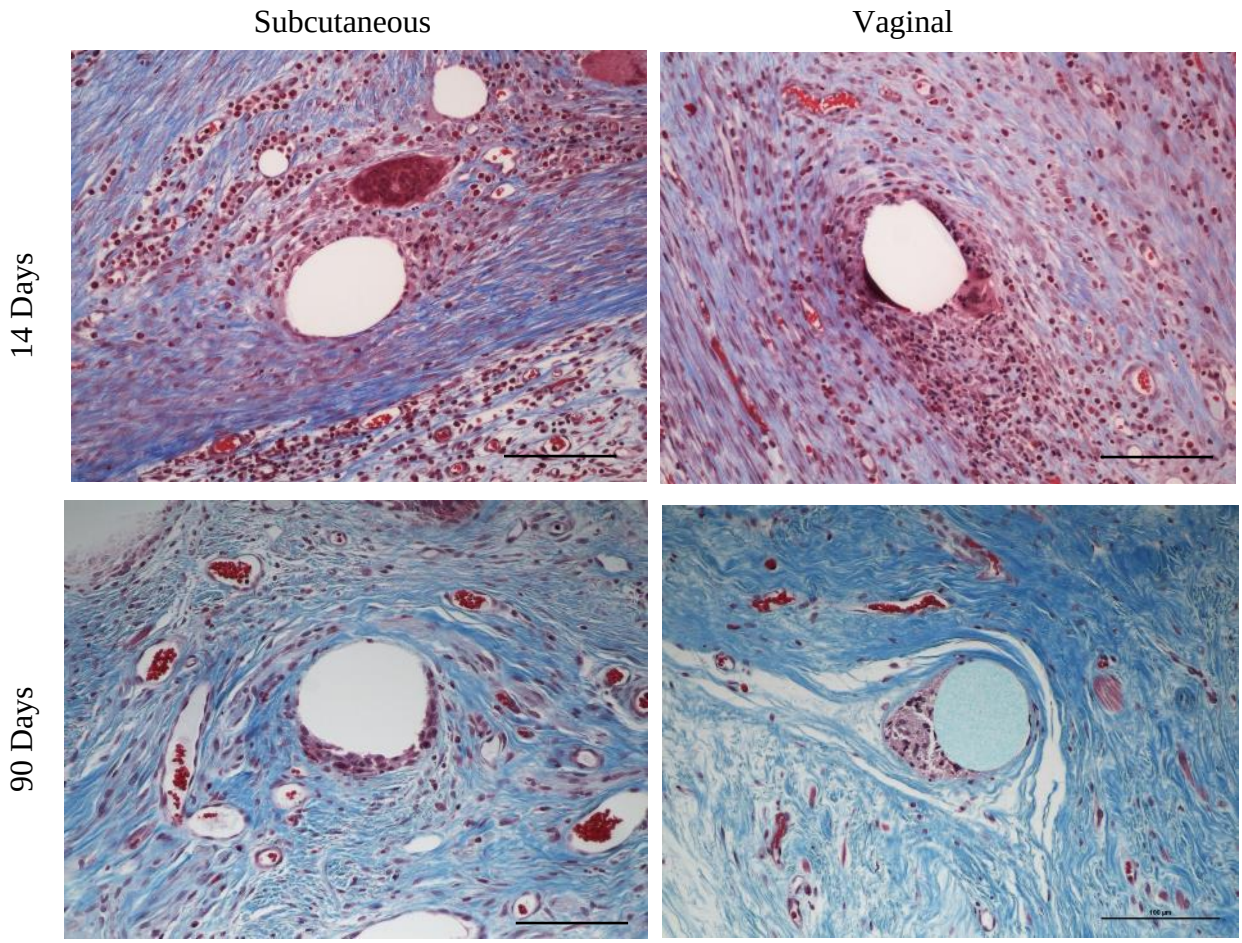

Figure 59: Representative images of Masson's Trichrome for subcutaneous and vaginal mesh-tissue implants at 14- and 90-days post-implantation of IL-4 coated mesh. All scale bars are 100 µm

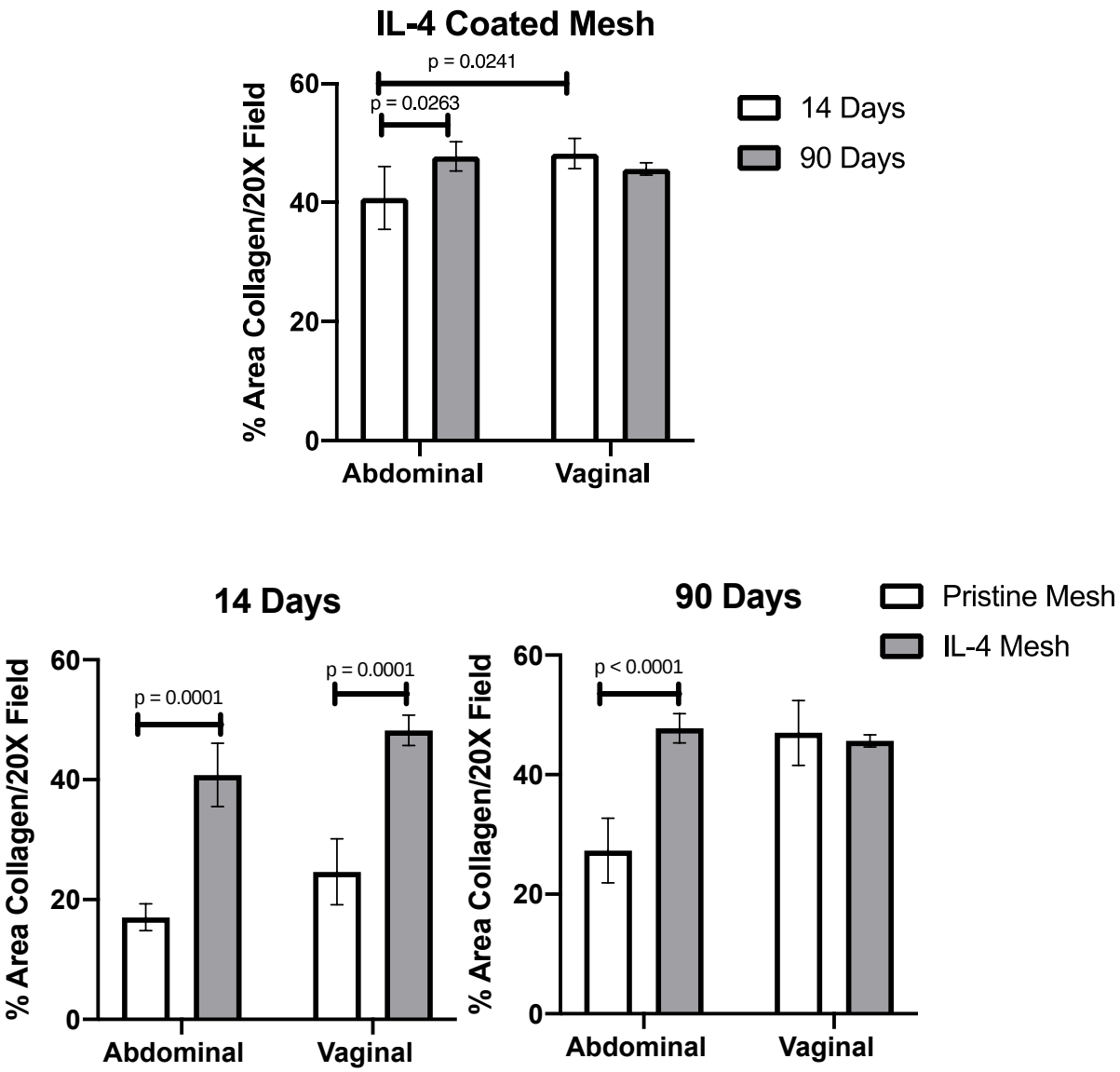

Figure 60: % Area Collagen Quantification of Masson's Trichrome staining using ImageJ algorithm. Data shown as mean ± SEM.

7.3.8 Angiogenesis Analysis

At both 14- and 90-days post-implantation, all IL-4 coated mesh implants showed the presence of blood vessels surrounding individual mesh fibers (Figure 61). In order to label endothelial cells lining blood vessels, especially those that are newly formed, a CD31 marker was used via immunohistochemistry techniques. Interestingly, there were no significant differences observed between groups of the IL-4 coated mesh implants at either 14 day or 90 days of implantation or based on anatomical location, either subcutaneous or vaginal. However, compared to the pristine mesh group, both subcutaneous and vaginal IL-4 coated mesh implants had significantly higher CD31+ blood vessel density found at both 14 days and 90 days (subcutaneous 14 days ($p = 0.0068$); vaginal 14 days ($p < 0.0001$), subcutaneous 90 days ($p = 0.0167$); vaginal 90 days ($p = 0.0128$)). This indicates a trend that the IL-4 coated mesh induced an increase in blood vessel density surrounding individual mesh fibers. This was confirmed through histological examination as mentioned in earlier sections (Figure 54).

A unique observation at 90 days was the presence of blood vessels directly outside the perimeter of individual mesh fibers of both subcutaneous and vaginal IL-4 coated mesh implants as noted in Figure 63. This indicates an enhanced vascular permeability shown in the response to the IL-4 coated mesh implants. Additionally, by visual qualitative observation, it was possible to notice an increase in the presence of blood vessels surrounding individual mesh fibers as noted in Figure 64.

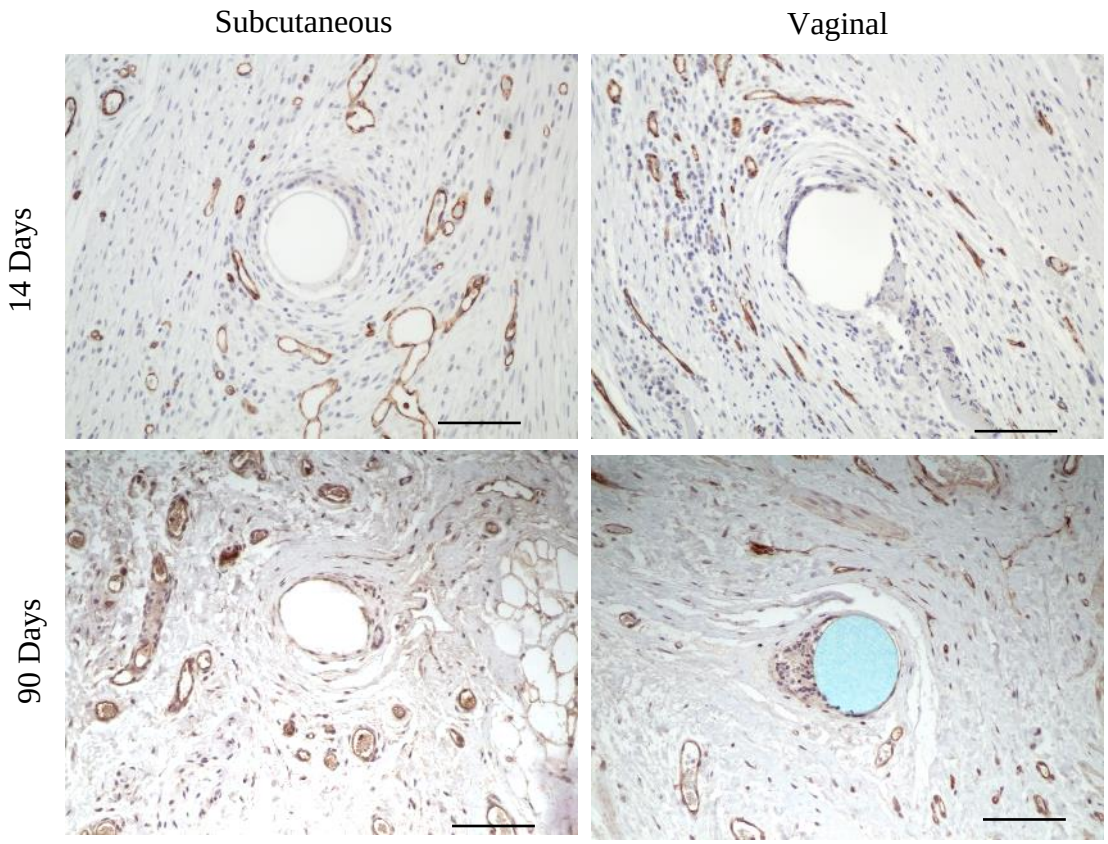

Figure 61: anti-CD31 immunolabeling of subcutaneous and vaginal IL-4 coated mesh implants 14- and 90-days post-implantation. All scale bars are 100 µm.

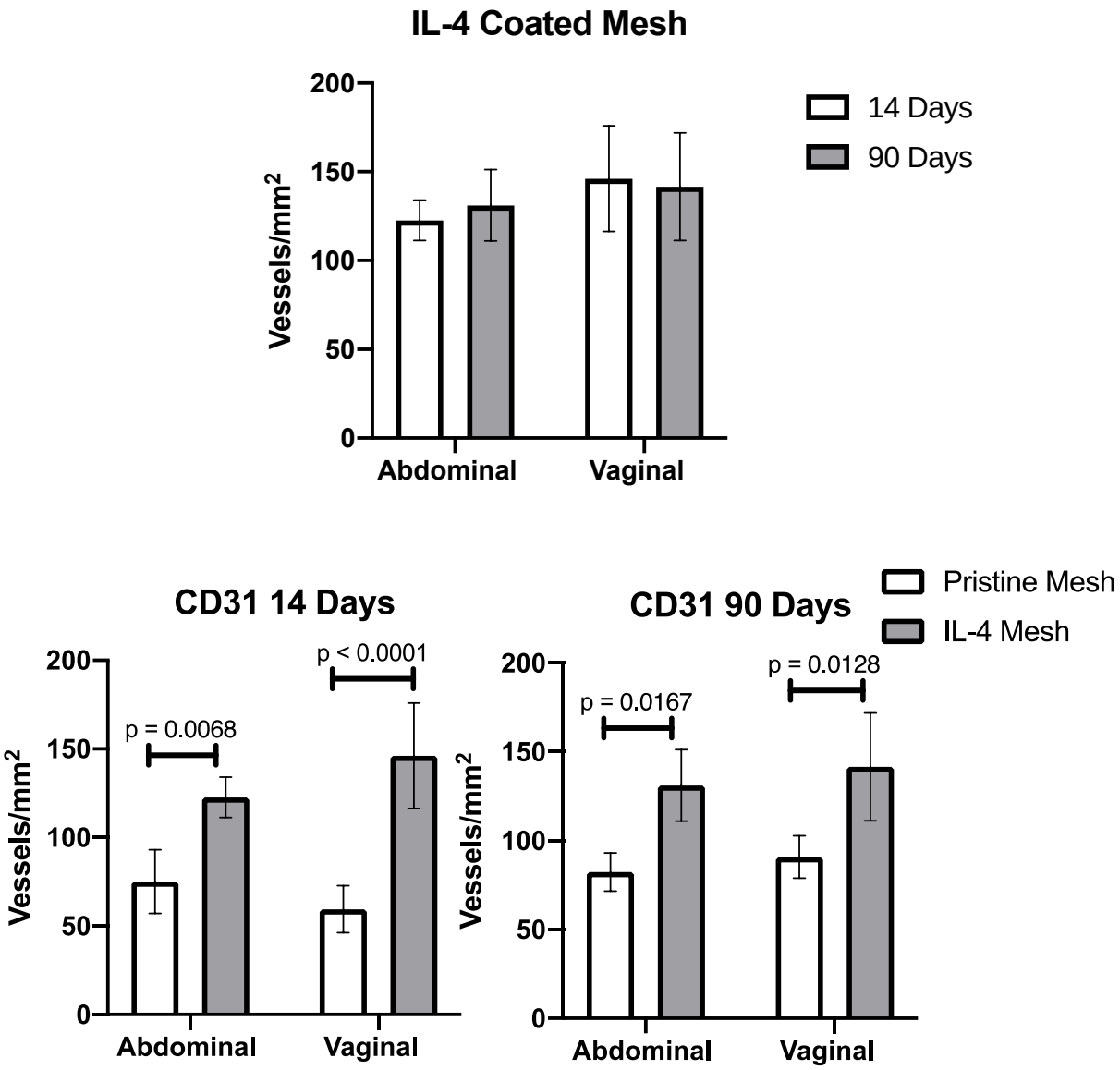

Figure 62: Quantitative analysis of CD31+ blood vessels in mesh implants. Data shown as mean ± SEM.

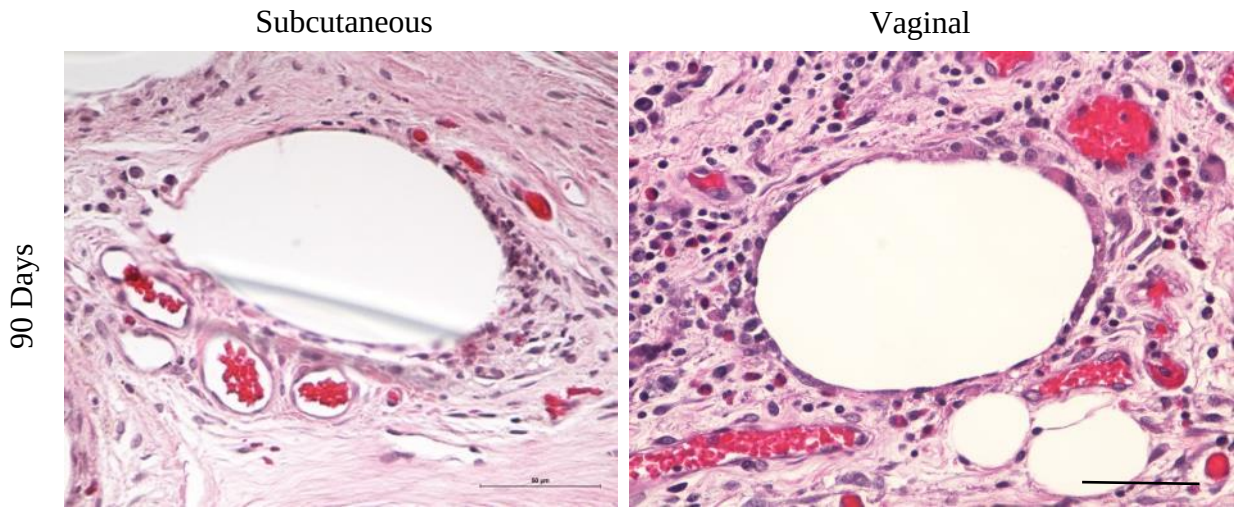

Figure 63: Notably increased blood vessels surrounding IL-4 coated mesh fibers in both subcutaneous and vaginal implants at 90 days post-implantation. All scale bars are 50 µm.

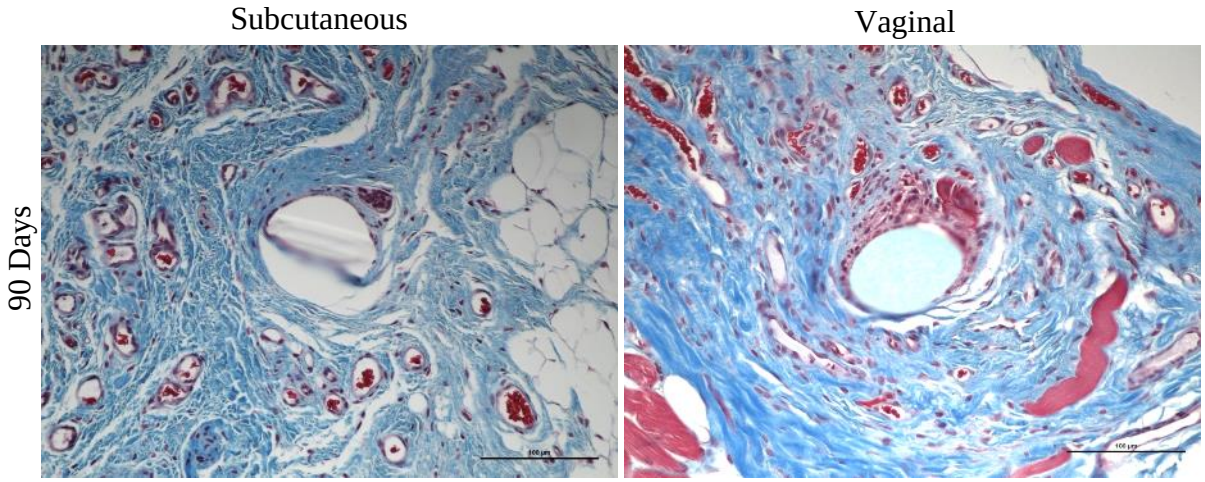

Figure 64: Notably increased presence of blood vessels surrounding individual IL-4 coated mesh fibers in another field of view with Masson's trichrome staining in both subcutaneous and vaginal implants at 90 days post-implantation. All scale bars are 100 µm.

7.3.9 Macrophage Analysis

All IL-4 coated mesh implants elicited an immune response at 14 days which remained present at 90 days post-implantation (Figure 65). A pan-macrophage marker, RAM11, was utilized to immunolabel the presence of macrophages surrounding individual mesh fibers. In the case of both subcutaneous and vaginal IL-4 coated mesh implants, there was a significant decrease in the number of macrophages (subcutaneous 35.2 % decrease, $p = 0.0033$; vaginal 44.8 % decrease, $p = 0.0003$) from 14 days to 90 days post-implantation (Figure 66). Upon comparing to the pristine mesh group, the IL-4 coated mesh had significantly higher macrophage number at 14 days in the subcutaneous implantation ($p < 0.0001$). However, there were no significant differences between the pristine mesh and IL-4 coated mesh in the vaginal implantation at 14 days. Interestingly, comparing vaginal implantation site at 90 days, there were significantly less macrophages in the IL-4 coated mesh implants than the pristine mesh implants ($p = 0.0036$). There were no significant differences observed in the subcutaneous implantation site when comparing between pristine mesh and IL-4 mesh groups at 90 days.

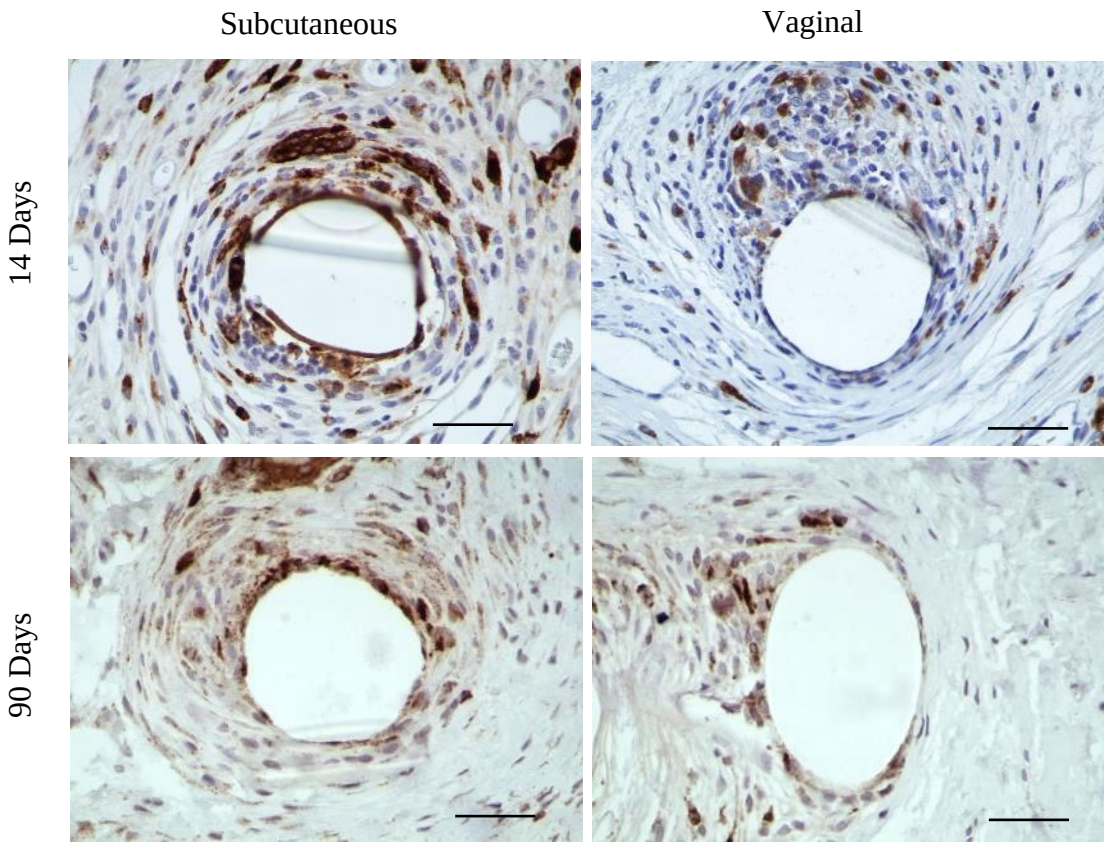

Figure 65: anti-RAM11 immunolabeling of subcutaneous and vaginal IL-4 coated mesh implants at 14- and 90-days post-implantation. All scale bars are 50 µm

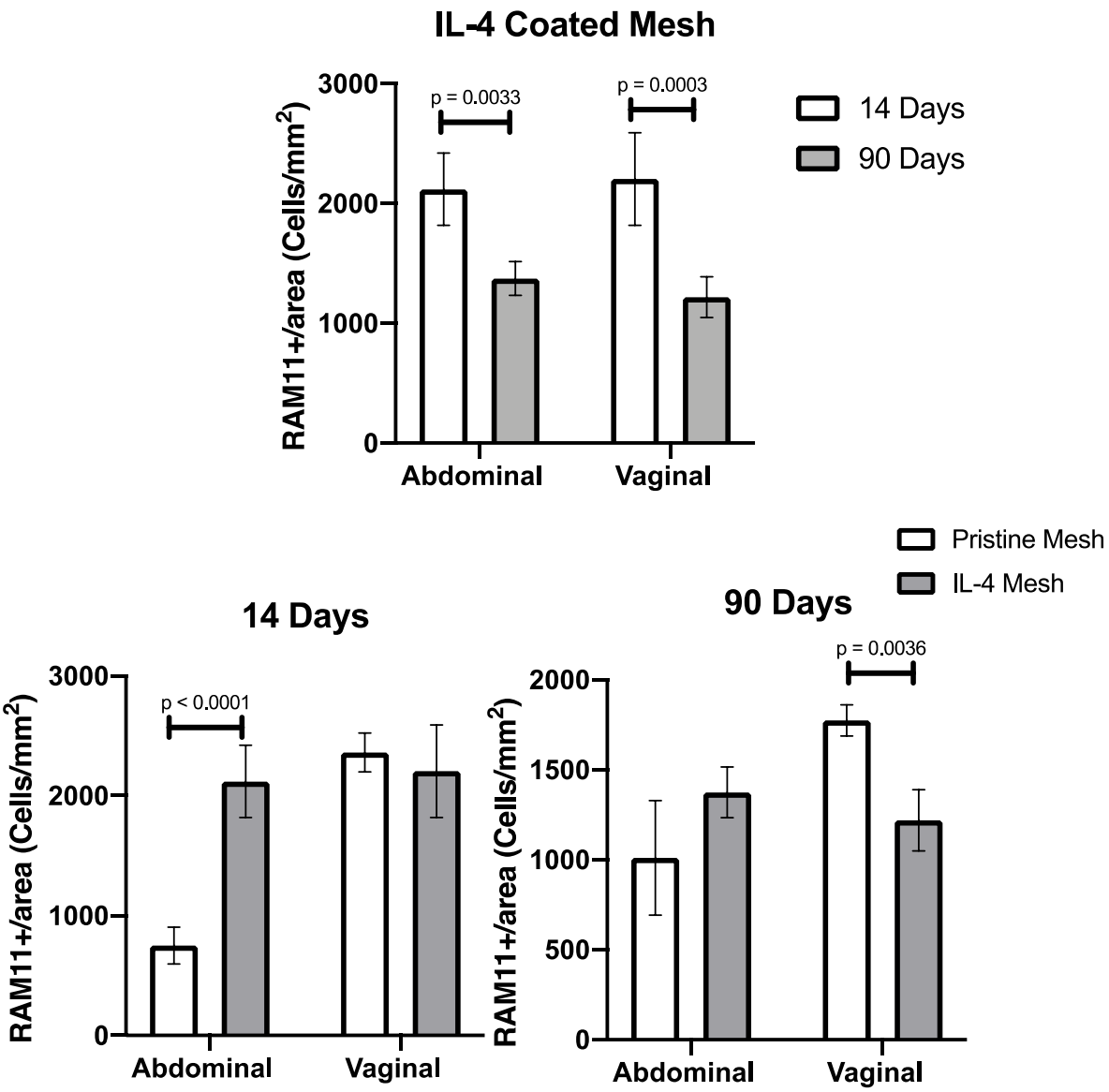

Figure 66: RAM11+ immunolabeling of macrophages surrounding individual mesh fibers both subcutaneous and vaginal implantation. Data shown as mean ± SEM.

7.3.10 Elastin Qualitative Analysis

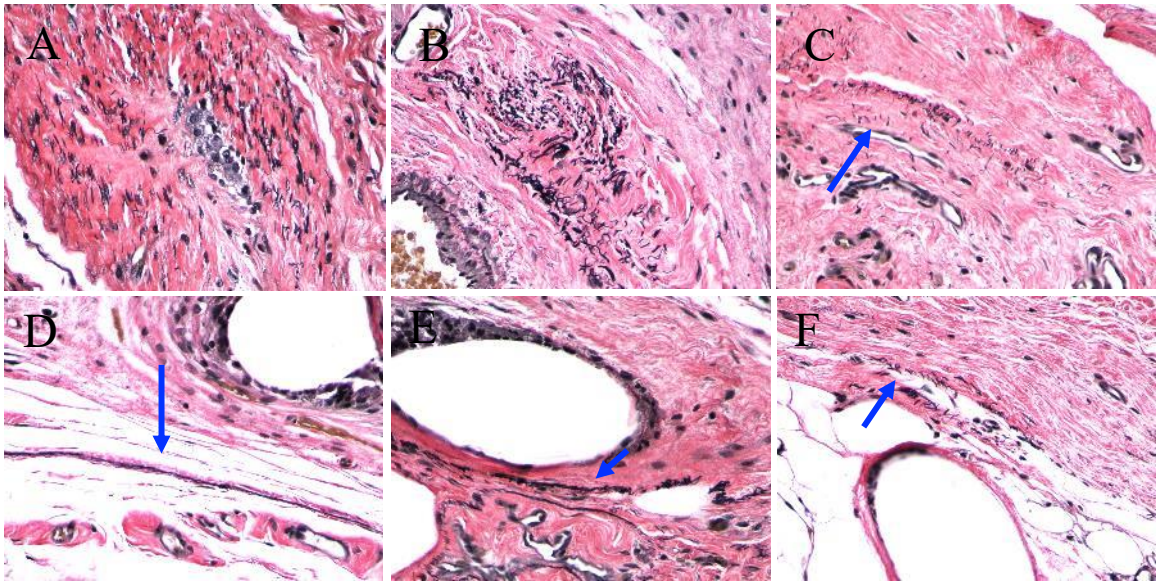

Figure 67: A, B, D, E. Elastic fibers in IL-4 coated mesh vaginal implants at 14 days post-implantation. C & F. Elastic fibers in IL-4 coated mesh vaginal implants at 90 days post-implantation.

Similar to the pristine mesh implants, a noticeable difference in the elastic fiber presence was observed at 14 days in the IL-4 coated mesh implants (Figure 67). Fragmented fibers were observed throughout the vaginal tissue and in particular near the mesh fibers, a fragmented singular elastic response was detected. Additionally, at 90 days post-implantation, similarly fragmented elastic fibers can be seen (Figure 67C). However, it was possible to observe elastic fibers in the vicinity of a mesh fiber, which was not possible with earlier pristine mesh implants (Figure 67F). Nevertheless, these fragmented elastic fibers are still indicative of a maladaptive tissue response.

7.3.11 Gene Expression Analysis

In order to further understand the inflammatory response in the tissue explants, TaqMan gene expression assays were performed using a series of pro-inflammatory and anti-inflammatory markers. All A_{260}/A_{280} ratios were found above or at 2.0, which confirms purity and well-solubilization of RNA extracted. The subcutaneous implants were normalized to abdominal muscle control tissue and vaginal implants were normalized to vaginal control tissue. At 14 days, subcutaneous pristine mesh implants showed increased expression in all pro-inflammatory markers, but significantly increased expression in IFN-γ and IL-1β when compared to abdominal muscle control (IFN-γ, $p = 0.0014$; IL-1β, $p = 0.0008$) and IL-4 coated mesh (IFN-γ, $p = 0.0011$, IL-1β, $p = 0.0003$) (Figure 68). However, IL-4 coated mesh implants were significantly upregulated in IL-6 expression when compared to abdominal muscle controls ($p = 0.0161$). There were no significant differences observed in iNOS expression, however both mesh implants did show a trend of increased expression.

At 14 days, the subcutaneous IL-4 coated mesh implants were associated with a significant increase in the anti-inflammatory markers (TGF-β, IL-10, and Mrc1) when compared to pristine mesh implants (TGF- β, $p = 0.0003$; IL-10, $p = 0.0030$; Mrc1, $p = 0.0348$) (Figure 69). There were no significant differences observed in the Arg1 expression between mesh groups. This indicates that the IL-4 eluted from the coating does have a direct impact on the inflammatory profile of the surrounding tissue. Similarly, at 14 days, the vaginal pristine mesh implants were significantly upregulated in the pro-inflammatory markers, IFN-γ and IL-1β when compared to the vaginal control (IFN-γ, $p = 0.0037$; IL-1β, $p = 0.0050$) and the IL-4 coated mesh implants (IFN-γ, $p = 0.0081$; IL-1β, $p = 0.0012$) (Figure 70). Similar to the abdominal implants, the IL-4 coated mesh implants were significantly upregulated in IL-6 expression when compared to the vaginal controls

(p = 0.0129). There were no significant differences observed for iNOS expression, however the values did trend towards an increase in expression in the mesh implants. The vaginal IL-4 coated mesh implants were significantly upregulated in Arg1 and TGF-β expression at 14 days (Arg1, p = 0.0316; TGF-β, p = 0.0167) (Figure 71). There were no significant differences observed in expression of IL-10 and Mrc1 between groups.

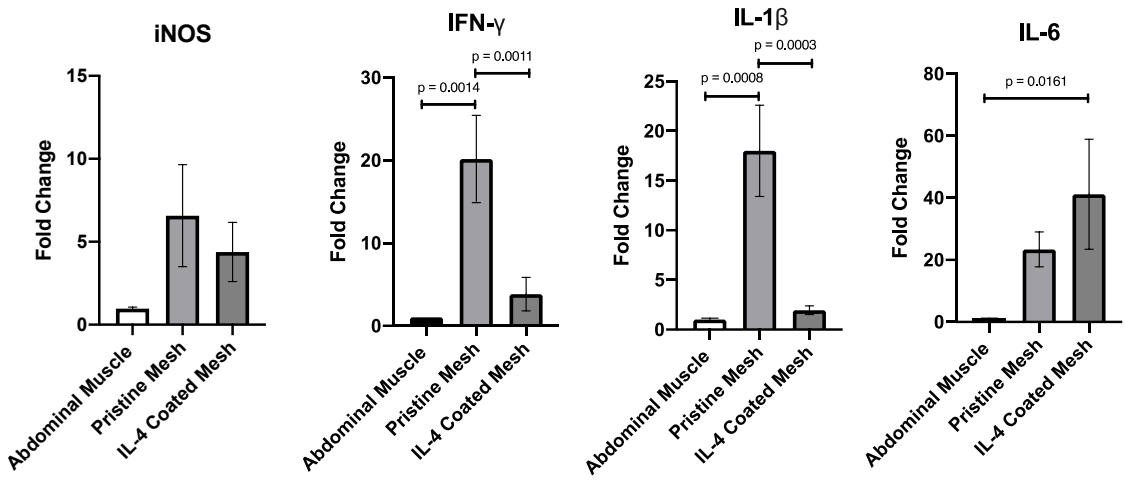

Figure 68: Rabbit Subcutaneous Pro-inflammatory profile at 14 days post-implantation. Samples are normalized to abdominal muscle control. Data is shown as (n = 3 – 5) biological replicates with (n = 3) technical replicates. Values are represented as mean fold change ± SEM

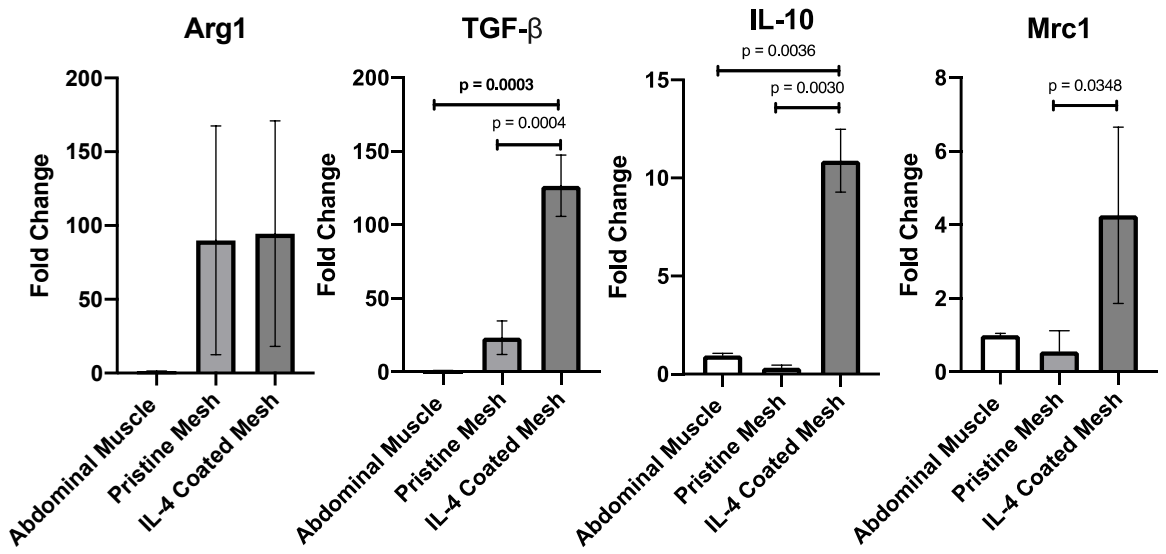

Figure 69: Rabbit Subcutaneous Anti-inflammatory profile at 14 days post-implantation. Samples are normalized to abdominal muscle control. Data is shown as (n = 3 – 5) biological replicates with (n = 3) technical replicates. Values are represented as mean fold change ± SEM

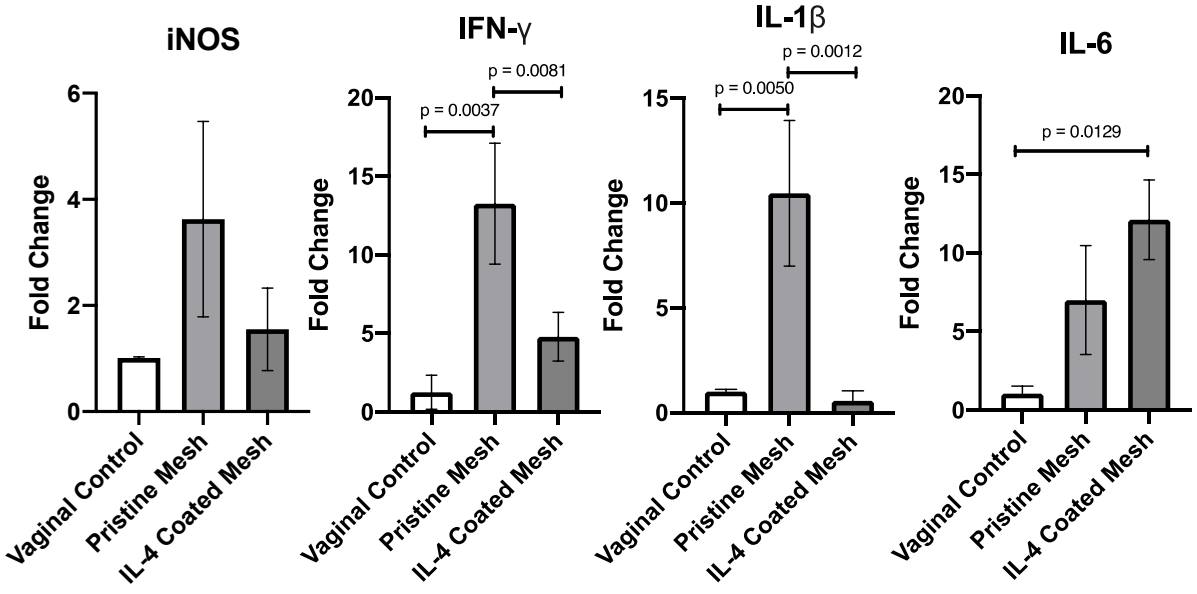

Figure 70: Rabbit Vaginal Pro-inflammatory profile at 14 days post-implantation. Samples are normalized to Vaginal control. Data is shown as (n = 3 – 5) biological replicates with (n = 3) technical replicates. Values are represented as mean fold change ± SEM

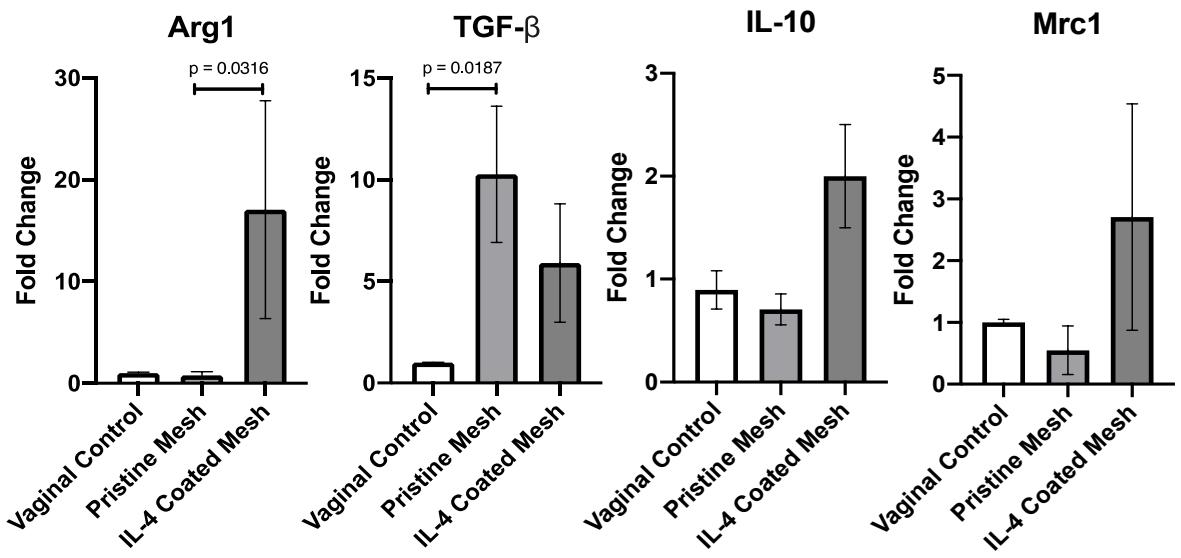

Figure 71: Rabbit Vaginal Anti-inflammatory profile at 14 days post-implantation. Samples are normalized to Vaginal control. Data is shown as (n = 3 – 5) biological replicates with (n = 3) technical replicates. Values are represented as mean fold change ± SEM

At 90 days, the subcutaneous pristine mesh implants expressed a significant increase in iNOS and IL-1β expression when compared to abdominal muscle control (iNOS, p = 0.0006; IL-1β, p = 0.0268), and pristine mesh implants (iNOS, p = 0.0004; IL-1β, p = 0.0215) (Figure 72). There were no significant differences observed in regulation of IFN-γ and IL-6 between groups. Interestingly, while there seemed to be a trend of increasing expression in the IL-4 coated mesh groups for the anti-inflammatory panel of markers, there were no significant differences found between groups in expression of Arg1, TGF-β, IL-10, and Mrc1 at 90 days for subcutaneous implants (Figure 73).

Pristine mesh vaginal implants showcased a significantly increased expression in all of the pro-inflammatory markers (iNOS, IFN-γ, IL-1β, and IL-6) when compared to vaginal controls (iNOS, p = 0.0336; IFN-γ, p = 0.0008; IL-1β, p = 0.0067; IL-6, p = 0.0180) (Figure 74). Pristine mesh vaginal implants also showed significantly increased expression when compared to IL-4 coated mesh for the pro-inflammatory markers IFN-γ (p= 0.0006) and IL-1β (p = 0.0043). At 90

days, the IL-4 coated mesh vaginal implants showcased a significant increase in the anti-inflammatory markers, Arg1 ($p = 0.0439$) and Mrc1 ($p = 0.0381$) when compared to pristine mesh implants indicating a possible mediating effect with the eluted IL-4 (Figure 75). There were no significant differences in the regulation of TGF-β and IL-10, thought the IL-4 coated mesh implants did show a trend of increased expression.

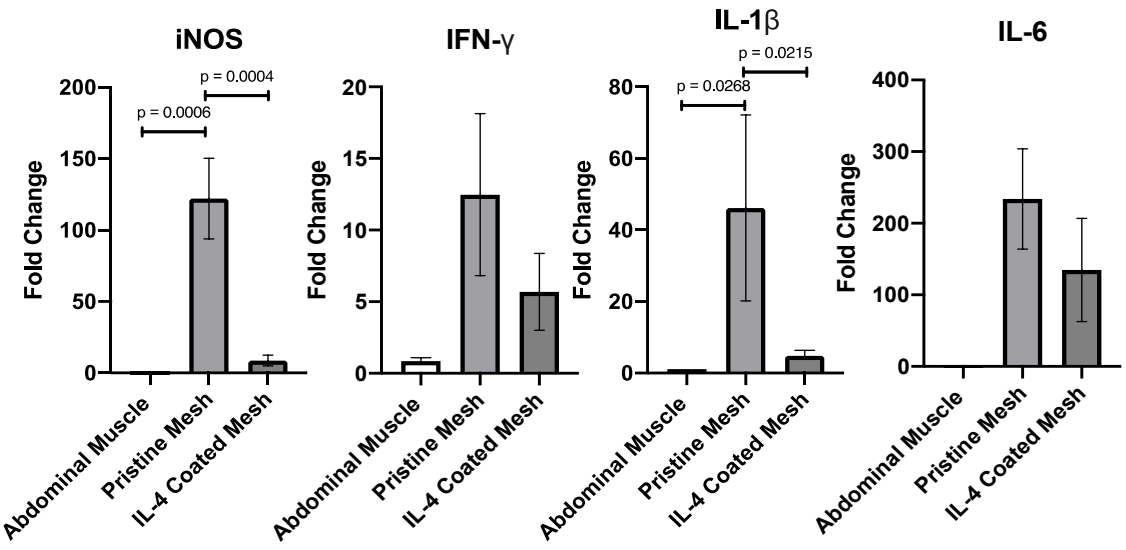

Figure 72: Rabbit Subcutaneous Pro-inflammatory profile at 90 days post-implantation. Samples are normalized to Abdominal Muscle control. Data is shown as (n = 3 – 5) biological replicates with (n = 3) technical replicates. Values are represented as mean fold change ± SEM

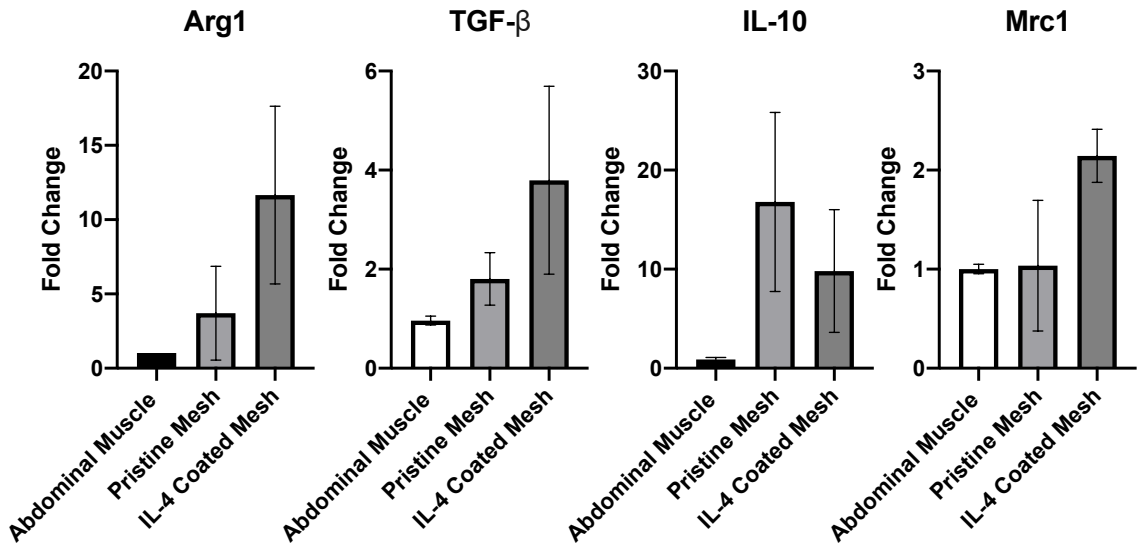

Figure 73: Rabbit Subcutaneous Anti-inflammatory profile at 90 days post-implantation. Samples are normalized to abdominal muscle control. Data is shown as (n = 3 – 5) biological replicates with (n = 3) technical replicates. Values are represented as mean fold change ± SEM

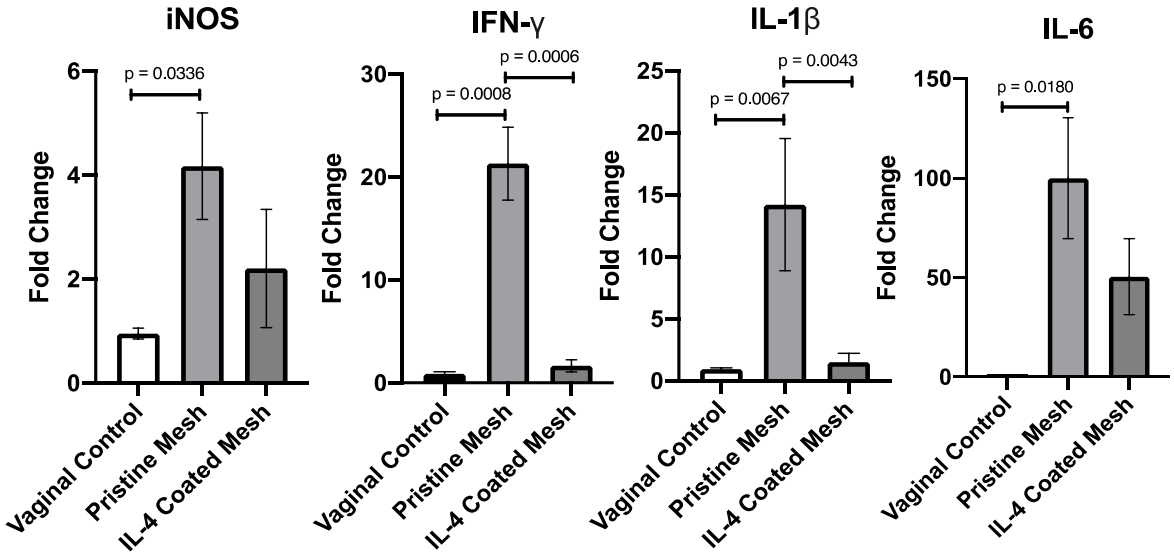

Figure 74: Rabbit Vaginal Pro-inflammatory profile at 90 days post-implantation. Samples are normalized to Vaginal control. Data is shown as (n = 3 – 5) biological replicates with (n = 3) technical replicates. Values are represented as mean fold change ± SEM

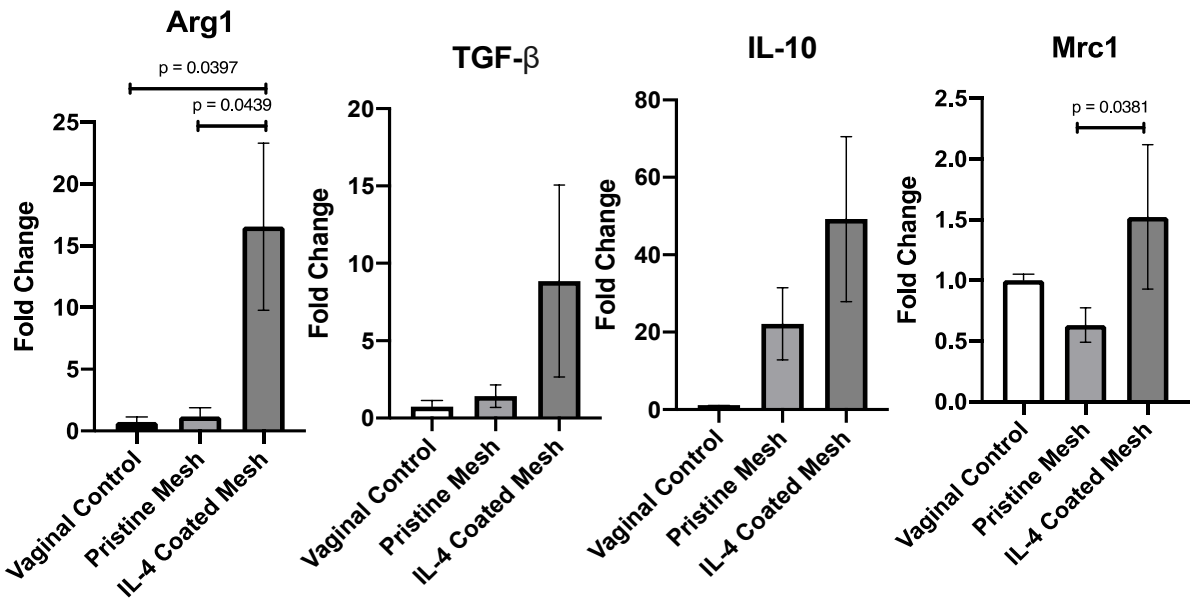

Figure 75: Rabbit Vaginal Anti-inflammatory profile at 90 days post-implantation. Samples are normalized to Vaginal control. Data is shown as (n = 3 – 5) biological replicates with (n = 3) technical replicates. Values are represented as mean fold change ± SEM

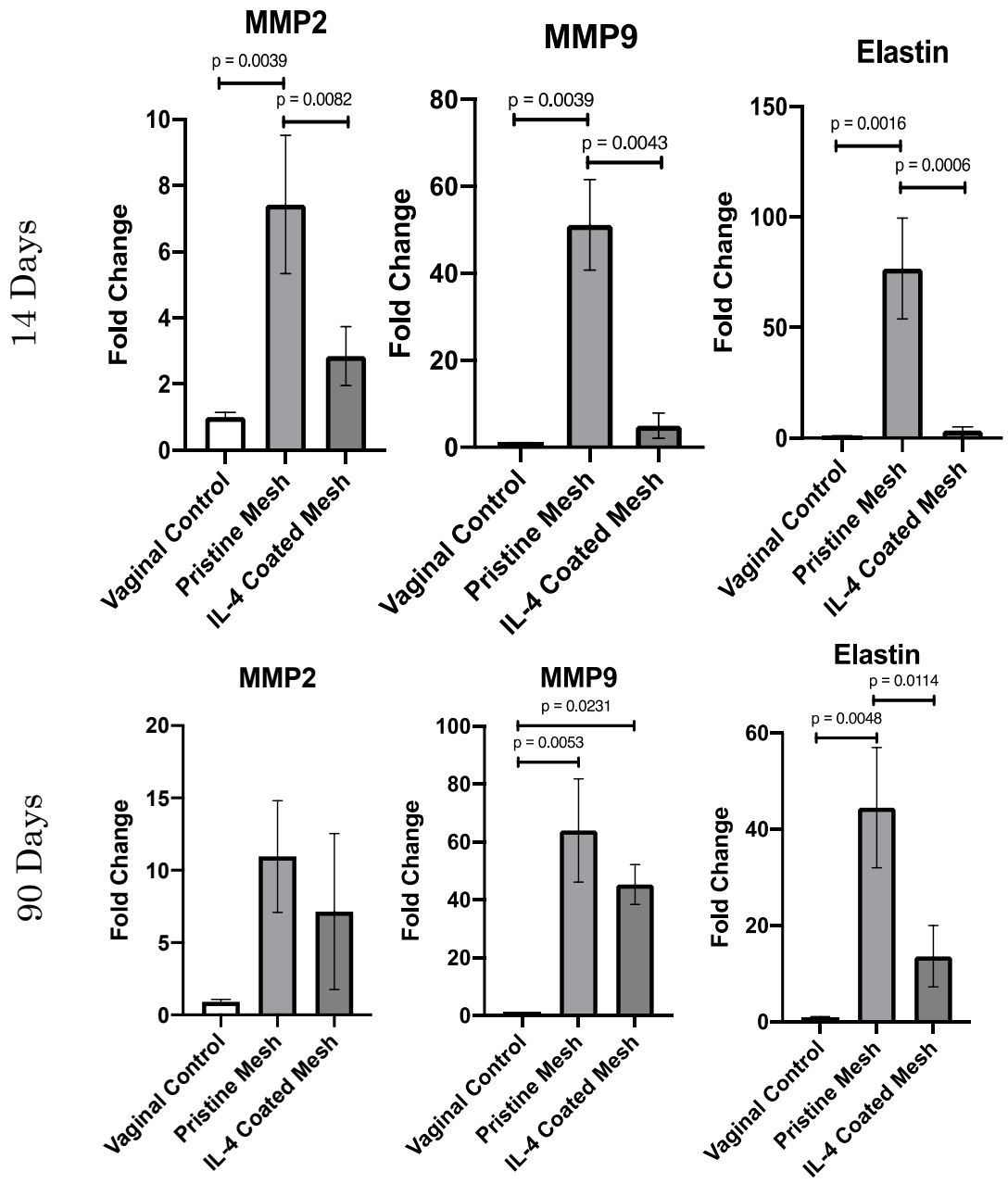

Figure 76: Rabbit vaginal matrix metalloproteinases and elastin expression at both 14- and 90-days post-implantation. Samples are normalized to vaginal control. Data shown as (n = 3 – 5) biological replicates with (n = 3) technical replicates. Values are represented as mean fold change ± SEM

Pristine mesh implants all expressed significantly higher MMP2 and MMP9 when compared to vaginal controls (MMP2, p = 0.0039; MMP9, p = 0.0039) and IL-4 coated mesh implants (MMP2, p = 0.0082; MMP9, p = 0.0043) at 14 days post-implantation (Figure 76).

However, pristine mesh implants also significantly expressed higher elastin when compared to vaginal controls ($p = 0.0016$) and IL-4 coated mesh ($p = 0.0006$). On the other hand, IL-4 coated mesh implants had markedly decreased expression in MMP9 and elastin at 14 days but an increase when compared to vaginal controls.

At 90 days, both the pristine mesh implants and IL-4 coated mesh implants showed increased MMP2, MMP9 and elastin expression when compared to vaginal controls. However, MMP9 expression was significantly increased when comparing to vaginal controls for pristine mesh ($p = 0.0053$) and for IL-4 coated mesh ($p = 0.0231$). In terms of elastin expression, pristine mesh implants had significantly higher expression ($p = 0.0048$) when compared to vaginal controls and ($p = 0.0114$) the IL-4 coated implants. This provides further insight into the histological findings of the maladaptive response regarding elastic fibers observed earlier. The increase in MMP2 and MMP9 expression can be associated with increased tissue degradation and changes in matrix remodeling.

7.3.12 Gelatinase Assay

In order to assess the matrix-metalloproteinase levels in the IL-4 coated mesh implants, a gelatinase substrate degradation assay was performed allowing for the measurement of gelatinase activity. There were no significant differences in gelatinase activity between the vaginal control and IL-4 coated mesh implanted vaginally after 14 days (Figure 77). However, there was a significant increase in activity at 90 days post-implantation of the IL-4 coated mesh ($p = 0.0106$) compared to the vaginal control, indicating MMP activity was upregulated during the chronic immune response (Figure 77). There was also a significant increase in activity at 90 days post-

implantation of the IL-4 coated mesh ($p = 0.0009$) compared to the IL-4 coated mesh at 14 days. Interestingly, at 14 days post-implantation, there was a significant decrease in gelatinase activity in the IL-4 coated mesh implants when compared to pristine mesh implants ($p = 0.0454$). A similar trend was observed at 90 days post-implantation, where the IL-4 coated mesh implants showed significantly less activity than the pristine mesh implants, indicating that the IL-4 coated mesh was capable of decreasing levels of gelatinase activity in the chronic host response.

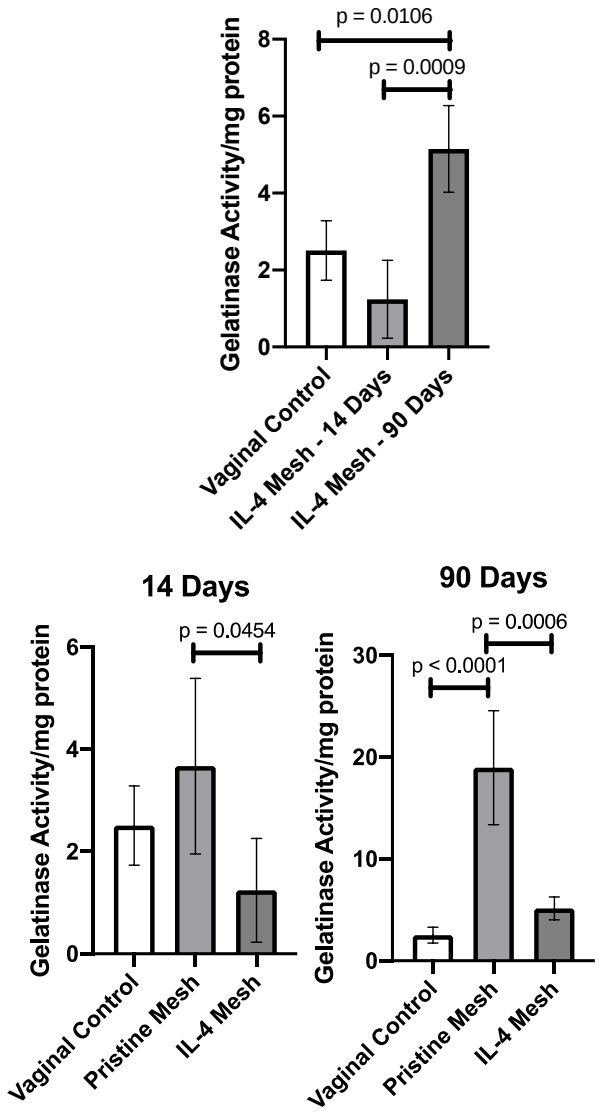

Figure 77: Gelatinase Activity comparing Vaginal Controls to 14- and 90-days post-implantation of pristine mesh and IL-4 coated mesh. Data shown as values ± SEM.

7.3.13 Ball Burst Mechanical Testing Outcomes

In order to estimate individual vaginal tissue structural properties, ball-burst mechanical tests were performed on the IL-4 coated mesh-tissue complexes at both 14- and 90-days post-implantation. Similar to the pristine mesh implants, there were no significant differences observed

in the estimated vaginal tissue contribution calculated at 14 days and 90 days post-implantation. However, upon comparison to pristine mesh implants, IL-4 mesh coated implants depicted a significantly higher estimated vaginal tissue contribution at both 14- and 90-days post-implantation ($p = 0.0452$, $p = 0.0059$). The higher vaginal stiffness indicates that there was less loss in structural integrity overall with the IL-4 mesh implants.

It is important to note that the polymer coated mesh was also mechanically tested for load and stiffness and no differences were observed in the mechanical integrity of the mesh when compared to pristine mesh samples.

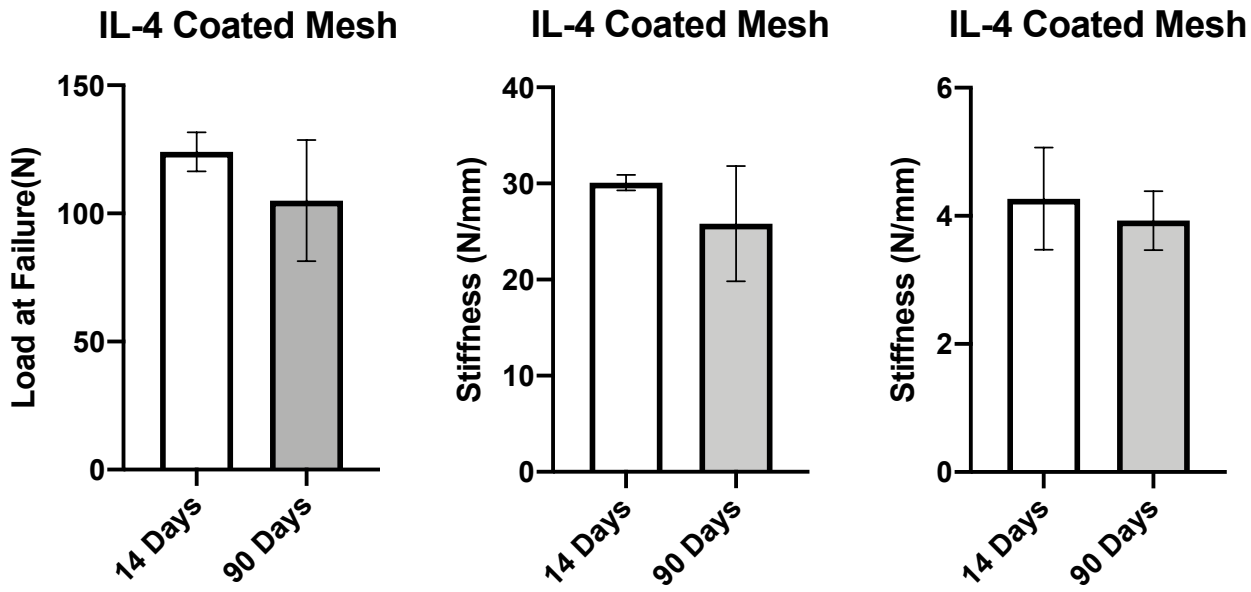

Figure 78: IL-4 Coated Mesh A. Load to Failure of mesh-tissue complex B. Stiffness of mesh-tissue complex C. Estimated Stiffness of Vaginal Tissue Contribution. Data shown as values ± SD.

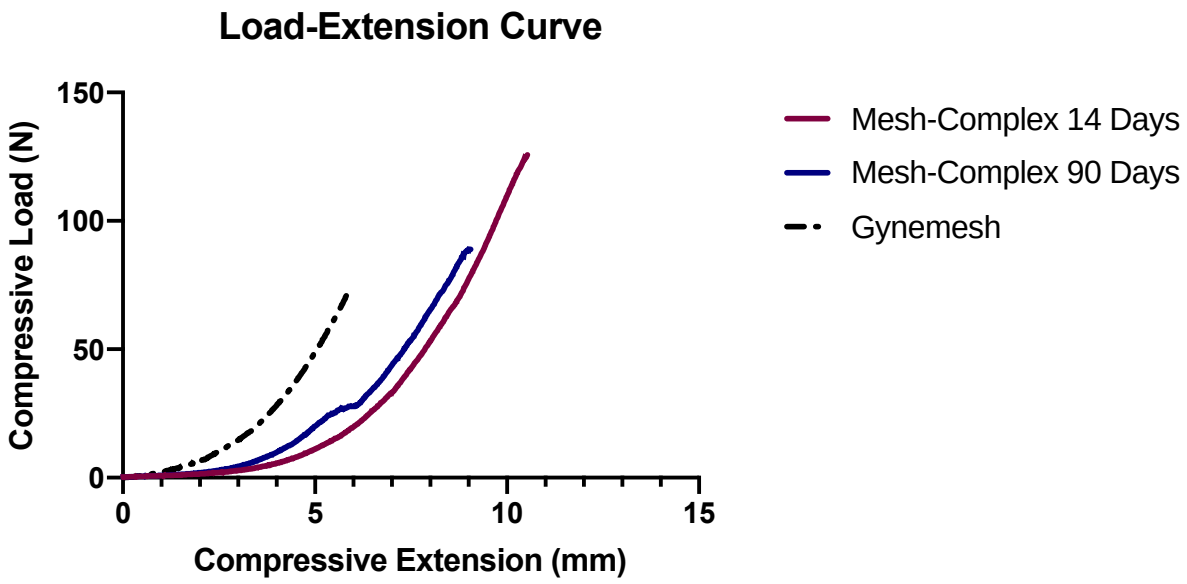

Figure 79: Representative Load-Extension curves for Gynemesh, Vaginal IL-4 Coated Mesh Implants at 14- and 90-days post-implantation

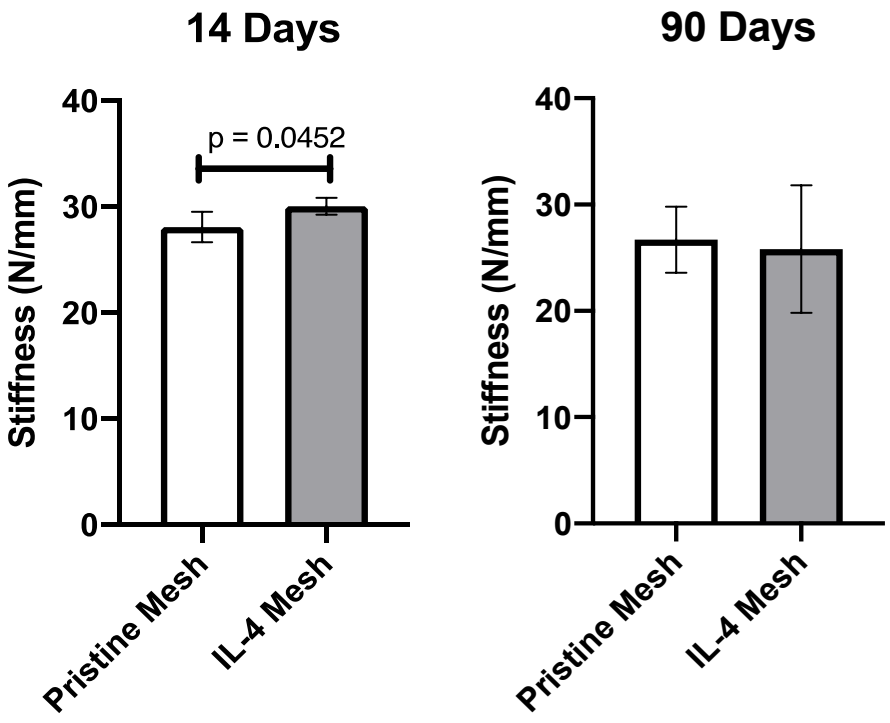

Figure 80: Stiffness of the Mesh-Tissue Complex for Pristine Mesh and IL-4 Coated Mesh at both 14- and 90-days post-implantation. Data shown as values ± SD.

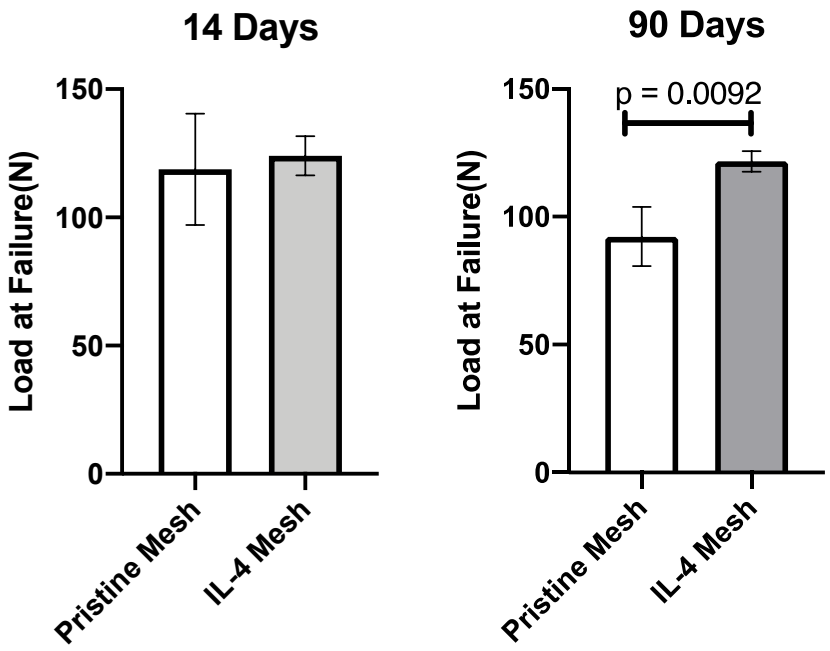

Figure 81: Load at Failure for Mesh-Tissue Complex for Pristine mesh and IL-4 Coated mesh at both 14- and 90-days post-implantation. Data shown as values ± SD.

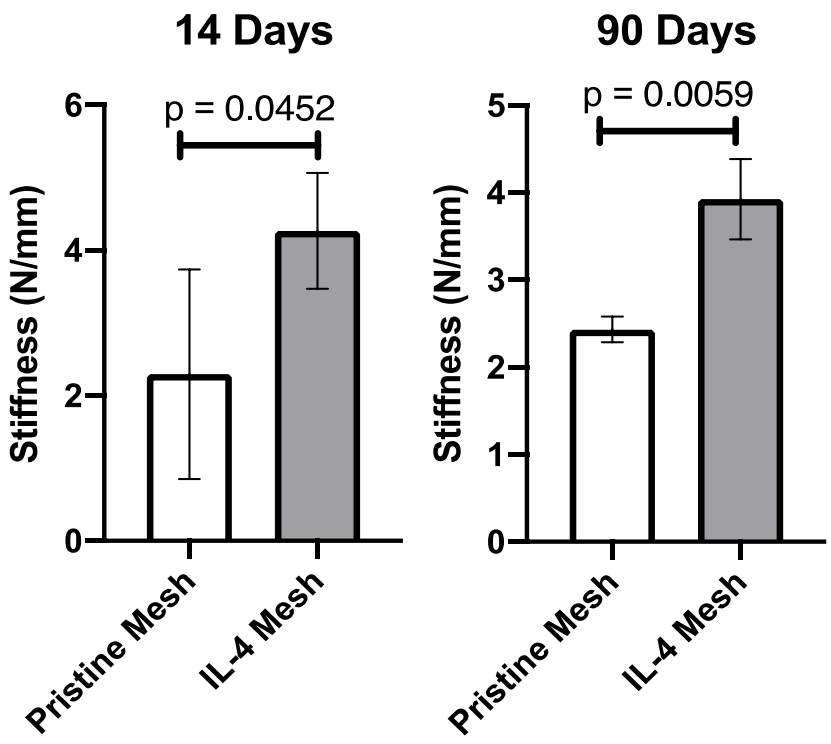

Figure 82: Estimated Vaginal Tissue Contribution for Pristine mesh and IL-4 Coated mesh at both 14- and 90-days post-implantation. Data shown as values ± SD.

7.4 Conclusions

Overall, the findings from the second aim can be split into two main categorical divisions. The first portion of the study was aimed at scaling up and validating the bioactive rabbit IL-4 release from a polymer coating. This principally involved utilizing *in vitro* assays and rabbit cytokines to understand the inflammatory spectrum. We were able to specifically observe the functionality of rabbit macrophages cultured *in vitro* and further characterize the pro-inflammatory and anti-inflammatory expression. We were able to incorporate recombinant rabbit IL-4 into a layer-by-layer coating followed determining a distinct release profile, consisting of 80% of IL-4

released in the first week. This follows our desired profile since IL-4 released in this acute phase is necessary to be impactful on macrophage polarization capabilities. This was in addition to macrophage polarization cultures confirmed through functional assays and gene expression to indicate the pro-inflammatory and anti-inflammatory profiles. The bioactivity assays from these macrophage cultures further elucidated the IL-4 being released was capable of polarizing naïve macrophages towards an M2-like profile.

Following this set of *in vitro* characterization, the second portion of this aim focused on *in vivo* implantation of the IL-4 coated mesh in a rabbit model of lumbar colpopexy. We found distinct host responses to IL-4 coated polypropylene mesh implanted both subcutaneously and vaginally with overall changes in tissue architecture indicating changes in remodeling that can be characterized through collagen deposition, vascularity, and a variety of immune expression markers. Upon further histological analysis, specifically observing collagen formation, the IL-4 coated mesh implants did showcase higher percentages in the area of collagen when compared to their pristine mesh counterparts. While a collagen response is usually one associated with the typical pathway of inflammation and fibrotic tissue formation [1, 39, 40], the important idea is to also consider specific characteristics regarding the collagen that is surrounding the implant. For instance, with the IL-4 coated mesh, we observed these oriented dense collagen fibers indicative of an active remodeling response related to tissue integration downstream and a homogenous architecture. Additionally, we must take into consideration the higher percentage of native collagen present in the tissues, especially in the vagina.

Evidence indicating that this increased collagen percentage does not necessarily correlate with the formation of scar tissue or a fibrotic capsule is the enhanced angiogenesis observed surrounding mesh fibers. In the case of scar development, it is possible to see dense collagen fibers,

but a lack of vascularity leading to the compacture component often seen surrounding implants or the wound site. Often, fibrotic reactions are harmful when considering the needs of the host and nutrient supply. However, in the case of the IL-4 coated mesh implants, we did detect heightened vascularity surrounding individual mesh fibers. This indicates that the surrounding tissue response not only consisted of an aligned homogenous connective tissue but also one that was adequately supplied in terms of vascularity. These are all factors to consider upon implant integration with tissue outcomes. Of course, with the observation of enhanced angiogenesis can also be a concern for mechanisms relying on tumor progression. However, it is also important to note that other indicators of tumor growth, such as changes in collagen where the connective tissue is progressively destroyed as seen in the cases of malignant cancer cells [39, 100, 101]. We did not detect any presence of lesions either.

This aim also focused on understanding the immune response to the IL-4 coated mesh using strategies unique methods of identifying macrophage behavior. We were able to recognize macrophages surrounding mesh fibers using the pan-macrophage marker, RAM11. However, we were limited in the abilities to label the subtype of macrophage that was surrounding each mesh fiber. Nevertheless, there are many assumptions we can make about characterizing the phenotype based on all other evidence gathered (collagen deposition, angiogenesis, IL-4 promotion, gene expression, etc.). For instance, we know that the anti-inflammatory M2 macrophage phenotypic subtype produce high levels of arginase, TGF- β, IL-10 and Mrc1[44, 47, 48, 72, 94, 102]. Additionally, M2 macrophages have previously been known to promote angiogenesis and recruit cells in constructive tissue remodeling.

Our methods of evaluating the immune response at a deeper level included using a marker for angiogenesis, anti-CD31, and characterizing gene expression in the implant-specific tissues at

each time point using a set of known pro-inflammatory and anti-inflammatory markers. As mentioned earlier, we did see increased vascularity surrounding the IL-4 coated mesh fibers at both 14- and 90-days post-implantation when comparing to pristine mesh implants at those time points in both subcutaneous and vaginal implants. This indicates an overall increase in vascularity regardless of location that begins at the early stage of the immune response and remains during longer times of implantation.

The panel of pro-inflammatory markers used to measure expression in the subsequent tissues consisted of characteristic indicators of macrophages that can be classified on the M1 phenotypic end of the spectrum. Pristine mesh implants consistently had increased iNOS, IFN-γ, IL-1β, and IL-6 expression when compared to control tissues in both vaginal and subcutaneous implants at both 14- and 90-days post-implantation. Interestingly, we began to see changes in the pro-inflammatory expression of the IL-4 coated mesh implants when compared to both control tissues and the pristine mesh implants. While there was an overall increase in expression compared to control tissues, we did observe a general decrease in pro-inflammatory expression in the IL-4 coated mesh implants compared to pristine mesh implants. These findings suggest that the IL-4 coated mesh is capable of decreasing the pro-inflammatory expression in tissues at both 14 and 90 days of implantation. Further indicators of this are derived with the anti-inflammatory panel of markers, Arg1, TGF-β, IL-10, and Mrc1, where pristine mesh implants in both subcutaneous and vaginal spaces and at both 14 and 90 days of implantation were decreased overall when compared to both control tissues and the IL-4 coated mesh. Interestingly, the overall finding of increased anti-inflammatory expression in the IL-4 coated mesh implants in all conditions further suggests the beneficiary effects of the coating being substantially present. While it was not possible to use surface markers to specifically label the subtype of macrophages, we have shown strong

indications for the population of macrophages that may have dominated in the host response to the IL-4 coated mesh as compared to the pristine mesh.

Overall, by targeting the early immune response, we have shown changes in the tissue degradation responses with indications of better mesh-tissue integration and formation. This was associated with enhanced mechanical contributions from the tissue instead of the mesh, suggesting an improvement in implant integration. We did not see the presence of an aggravated scar formation nor any indications of tumoral factors, instead there was a reduction in the tissue adhesions and changes in the overall immune response. There is stronger evidence in the dynamic tissue remodeling process as these findings are able to capture trends that may have been observed on separate occasions, but not together in the same study.

8.0 Translational Impact

The use of polypropylene mesh provides mechanical support to many requiring prolapse repair. However, the literature has shown over time, that with the implantation of mesh, also coincides the degradation of the surrounding tissues. Persistent inflammation has been linked to women experiencing complications with mesh.

In an attempt to increase chances of success, robust studies from clinical trials assessing differences in the vaginal surgical procedures have found that introducing behavioral intervention such as pelvic floor muscle training did not improve urinary symptoms at 6 months or prolapse outcomes two years post-surgery[28, 103]. This suggests that there may be more complicated mechanisms leading to the symptoms experienced. As noted, there are so many biological and chemical changes with the implantation of mesh itself, it seems a complex solution would be necessary to address an overall improvement in mesh-tissue interactions.

Restoring apical support is the most common surgical procedure, and yet there remains to be little known about the safety and efficacy. The complications experienced are still high in number and surgical models like the rabbit lumbar colpopexy allow for a cost-effective method to understanding different stages of mesh impacting the host response. Models such as these can provide further information for the reasoning behind success rates and complication rates that are seen in the clinic.

9.0 Limitations and Future Directions

There were several limitations in this study that must be noted. Most significantly upon assessing the inflammatory response, the lack of rabbit M1 and M2 specific antibodies. While it was possible to label cells with a validated pan-macrophage marker, the limitation in the rabbit model for getting into the specificity of the macrophage spectrum led to focusing on other aspects of the host immune response. However, attempts to mitigate this were completed by utilizing other methods of evidence for characterizing the macrophage profile such as the use of gene expression and functional assays.

However, there still remains numerous other aspects of the host response that one can delve deeply into. The scope of this dissertation pertained to developing characteristics related to the macrophage response and related extracellular events. However, it is certainly possible to go further into assessing other factors of the immune response, such as specific changes in other growth factors and protein molecules. Further information about the downstream effects by considering fibroblast behavior and environmental indicators of tissue degradation.

It is also important to note that the use of New Zealand white rabbit provided advantages, also has its disadvantages in the translational hierarchy. While it served as a moderately-sized animal for mesh implantation via lumbar colpopexy, there remains the future steps that need to be taken in primate implants and human trials before translating the concepts to the clinic.

An important limitation was the lack of comparison to native vaginal tissue in the ball-burst mechanical testing outcomes. While it most certainly serves as an appropriate control, due to the lack of resources in obtaining native rabbit vagina, the data presented earlier utilizes the

different groups of mesh. Future development would most definitely include native vaginal tissue as well to better understand the structural properties.

This study focused on an overall histological characterization utilizing multiple staining methodologies to evaluate mesh host response. Another limitation is that it is possible to expand the analyses with even more metrics of immunolabeling with other characteristic markers of the dynamic immune response, such as fibroblasts and T cells along with markers of apoptosis and cellular proliferation to better understand the stages of tissue remodeling and the wound healing process. In the case of elastin metabolism, it would greatly add to the study if further analyses on markers of elastin metabolism, such as lysyl oxidase like-1, fibulin-5, and matrix-metalloproteinases were included. Overall, another distinction in this study was to assess the response to mesh, without inducing prolapse in the animal model itself, nor utilizing a specific knockout model that may represent prolapse conditions. This study is just the beginning of developing an overarching system of analysis for mesh host response at different time points. Given future work, it would be ideal to look into validating these limitations with new studies.

Appendix A Coating Stability information

Table 8: Coating Stability Requirements

Type	Storage/Stability
Pristine Mesh	Room Temperature (Desiccator) (indefinitely)
Plasma Irradiated Mesh	Room Temperature (Desiccator) (use within 1 - 2 weeks)
Core Coating Mesh (no cytokines)	4°C, Fridge (1 month)
Cytokine + coating Mesh	-20°C, Freezer (1 month)
Polymer	0.2 um Filtering everything
Chitosan (RT, chemical cabinet)	2 mg/mL in 0.5% Acetic Acid with UltraPure Water
Dermatan Sulfate (4°C box)	10 mg/mL stock in UltraPure Water, then create 2 mg/mL

Appendix B Immunohistochemistry M1/M2 Macrophage Surface Markers

Table 9: Immunohistochemistry M1/M2 Marker Validation

Type	Antibody	Dilution	H_2O_2	Blocking	Antigen Retrieval
M2	Mouse anti-CD163 [GHI/61] ab111250	1:25 1:50	1X PBS	Donkey	Citric Acid Buffer
		1:100 1:200		Goat	Tris EDTA
				Horse	
	Mouse anti-CD206 MCA2155	1:50 1:100			
	Guinea Pig Arginase PAB120Rb51	1:10 1:20 1:50 1:100 1:200	Methanol	BSA	Proteinase k
	Goat anti-Liver Arginase ab92274	1:50 1:100 1:200	1X PBS Methanol	Donkey Horse	Citric Acid Buffer
	Mouse anti- Liver Arginase [4E6] ab117989	1:50 1:100 1:200	1X PBS Methanol	Donkey Goat Horse	Citric Acid Buffer
	Mouse anti-CD163 [10D6] ab201461	1:50 1:100 1:200	1X PBS Methanol	Donkey Goat	Citric Acid Buffer
M1	Mouse anti-HLA-DR ab20181	1:50 1:100 1:200	1X PBS Methanol	Donkey	Citric Acid Buffer
	Mouse anti-HLA-DR [LN-3] ab166777	1:50 1:100 1:200	1X PBS Methanol	Donkey Goat Horse	Citric Acid Buffer

Bibliography

1. Luttikhuizen, D.T., M.C. Harmsen, and M.J. Van Luyn, *Cellular and molecular dynamics in the foreign body reaction.* Tissue Eng, 2006. **12**(7): p. 1955-70.

2. Abdool, Z., H.P. Dietz, and B.G. Lindeque, *Prolapse symptoms are associated with abnormal functional anatomy of the pelvic floor.* Int Urogynecol J, 2017. **28**(9): p. 1387-1391.

3. Ashton-Miller, J.A. and J.O. DeLancey, *Functional anatomy of the female pelvic floor.* Ann N Y Acad Sci, 2007. **1101**: p. 266-96.

4. Corton, M.M., *Anatomy of pelvic floor dysfunction.* Obstet Gynecol Clin North Am, 2009. **36**(3): p. 401-19.

5. DeLancey, J.O., *The anatomy of the pelvic floor.* Curr Opin Obstet Gynecol, 1994. **6**(4): p. 313-6.

6. Maher, C., et al., *Surgical management of pelvic organ prolapse in women.* Cochrane Database Syst Rev, 2010(4): p. CD004014.

7. Jones, K.A. and P.A. Moalli, *Pathophysiology of pelvic organ prolapse.* Female Pelvic Med Reconstr Surg, 2010. **16**(2): p. 79-89.

8. Maldonado, P.A. and C.Y. Wai, *Pelvic Organ Prolapse: New Concepts in Pelvic Floor Anatomy.* Obstet Gynecol Clin North Am, 2016. **43**(1): p. 15-26.

9. Dällenbach, P., *To mesh or not to mesh: a review of pelvic organ reconstructive surgery.* International Journal of Women's Health, 2015. **7**: p. 331-343.

10. Ghetti, C., et al., *Depressive symptoms in women seeking surgery for pelvic organ prolapse.* Int Urogynecol J, 2010. **21**(7): p. 855-60.

11. Iglesia, C.B. and K.R. Smithling, *Pelvic Organ Prolapse.* Am Fam Physician, 2017. **96**(3): p. 179-185.

12. FDA, *Surgical Mesh for Transvaginal Repair of Pelvic Organ Prolapse in the Anterior Vaginal Compartment* 2019.

13. Persu, C., et al., *Pelvic Organ Prolapse Quantification System (POP-Q) - a new era in pelvic prolapse staging.* J Med Life, 2011. **4**(1): p. 75-81.

14. Aukee, P., J.P. Usenius, and P. Kirkinen, *An evaluation of pelvic floor anatomy and function by MRI.* Eur J Obstet Gynecol Reprod Biol, 2004. **112**(1): p. 84-8.

15. Baytur, Y.B., et al., *Pelvic floor function and anatomy after childbirth.* J Reprod Med, 2007. **52**(7): p. 604-10.

16. Berger, A.A., S. Abramowitch, and P.A. Moalli, *3D vascular anatomy of the presacral space: impact of age and adiposity.* Int Urogynecol J, 2019. **30**(3): p. 401-407.

17. Betschart, C., A. Singer, and D. Scheiner, *[Female pelvic floor: anatomy and normal function]*. Ther Umsch, 2019. **73**(9): p. 529-534.

18. Bharucha, A.E., *Pelvic floor: anatomy and function.* Neurogastroenterol Motil, 2006. **18**(7): p. 507-19.

19. Bordoni, B., K. Sugumar, and S.W. Leslie, *Anatomy, Abdomen and Pelvis, Pelvic Floor*, in *StatPearls*. 2019: Treasure Island (FL).

20. Eickmeyer, S.M., *Anatomy and Physiology of the Pelvic Floor.* Phys Med Rehabil Clin N Am, 2017. **28**(3): p. 455-460.

21. Grasby, E.D., *Anatomy and physiology of the pelvic floor.* Nurs Mirror Midwives J, 1947. **86**(2228): p. 211.

22. Guo, M. and D. Li, *Pelvic floor images: anatomy of the levator ani muscle.* Dis Colon Rectum, 2007. **50**(10): p. 1647-55.

23. Herschorn, S., *Female pelvic floor anatomy: the pelvic floor, supporting structures, and pelvic organs.* Rev Urol, 2004. **6 Suppl 5**: p. S2-S10.

24. Lawson, J.O., *Pelvic anatomy. I. Pelvic floor muscles.* Ann R Coll Surg Engl, 1974. **54**(5): p. 244-52.

25. DeLancey, J.O., *What's new in the functional anatomy of pelvic organ prolapse?* Curr Opin Obstet Gynecol, 2016. **28**(5): p. 420-9.

26. FDA, *Reclassification of Urogynecologic Surgical Mesh Instrumentation.* 2016.

27. FDA, *Surgical Mesh for Treatment of Women with Pelvic Organ Prolapse and Stress Urinary Incontinence.* 2011.

28. Jelovsek, J.E., et al., *Effect of Uterosacral Ligament Suspension vs Sacrospinous Ligament Fixation With or Without Perioperative Behavioral Therapy for Pelvic Organ Vaginal Prolapse on Surgical Outcomes and Prolapse Symptoms at 5 Years in the OPTIMAL Randomized Clinical Trial.* JAMA, 2018. **319**(15): p. 1554-1565.

29. El Kassis, N., et al., *Surgical management of pelvic organ prolapse in women: how to choose the best approach.* J Med Liban, 2013. **61**(1): p. 36-47.

30. Cohen, A.M., M.A. Kahn, and S. Brown, *Comments to: surgical management of pelvic organ prolapse in women.* Tech Coloproctol, 2016. **20**(5): p. 327-330.

31. Fialkow, M.F., et al., *Lifetime risk of surgical management for pelvic organ prolapse or urinary incontinence.* Int Urogynecol J Pelvic Floor Dysfunct, 2008. **19**(3): p. 437-40.

32. Maher, C., et al., *Surgical management of pelvic organ prolapse in women.* Cochrane Database Syst Rev, 2013(4): p. CD004014.

33. Brown, B.N., et al., *Characterization of the host inflammatory response following implantation of prolapse mesh in rhesus macaque.* Am J Obstet Gynecol, 2015. **213**(5): p. 668.e1-10.

34. Nolfi, A.L., et al., *Host response to synthetic mesh in women with mesh complications.* Am J Obstet Gynecol, 2016. **215**(2): p. 206.e1-8.

35. Liang, R., et al., *Vaginal degeneration following implantation of synthetic mesh with increased stiffness.* BJOG: An International Journal of Obstetrics & Gynaecology, 2013. **120**(2): p. 233-243.

36. Bilsel, Y. and I. Abci, *The search for ideal hernia repair; mesh materials and types.* International Journal of Surgery, 2012. **10**(6): p. 317-321.

37. Jonsson Funk, M., et al., *Trends in use of surgical mesh for pelvic organ prolapse.* Am J Obstet Gynecol, 2013. **208**(1): p. 79.e1-7.

38. Mironska, E., C. Chapple, and S. MacNeil, *Recent advances in pelvic floor repair.* F1000Res, 2019. **8**.

39. Ruud A. Bank, P., Jurjen Zandstra, PhD, Hilde Room, Arjen H. Petersen, and Sander M. van Putten, PhD, *Biomaterial Encapsulation Is Enhanced in the Early Stages of the*

Foreign Body Reaction During Conditional Macrophage Depletion in Transgenic Macrophage Fas-Induced Apoptosis Mice. Tissue Engineering Part A, 2017.

40. Anderson, J.M., A. Rodriguez, and D.T. Chang, *Foreign body reaction to biomaterials.* Semin Immunol, 2008. **20**(2): p. 86-100.

41. Holger Gerullis, 2 Evangelos Georgas,1 Mihaly Borós,3 Bernd Klosterhalfen,4 Christoph Eimer,1 Christian Arndt,1 Stephan Otto,2,5 Dimitri Barski,1 Dirk Ysebaert,6 Albert Ramon,7 and Thomas Otto1,2, *Inflammatory Reaction as Determinant of Foreign Body Reaction Is an Early and Susceptible Event after Mesh Implantation.* Biomed Res Int, 2014.

42. Gerullis, H., et al., *Inflammatory reaction as determinant of foreign body reaction is an early and susceptible event after mesh implantation.* Biomed Res Int, 2014. **2014**: p. 510807.

43. Schutte, R.J., et al., *In vivo cytokine-associated responses to biomaterials.* Biomaterials, 2009. **30**(2): p. 160-8.

44. Brown, B.N., et al., *Macrophage phenotype as a predictor of constructive remodeling following the implantation of biologically derived surgical mesh materials.* Acta Biomater, 2012. **8**(3): p. 978-87.

45. Spiller, K.L., et al., *Sequential delivery of immunomodulatory cytokines to facilitate the M1-to-M2 transition of macrophages and enhance vascularization of bone scaffolds.* Biomaterials, 2015. **37**: p. 194-207.

46. Mills, C.D., *Anatomy of a discovery: m1 and m2 macrophages.* Front Immunol, 2015. **6**: p. 212.

47. Zhu, L., et al., *Cellular metabolism and macrophage functional polarization.* Int Rev Immunol, 2015. **34**(1): p. 82-100.

48. Murray, P.J., et al., *Macrophage activation and polarization: nomenclature and experimental guidelines.* Immunity, 2014. **41**(1): p. 14-20.

49. Brown, B.N., B.M. Sicari, and S.F. Badylak, *Rethinking Regenerative Medicine: A Macrophage-Centered Approach.* Frontiers in Immunology, 2014. **5**: p. 510.

50. Hachim, D., et al., *Shifts in macrophage phenotype at the biomaterial interface via IL-4 eluting coatings are associated with improved implant integration.* Biomaterials, 2017. **112**: p. 95-107.

51. Dziki, J.L., et al., *Extracellular Matrix Bioscaffolds as Immunomodulatory Biomaterials<sup/>*. Tissue Eng Part A, 2017. **23**(19-20): p. 1152-1159.

52. Minardi, S., et al., *IL-4 Release from a Biomimetic Scaffold for the Temporally Controlled Modulation of Macrophage Response.* Ann Biomed Eng, 2016. **44**(6): p. 2008-19.

53. den Dekker, E., et al., *Monocyte cell surface glycosaminoglycans positively modulate IL-4-induced differentiation toward dendritic cells.* J Immunol, 2008. **180**(6): p. 3680-8.

54. Daucher, J.A., et al., *Adaptations of the rat vagina in pregnancy to accommodate delivery.* Obstet Gynecol, 2007. **109**(1): p. 128-35.

55. Jiang, K., et al., *Local release of dexamethasone from macroporous scaffolds accelerates islet transplant engraftment by promotion of anti-inflammatory M2 macrophages.* Biomaterials, 2017. **114**: p. 71-81.

56. Keeney, M., et al., *Mutant MCP-1 protein delivery from layer-by-layer coatings on orthopedic implants to modulate inflammatory response.* Biomaterials, 2013. **34**(38): p. 10287-95.

57. Pavlukhina, S. and S. Sukhishvili, *Polymer assemblies for controlled delivery of bioactive molecules from surfaces.* Advanced Drug Delivery Reviews, 2011. **63**(9): p. 822-836.

58. Liu, X., et al., *Elastic fiber homeostasis requires lysyl oxidase-like 1 protein.* Nat Genet, 2004. **36**(2): p. 178-82.

59. Liu, X., et al., *Failure of elastic fiber homeostasis leads to pelvic floor disorders.* Am J Pathol, 2006. **168**(2): p. 519-28.

60. Budatha, M., et al., *Extracellular matrix proteases contribute to progression of pelvic organ prolapse in mice and humans.* J Clin Invest, 2011. **121**(5): p. 2048-59.

61. Drewes, P.G., et al., *Pelvic organ prolapse in fibulin-5 knockout mice: pregnancy-induced changes in elastic fiber homeostasis in mouse vagina.* Am J Pathol, 2007. **170**(2): p. 578-89.

62. Wolf, M.T., et al., *Macrophage polarization in response to ECM coated polypropylene mesh.* Biomaterials, 2014. **35**(25): p. 6838-49.

63. Hilger, W.S., et al., *Histological and biomechanical evaluation of implanted graft materials in a rabbit vaginal and abdominal model.* Am J Obstet Gynecol, 2006. **195**(6): p. 1826-31.

64. Couri, B.M., et al., *Animal models of female pelvic organ prolapse: lessons learned.* Expert Rev Obstet Gynecol, 2012. **7**(3): p. 249-260.

65. Bellon, J.M., et al., *Comparing the behavior of different polypropylene meshes (heavy and lightweight) in an experimental model of ventral hernia repair*. J Biomed Mater Res B Appl Biomater, 2009. **89**(2): p. 448-55.

66. Endo, M., et al., *Cross-linked xenogenic collagen implantation in the sheep model for vaginal surgery.* Gynecol Surg, 2015. **12**(2): p. 113-122.

67. Mansoor, A., et al., *Development of an ovine model for training in vaginal surgery for pelvic organ prolapse.* Int Urogynecol J, 2017. **28**(10): p. 1595-1597.

68. Abramowitch, S.D., et al., *Tissue mechanics, animal models, and pelvic organ prolapse: a review*. Eur J Obstet Gynecol Reprod Biol, 2009. **144 Suppl 1**: p. S146-58.

69. Hympanova, L., et al., *Assessment of Electrospun and Ultra-lightweight Polypropylene Meshes in the Sheep Model for Vaginal Surgery.* Eur Urol Focus, 2018.

70. Jallah, Z., et al., *The impact of prolapse mesh on vaginal smooth muscle structure and function.* BJOG, 2016. **123**(7): p. 1076-85.

71. Liang, R., et al., *Impact of prolapse meshes on the metabolism of vaginal extracellular matrix in rhesus macaque.* Am J Obstet Gynecol, 2015. **212**(2): p. 174 e1-7.

72. Badylak, S.F., et al., *Macrophage phenotype as a determinant of biologic scaffold remodeling.* Tissue Eng Part A, 2008. **14**(11): p. 1835-42.

73. Huffaker, R.K., et al., *Histologic response of porcine collagen-coated and uncoated polypropylene grafts in a rabbit vagina model.* Am J Obstet Gynecol, 2008. **198**(5): p. 582.e1-7.

74. Socarras, T.O., et al., *Foreign body response to subcutaneous implants in diabetic rats.* PLoS One, 2014. **9**(11): p. e110945.

75. Udpa, N., et al., *Effects of Chitosan Coatings on Polypropylene Mesh for Implantation in a Rat Abdominal Wall Model.* Tissue Engineering. Part A, 2013. **19**(23-24): p. 2713-2723.

76. Ulrich, D., et al., *Changes in pelvic organ prolapse mesh mechanical properties following implantation in rats.* Am J Obstet Gynecol, 2016. **214**(2): p. 260 e1-260 e8.

77. Wolf, M.T., et al., *Polypropylene Surgical Mesh Coated with Extracellular Matrix Mitigates the Host Foreign Body Response.* Journal of biomedical materials research. Part A, 2014. **102**(1): p. 234-246.

78. Weidner, N., *Current pathologic methods for measuring intratumoral microvessel density within breast carcinoma and other solid tumors.* Breast Cancer Res Treat, 1995. **36**(2): p. 169-80.

79. Liang, R., et al., *Towards rebuilding vaginal support utilizing an extracellular matrix bioscaffold.* Acta Biomater, 2017. **57**: p. 324-333.

80. Stegemann, H. and K. Stalder, *Determination of hydroxyproline.* Clin Chim Acta, 1967. **18**(2): p. 267-73.

81. Feola, A., et al., *Characterizing the ex vivo textile and structural properties of synthetic prolapse mesh products.* Int Urogynecol J, 2013. **24**(4): p. 559-64.

82. Bolnick, A., J. Bolnick, and M.P. Diamond, *Postoperative adhesions as a consequence of pelvic surgery.* J Minim Invasive Gynecol, 2015. **22**(4): p. 549-63.

83. Hibbs, M.S., C.L. Mainardi, and A.H. Kang, *Type-specific collagen degradation by eosinophils.* Biochem J, 1982. **207**(3): p. 621-4.

84. Jaillon, S., et al., *The humoral pattern recognition receptor PTX3 is stored in neutrophil granules and localizes in extracellular traps.* J Exp Med, 2007. **204**(4): p. 793-804.

85. Zong, W., et al., *Alteration of vaginal elastin metabolism in women with pelvic organ prolapse.* Obstet Gynecol, 2010. **115**(5): p. 953-61.

86. Karsdal, M.A. and ProQuest (Firm), *Biochemistry of collagens, laminins and elastin : structure, function and biomarkers*. 2016, Academic Press is an imprint of Elsevier,: London, United Kingdom ; San Diego, CA, United States. p. 1 online resource.

87. Katrina M. Knight1, A.M.A.M.R.R.G.E.K.S.D.A., 4 & Pamela A. Moalli3,4, *New Zealand white rabbit: a novel model for prolapse mesh implantation via a lumbar colpopexy.* International Urogynecology Journal, 2019.

88. Liang, R., et al., *Extracellular matrix regenerative graft attenuates the negative impact of polypropylene prolapse mesh on vagina in rhesus macaque.* Am J Obstet Gynecol, 2017. **216**(2): p. 153 e1-153 e9.

89. Moalli, P.A., et al., *Regulation of matrix metalloproteinase expression by estrogen in fibroblasts that are derived from the pelvic floor.* Am J Obstet Gynecol, 2002. **187**(1): p. 72-9.

90. Feola, A., et al., *Deterioration in biomechanical properties of the vagina following implantation of a high-stiffness prolapse mesh.* BJOG, 2013. **120**(2): p. 224-232.

91. Lapèíková, B., et al., *Application of radio frequency glow discharge plasma for enhancing adhesion bonds in polymer/polymer joints.* Journal of Applied Polymer Science, 2006. **102**(2): p. 1827-1833.

92. Winchester, M.R. and R. Payling, *Radio-frequency glow discharge spectrometry:: A critical review.* Spectrochimica Acta Part B: Atomic Spectroscopy, 2004. **59**(5): p. 607-666.

93. Correa, S., et al., *Highly Scalable, Closed-Loop Synthesis of Drug-Loaded, Layer-by-Layer Nanoparticles.* Advanced Functional Materials, 2016. **26**(7): p. 991-1003.

94. Mosser, D.M. and J.P. Edwards, *Exploring the full spectrum of macrophage activation.* Nat Rev Immunol, 2008. **8**(12): p. 958-69.

95. Mazuji, M.K., K. Kalambaheti, and B. Pawar, *Prevention of Adhesions with Polyvinylpyrrolidone. Preliminary Report.* Arch Surg, 1964. **89**: p. 1011-5.

96. Irkorucu, O., et al., *Reduction of postsurgical adhesions in a rat model: a comparative study.* Clinics (Sao Paulo), 2009. **64**(2): p. 143-8.

97. Lin, J., et al., *Mechanical roles in formation of oriented collagen fibers.* Tissue Eng Part B Rev, 2019.

98. Valentin, J.E., et al., *Extracellular matrix bioscaffolds for orthopaedic applications. A comparative histologic study.* J Bone Joint Surg Am, 2006. **88**(12): p. 2673-86.

99. Sicari, B.M., et al., *The promotion of a constructive macrophage phenotype by solubilized extracellular matrix.* Biomaterials, 2014. **35**(30): p. 8605-12.

100. Bygd, H.C., K.D. Forsmark, and K.M. Bratlie, *The significance of macrophage phenotype in cancer and biomaterials.* Clin Transl Med, 2014. **3**(1): p. 62.

101. Adjei, I.M. and S. Blanka, *Modulation of the tumor microenvironment for cancer treatment: a biomaterials approach.* J Funct Biomater, 2015. **6**(1): p. 81-103.

102. Mills, C.D., *M1 and M2 Macrophages: Oracles of Health and Disease.* Crit Rev Immunol, 2012. **32**(6): p. 463-88.

103. Barber, M.D., et al., *Comparison of 2 transvaginal surgical approaches and perioperative behavioral therapy for apical vaginal prolapse: the OPTIMAL randomized trial.* JAMA, 2014. **311**(10): p. 1023-34.